INFORMATION TO USERS

This manuscript has been reproduced from the microfilm master. UMI films the text directly from the original or copy submitted. Thus, some thesis and dissertation copies are in typewriter face, while others may be from any type of computer printer.

The quality of this reproduction is dependent upon the quality of the copy submitted. Broken or indistinct print, colored or poor quality illustrations and photographs, print bleedthrough, substandard margins, and improper alignment can adversely affect reproduction.

In the unlikely event that the author did not send UMI a complete manuscript and there are missing pages, these will be noted. Also, if unauthorized copyright material had to be removed, a note will indicate the deletion.

Oversize materials (e.g., maps, drawings, charts) are reproduced by sectioning the original, beginning at the upper left-hand corner and continuing from left to right in equal sections with small overlaps. Each original is also photographed in one exposure and is included in reduced form at the back of the book.

Photographs included in the original manuscript have been reproduced xerographically in this copy. Higher quality 6" x 9" black and white photographic prints are available for any photographs or illustrations appearing in this copy for an additional charge. Contact UMI directly to order.

UMI

A Bell & Howell Information Company
300 North Zeeb Road, Ann Arbor MI 48106-1346 USA
313/761-4700 800/521-0600

EXPERIMENTAL DETERMINATION OF THE SYMMETRY OF THE SUPERCONDUCTING PAIRING STATE IN YBCO

BY

DAVID ANDERS WOLLMAN

B.S., Michigan State University, 1990
M.S., University of Illinois, 1992

THESIS

Submitted in partial fulfillment of the requirements
for the degree of Doctor of Philosophy in Physics
in the Graduate College of the
University of Illinois at Urbana-Champaign, 1996

Urbana, Illinois

UNIVERSITY OF ILLINOIS AT URBANA-CHAMPAIGN

THE GRADUATE COLLEGE

OCTOBER 1995

WE HEREBY RECOMMEND THAT THE THESIS BY

DAVID ANDERS WOLLMAN

ENTITLED EXPERIMENTAL DETERMINATION OF THE SYMMETRY OF THE SUPERCONDUCTING PAIRING STATE IN YBCO

BE ACCEPTED IN PARTIAL FULFILLMENT OF THE REQUIREMENTS FOR THE DEGREE OF DOCTOR OF PHILOSOPHY

Director of Thesis Research

Head of Department

Committee on Final Examination†

Chairperson

† Required for doctor's degree but not for master's.

O 517

EXPERIMENTAL DETERMINATION OF THE SYMMETRY OF THE SUPERCONDUCTING PAIRING STATE IN YBCO

David Anders Wollman, Ph.D.
Department of Physics
University of Illinois at Urbana-Champaign, 1996
Dale J. Van Harlingen, Advisor

In this thesis I present measurements of bimetallic Pb-Au-YBCO dc SQUIDs (Superconducting QUantum Interference Devices) and Josephson junctions that provide an important clue to the origin of the pairing mechanism for high temperature superconductivity in the cuprates. By probing the momentum space anisotropy of the phase of the superconducting order parameter, we can experimentally determine the symmetry of the superconducting pairing state in YBCO and distinguish between the leading candidate states that have been proposed. We find that the superconducting order parameter in YBCO changes sign between orthogonal directions in momentum space, unlike the isotropic order parameter in conventional superconductors. The sign change of the order parameter is consistent with a $d_{x^2-y^2}$ pairing state symmetry.

To Susan, Thomas and Sarah

ACKNOWLEDGMENTS

First of all, I would like to thank my advisor Dale Van Harlingen for his considerable interest and guidance in this work. He has been the ideal advisor, both in lab and as a friend and mentor. I personally appreciate that he took the time to share his thoughts on all aspects of academic life, both good and bad, as well as going out of his way to see that I received attention for my role in this work.

I would also like to acknowledge my fellow DVH group members (past and present) for many helpful and enjoyable discussions on subjects ranging from physics to politics. In particular, I would like to thank Mark Wistrom for turning valves and flipping switches for me late at night so that I could stay at home with my family. When I was just starting, Ralph Schweinfurth always found the time to explain things and train me on equipment. I thank Joe Walko for help with his data acquisition program as well as support during political discussions. Subashri (Suba) Rao and Lan Vu made life in lab interesting and fun. I would also like to thank Britton Plourde and Stu Tessmer for helping me use the STM on YBCO surfaces, and Brian Yanoff and Adam Schwartz for helping with the SEM maintenance. I wish Brian and our newest member, Joe Hilliard, good luck in the future as they continue working on other aspects of the pairing state symmetry problem.

Outside of my research group, I would like to acknowledge many of the faculty and fellow students at Illinois for stimulating and helpful conversations, particularly Tony Leggett, David Pines, Laura Greene, Alwyn Eades, Don Ginsberg, John

Giapintzakis, Ioan Kosztin, and Mark Covington. The MRL support staff made life much easier for me, particularly Ray Strange in the Microfabrication Lab, Carroll and Liz in the Storeroom, and Roxanne, Ramona, and Susan in the MRL offices. I would especially like to thank Irena Dumlar for all of her help with electron microscopy and maintaining our SEM.

Words cannot express my appreciation and love for my best friend (and wife) Susan. She had an essential role in the writing of this thesis, helping me to set high standards and achieve them, all while taking care of our two wonderful kids, Thomas and Sarah. I would also like to thank my parents for their constant love and support.

At the end of this list of acknowledgements but first in my heart, I thank God, from whom all blessings flow. But by His grace, I would not even exist, let alone have the opportunity to study His glorious creation. I also acknowledge the love and support of Jesus Christ, who has always watched over me in the past as my personal Savior, and will continue to do so always.

This work was supported by you (or more specifically, your taxes) through the National Science Foundation and the Frederick Seitz Materials Research Laboratory under grant NSF DMR 89-20538, and by the NSF Science and Technology Center for Superconductivity under grant NSF DMR 91-20000. I gratefully acknowledge receiving a National Science Foundation (NSF) Graduate Research Fellowship from August, 1990 to August, 1993. I also acknowledge extensive use of the facilities of the MRL Microfabrication Laboratory.

TABLE OF CONTENTS

Chapter Page

1. INTRODUCTION. 1

2. STRUCTURE AND PHYSICAL PROPERTIES OF THE CUPRATES. 5

Structure. 5
Physical properties. 9
Normal state properties. 9
Superconducting state properties. 13

3. PROPOSED THEORIES OF THE CUPRATES. 21

4. SYMMETRY OF THE SUPERCONDUCTING PAIRING STATE. 34

Predicted symmetries. 35
Experimental determination of symmetry. 46

5. EXPERIMENTAL TECHNIQUES. 54

Crystal growth. 54
Junction fabrication. 58
Measurement setup. 63

6. DC SQUIDS: EXPERIMENTAL RESULTS AND ANALYSIS. 71

7. JOSEPHSON JUNCTIONS:
EXPERIMENTAL RESULTS AND ANALYSIS. 88

8. OTHER PHASE-SENSITIVE EXPERIMENTS. 103

9. UNFINISHED BUSINESS. 112

Other cuprates. 113
Non-orthogonal angle measurements. 117
c-axis tunneling. 120

10. CONCLUSION. 130

REFERENCES. 135

VITA. 146

Chapter 1

INTRODUCTION

The discovery of the high temperature cuprate superconductors (Bednorz and Muller, 1986) has sparked much interest and activity in the scientific community over the last ten years. These superconducting ceramics have many anomalous properties both in the normal and superconducting states and have provided immense challenges to experimentalists and theorists.

Although a microscopic theory of superconductivity in the cuprates has not been constructed, much progress has been made in the understanding of the cuprates. That is not to say that any theoretical consensus has been reached, although the antiferromagnetic spin fluctuation scenario of David Pines and others has gathered considerable support recently. Experiments, meanwhile, have been converging, as the availability of high-quality samples in the past few years has allowed accurate measurement of the intrinsic physical properties of the cuprates.

The situation is similar to that just before the Bardeen-Cooper-Schrieffer (BCS) theory of superconductivity was introduced. For nearly a half century after the discovery of superconductivity in mercury by Kammerlingh Onnes in 1911, superconductivity remained unexplained, despite the efforts of many distinguished physicists. Several phenomenological theories were advanced to explain aspects of superconductivity, including London theory, the two-fluid model, Pippard's coherence length, and Ginzburg-Landau theory.

Experimentally, the important facts were already known. The Meissner effect showed that the lowest free energy state of a superconductor occurs in the absence of a magnetic field. It was also known from measurements of the electronic heat capacity and electronic thermal conductivity that there was an energy gap in the excitation spectrum. This energy gap is of order $k_B T_c$ in magnitude, where k_B is Boltzmann's constant and T_c is the superconducting transition temperature. In addition, it was discovered that different isotopes of the same element have different transition temperatures.

The isotope effect eventually proved to be the key to a complete understanding of conventional superconductivity, as it revealed the important role played by electron-phonon coupling. Even with this knowledge, it was several years until the BCS theory was formulated in 1957. The BCS theory was based on an electron-electron attraction near the Fermi surface that resulted from a retarded electron-phonon interaction. The BCS theory was amazingly successful in explaining the observed experimental properties and predicting new ones. It provides the framework in which we try to explain pairing in all new superconducting materials. In fact, BCS theory has been extended to such diverse systems as neutron stars, helium-3, and strong-coupling superconductors.

The present challenge of the high temperature superconducting cuprates is to determine whether BCS pairing theory is applicable or whether some fundamentally new theory must be developed. One way to answer this question is to determine the symmetry of the superconducting order parameter in the cuprates. This would

provide insight into the microscopic origins of high temperature superconductivity, and significantly constrain proposed theories of superconductivity in these materials.

In this thesis I will present measurements of bimetallic Pb-Au-YBCO dc SQUIDs (Superconducting QUantum Interference Devices) and Josephson junctions that I believe provide an important clue to the origin of the pairing mechanism for high temperature superconductivity in the cuprates. We find that the superconducting order parameter in $YBa_2Cu_3O_{6.95}$ changes sign between orthogonal directions in momentum space, unlike the isotropic order parameter in conventional superconductors. The sign change and corresponding nodes are consistent with a $d_{x^2-y^2}$ pairing state symmetry.

I provide the following overview of this thesis. In Chapter 2, I begin with a discussion of the physical structure of the cuprate materials, followed by a brief review of experiments in the normal and superconducting states. The normal state of the cuprates is shown to deviate experimentally from a conventional Fermi liquid picture. Experimental evidence for an unconventional superconducting state is also reviewed.

This leads to a discussion in Chapter 3 of several proposed theories of both the normal and superconducting states. To differentiate experimentally between the competing theories, it is necessary to determine the symmetry of the superconducting state. In Chapter 4, I show that the most direct approach to determining the symmetry of the pairing state of the high temperature superconductors is to probe the spatial anisotropy of the relative phase of the order parameter. In contrast to magnitude measurements, the phase shows a clear distinction between the leading

candidate states: the anisotropic *s*-wave pairing state of Philip Anderson and others, the $d_{x^2-y^2}$ pairing state that is unambiguously predicted by the spin fluctuation scenario of David Pines and others, and the extended *s*-wave pairing state proposed by C.M. Varma and others.

In Chapter 5, the experimental techniques used to make the $YBa_2Cu_3O_{6.95}$ crystals and bimetallic dc SQUIDs are discussed, as well as other experimental details. In Chapters 6 and 7, I present measurements of the phase coherence of bimetallic dc SQUIDs and Josephson junctions that show very strong evidence for an intrinsic phase shift of π between orthogonal directions in $YBa_2Cu_3O_{6.95}$. The observed π phase shift is equivalent to a sign change in the order parameter and is consistent with a $d_{x^2-y^2}$ pairing state symmetry. A discussion of complicating factors and theoretical modeling is also provided.

After our initial SQUID experiment was reported, it sparked many subsequent experiments that confirmed and extended our measurements. These other phase-sensitive measurements are reviewed in Chapter 8. Our attempts to extend our phase shift measurements to other cuprate materials as well as to explain the observation of supercurrent in *c*-axis Pb-YBCO tunnel junctions are discussed in Chapter 9. Finally, I conclude with a few personal observations of life in the scientific spotlight.

Chapter 2

STRUCTURE AND PHYSICAL PROPERTIES OF THE CUPRATES

Structure. The unique physical properties of the high T_c cuprates are not altogether surprising, considering their structural complexity and variability. The unifying structural feature of all the cuprates is one or more CuO_2 planes, in which each copper atom is strongly bonded to four oxygen atoms in a square planar array. The CuO_2 planes can be stacked in a group with metal ions, such as yttrium or other rare earth elements, sandwiched between planes. The spacing of the planes in each stack is approximately 3.2 Å, and the stacks are separated from each other by a relatively thick layer of other atoms (such as La, Ba, Cu, Tl, Bi and O). This leads to a tetragonal or nearly tetragonal crystal structure with unit cell lattice parameters a, b, and c such that $a \sim b$ (in the CuO_2 plane) and $c << a, b$.

Since the stack of CuO_2 planes is responsible for electrical conduction and superconductivity, it is referred to as the conduction layer. The number of carriers in the planes is controlled by the chemistry and structure of the intervening layer, called the charge reservoir layer (Jorgensen, 1991 and references therein). The carriers are holes, except for a few cases such as the Nd_2CuO_4 family in which the carriers are electrons. By adding or removing oxygen or substituting a fraction of metal ions having different valences (for example, Ba^{2+} for La^{3+} in $La_{2-x}Ba_xCuO_4$) it is possible to continuously modify the hole concentration in the conduction layer.

As the hole concentration is varied, the magnetic and transport properties change dramatically. I refer the reader to Annett *et al.* (1990; to be published), Batlogg (1991), Kampf (1994), and Vijayaraghavan and Gupta (1995) for recent reviews of the physical properties of the cuprates. The undoped parent materials are anisotropic insulating antiferromagnets. As holes are added, the magnetic ordering becomes short-ranged and an insulator-superconductor transition occurs in the limit of low temperature. The maximum superconducting transition temperature in a given compound family occurs with roughly 0.15 - 0.2 holes per CuO_2 in the conduction layer (Batlogg, 1991). When overdoped, the materials are metallic with less unusual electrical properties. The close connection between magnetism and superconductivity leads naturally to theories based on the exchange of antiferromagnetic spin fluctuations which will be discussed in Chapter 3.

One of the best-characterized cuprate families is $YBa_2Cu_3O_{6+x}$ $(0 \leq x \leq 1)$, often referred to as YBCO or 1-2-3. High quality single crystals of YBCO have been grown and extensively studied. The crystal structure for the fully-oxygenated $YBa_2Cu_3O_7$ is shown in Figure 2.1, which is adapted from Jorgensen (1991). The unit cell consists of a conduction layer of two CuO_2 planes separated by an yttrium ion, and a charge reservoir layer composed of barium, oxygen and copper atoms.

Copper serves a dual role in this material. In addition to the CuO_2 planes, there are copper atoms in the charge reservoir that form one-dimensional copper-oxygen chains, oriented along the *b*-axis. These Cu-O chains are fully formed and ordered for $x = 1$, resulting in an orthorhombic structure. At an oxygen content

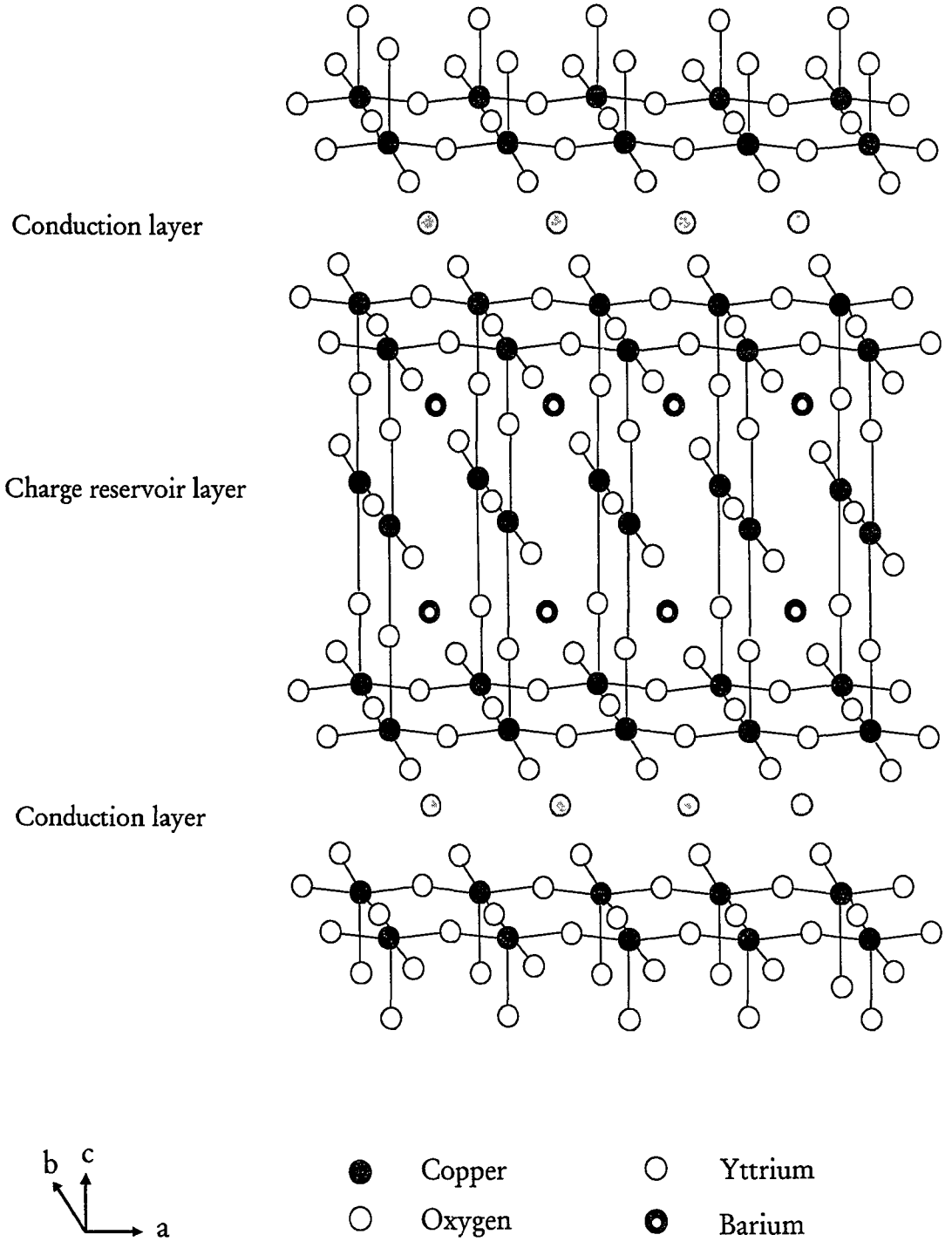

Figure 2.1. Structure of $YBa_2Cu_3O_7$ showing conduction and charge reservoir layers (adapted from Jorgensen, 1991).

x = 0 there are no chains and the structure is tetragonal. As shown in Figure 2.2 (adapted from Dagotto, 1994 and Burns, 1992), for x close to 0, $YBa_2Cu_3O_{6+x}$ is an antiferromagnet with a Néel temperature (T_N) of about 500 K. As x is increased, disordered CuO_x chains are formed. The structure changes to orthorhombic at a doping of x = 0.3 , where long-range antiferromagnetic ordering disappears, giving way to superconductivity. The optimal doping (that giving the highest superconducting

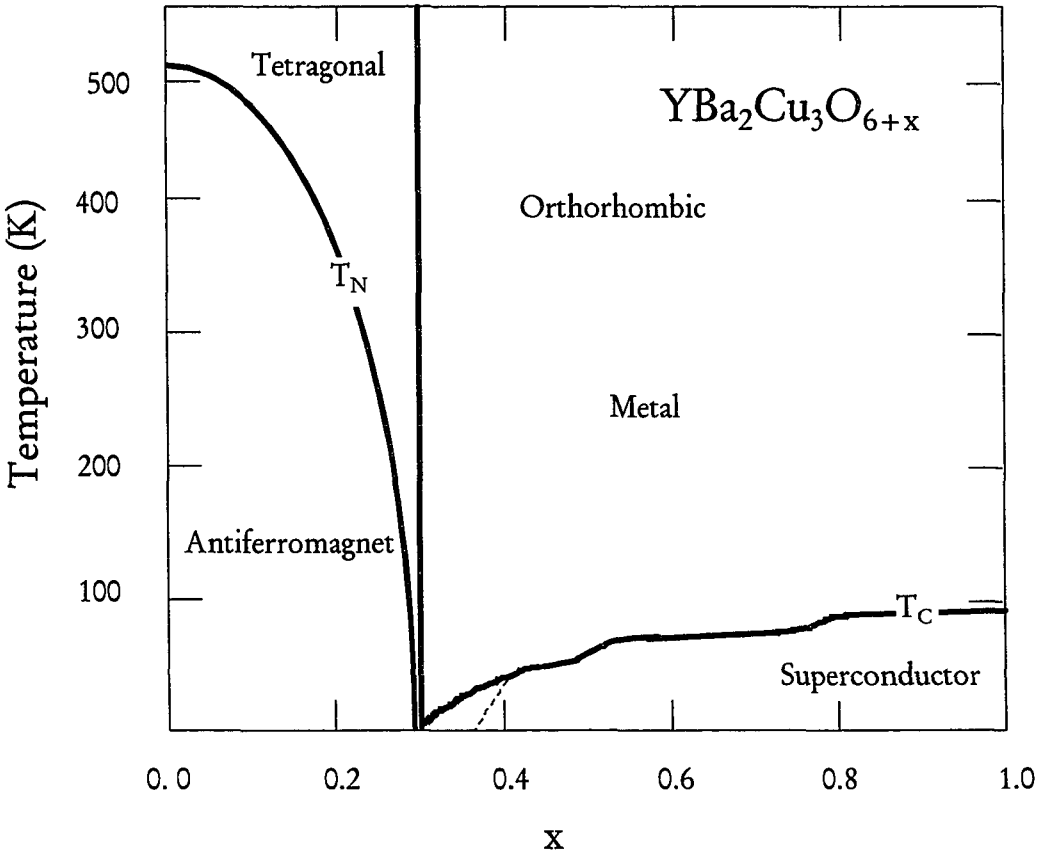

Figure 2.2. Phase diagram of $YBa_2Cu_3O_{6+x}$ (adapted from Dagotto, 1994 and Burns, 1992). The dotted line indicates that there may be a separation between the insulating and superconducting regions, as different methods of sample preparation (*e.g.*, Zr gettering and high temperature quenching) give different results.

transition temperature, $T_c = 93\,K$) occurs at approximately $x = 0.95$. The experiments described in this thesis have been done on optimally-doped YBCO.

Physical properties. Much effort has gone into determining the physical properties of the high T_c cuprates. This requires good experiments on good crystals. Many researchers focused on YBCO because it was possible to grow high-quality single crystals, as will be described in Chapter 5. Only within the last few years have we realized just how good the crystals must be to give us meaningful information about intrinsic physical properties, particularly at low temperatures.

Because of the anisotropy of YBCO, one must measure physical properties independently along both the *a*- and *b*-axes to separate the effects of the planes and chains. Twinning, an interchange of the *a*- and *b*-axes along a (110) twin plane that relieves stresses that occur during growth, makes these measurements difficult. Significant progress in crystal growth has led to the availability of untwinned single crystals of exceptional quality, allowing us to do the experiments described in this thesis.

Normal state properties. The transport properties of any conductor are determined by the electronic states near the Fermi energy. In a simple metal, there exists a Fermi surface which is nearly spherical. The Fermi surface is defined in momentum space as the set of points where the electronic state occupation drops sharply and the energy needed to create particle-hole excitations vanishes. Photoemission electron spectroscopy experiments done on $Bi_2Sr_2CaCu_2O_8$ (Olson *et*

al., 1989; Mante *et al.*, 1990) agree with band theory calculations, confirming the presence of a Fermi surface in the cuprates. This implies that the normal state of the cuprates should be described as a band-metallic state instead of a doped Mott-insulator.

The major question that arises is whether the metallic state above T_c can be described using the standard Fermi liquid theory that works so well with conventional metals. This is a very controversial issue, with prominent theorists on both sides. In the remainder of this section, I will show that the cuprates deviate experimentally from a simple Fermi liquid picture, leaving a discussion of theoretical ramifications to the next chapter.

The first property that we will examine is electrical transport in the cuprates. The electrical properties are very anisotropic, reflecting the crystal structure. For the extreme case of $Bi_2Sr_2CaCu_2O_8$, the electrical resistivity in the *c*-axis direction, ρ_c, is roughly 10^5 larger than the resistivity in the plane, ρ_{ab}. The least anisotropic cuprate may be YBCO, for which ρ_c is only 50 times larger than ρ_{ab}. For most cuprates at low temperatures, ρ_c is semiconducting in character (decreasing upon heating) while ρ_{ab} is metallic (increasing upon heating). The in-plane resistivity per CuO_2 plane is similar in value across the cuprates, but the ratio (ρ_c/ρ_{ab}) depends on the composition of the charge reservoir layers and thus varies from one cuprate to the next.

Fermi liquid theory predicts that the resistivity should have a quadratic temperature dependence at low temperatures (which is usually masked by electron-

phonon scattering). For optimally-doped cuprates, $\rho_{ab}(T)$ is linear in temperature over a large temperature range with remarkably similar values of $\frac{d\rho}{dT} \sim 0.7 \frac{\mu\Omega\,cm}{K}$, evidence that the linear behavior is an intrinsic property of the optimally-doped cuprates (Martin *et al.*, 1988; Batlogg, 1991). The linear dependence of the resistivity is seen down to 10 K in $Bi_2Sr_2CuO_{6+x}$ (Martin *et al.*, 1990), showing that the onset of superconductivity at a high T_c does not hide (what would be) Fermi-liquid behavior at lower temperatures. The linear resistivity strongly suggests that the normal state of the cuprates is much different than that of conventional metals.

Another complication for a Fermi liquid description is the general absence of residual resistivity in $\rho_{ab}(T)$. The residual resistivity of (off-stoichiometric) dopant ions can be easily calculated and should be significant, but is missing in the cuprates (Anderson, 1992). Nor can any resistivity be attributed to conventional phonon scattering. Although phonons are clearly visible in infrared and Raman spectra, they do not have a significant effect on electronic properties (Anderson, 1992). Bonn *et al.* (1992; 1993) have measured the microwave surface impedance to obtain the inelastic scattering rate, $\frac{1}{\tau}$, which decreases linearly with temperature in the normal state, but is rapidly suppressed below T_c. This is an important result, as it implies that the dominant scattering process in the normal state is electronic in origin, and is suppressed below T_c with the opening of the superconducting gap in the excitation spectrum (Kampf, 1994).

The temperature dependence of the *c*-axis resistivity provides additional evidence against a simple Fermi liquid description of the cuprates. For most underdoped to optimum-doped cuprates, $\rho_c(T)$ increases with decreasing temperature at low temperatures. If not for superconductivity, the cuprates would apparently be excellent 2D conductors in the planes but insulating perpendicular to the planes (Ong, 1994). A possible exception is ρ_c in fully-oxygenated YBCO, which is metallic in character and only 50 times larger than ρ_{ab}. The high transition temperature prevents us from knowing if ρ_c would actually go insulating below T_c in the absence of superconductivity.

In a recent review, Ong (1994) critically examines two explanations within conventional theory for the behavior of ρ_c. The first is that the value of $\rho_c \sim 7\,\mathrm{m\Omega\,cm}$ in optimally-doped YBCO corresponds to the Mott minimum conductivity, which divides the *c*-axis conductivity into metallic and insulating behavior. In other cuprate families, the crossover from insulating to metallic behavior occurs at much larger values of ρ_c, implying that there is no universal Mott value for all cuprates and making this explanation doubtful. The second explanation that Ong considers involves Anderson localization along the *c*-axis but not in the planes. He concludes that this, too, is unlikely because the high dephasing rate in the planes destroys the phase memory necessary for localization before an electron can tunnel between planes.

Another anomalous property of the cuprates is the Hall effect, which involves the off-diagonal components of the conductivity tensor. In Fermi-liquid theory, the in-plane Hall resistivity, $\rho_{xy} = R_H B$, has very little temperature dependence (where B is the magnetic field perpendicular to the planes and R_H is the Hall coefficient). Measurements of the Hall effect in the cuprates are reviewed by Ong (1990). In YBCO, the charge carriers in the CuO_2 planes are hole-like and R_H is positive above T_c. Below T_c, R_H goes negative over a range of magnetic fields and temperatures in the mixed state. In addition, R_H shows a strong $\frac{1}{T}$ temperature dependence over a range that is inconsistent with simple Fermi-liquid theory. In ordinary metals, strong temperature dependences of R_H are only seen at temperatures much smaller than the Debye temperature, Θ_D. This is not the case experimentally, as $\Theta_D \sim 450\,K$ in YBCO. Thus the anomalous temperature dependence of R_H provides further evidence that the normal state of the cuprates cannot be described using simple Fermi-liquid theory.

Superconducting state properties. The basic building block of superconductivity is the pairing of charge carriers. This holds true in the cuprates, as was established shortly after their discovery. Early in 1987, Gough *et al.* (1987) showed that magnetic flux was quantized in a superconducting ring of YBCO in units of $\Phi_0 = (0.97 \pm 0.04)\frac{hc}{2e}$, consistent with an effective pair charge of $e^* = 2e$. This was further supported by the observation of Shapiro steps in the current-voltage (I - V)

characteristics of Josephson tunnel junctions. In addition, Andreev scattering experiments showed that the superconducting condensate is composed of pairs of electrons with opposite momentum and spin (Annett *et al.*, 1990 and references therein).

The anisotropic structure of the cuprates influences their superconducting properties. The coherence length ξ, a measure of the spatial extent of a superconducting pair, is very short and anisotropic compared to conventional superconductors. In YBCO (one of the least anisotropic cuprates), the zero temperature coherence lengths are $\xi_{ab}(0) \cong 15\,\text{Å}$ and $\xi_c(0) \cong 4\,\text{Å}$. The coherence length in the *c*-axis direction is smaller than the distance between groups of superconducting planes, implying that transport along the *c*-axis occurs via Josephson tunneling. In conventional superconductors (with coherence lengths of roughly 500 Å to 10,000 Å) there are many Cooper pairs that overlap in a coherence volume, allowing an accurate mean-field BCS description of the condensate. In the cuprates there is a low carrier density and only a few pairs per coherence volume, making mean-field approximations questionable (Dagotto, 1994).

The low carrier density prevents the cuprates from effectively shielding an external magnetic field, leading to a large penetration depth, λ. In YBCO at $T = 0\ \text{K}$, $\lambda_{ab}(0) = 1400\,\text{Å}$ and $\lambda_c(0) = 7000\,\text{Å}$ (reviewed in Annett *et al.*, 1990). Therefore, the cuprates are extreme Type II superconductors ($\frac{\lambda}{\xi} >> 1$), and are in the "clean" limit

since the electron mean free path (100 Å - 200 Å) is much longer than $\xi(T = 0)$ (Batlogg, 1991).

The short coherence length leads to a high upper critical field $H_{c2} \sim \frac{\Phi_0}{2\pi\xi^2}$, the highest field in which a type II superconductor remains superconducting. In YBCO, H_{c2} can reach nearly 1000 T (far beyond our direct measurement capabilities) with field applied perpendicular to the CuO_2 planes, and is potentially important for commercial applications. The lower critical field $H_{c1} \sim \frac{\Phi_0}{2\pi\lambda^2}$ of YBCO is small due to the large penetration depth, with $H_{c1} \approx 200 - 500\,G$ for magnetic field applied along the *c*-axis. This allows vortices (containing magnetic flux equal to a multiple of one flux quantum Φ_0) to be introduced at relatively low magnetic fields. Vortex dynamics significantly affect the transport properties, and are the focus of much research.

So far I have considered properties that, while significantly different than in conventional superconductors, do not suggest that superconductivity in the cuprates is unconventional. By unconventional, I mean that the superconducting pairing state has a lower symmetry than the point group symmetry of the crystal (Annett *et al.*, 1990). In the remainder of this chapter I will focus on experiments indicating that superconductivity in the cuprates cannot be described with the usual isotropic *s*-wave BCS-type pairing. Because high temperature superconductivity is such an active field, I will not be able to do an exhaustive review of experiments and instead refer the reader

to reviews by Annett *et al.* (1990; to be published) and the other articles referenced at the start of this chapter. I will concentrate on work done prior to our experiment, setting the stage for a discussion in the next chapter in which I will outline the predictions made for the symmetry of the superconducting gap based on different theories of the pairing mechanism in the cuprates.

One of the most remarkable features of conventional superconductors is the existence of an energy gap $\Delta(\mathbf{k}, T)$ for quasiparticle excitations, where $\mathbf{k}$ is the wavevector in momentum space and T is the temperature. The threshold energy needed to break a Cooper pair and create two quasiparticles is $2\Delta_{min}$, the minimum value of $2|\Delta(\mathbf{k}, T)|$ on the Fermi surface. In conventional superconductors $\Delta_{min}(T) > 0$, leading to an absence of low energy excitations at low temperatures where $kT << \Delta_{min}(T)$. The gap in conventional superconductors is very nearly isotropic in $\mathbf{k}$-space, such that $\Delta \approx \Delta_{min} \approx \Delta_{max}$. It is possible to observe a small anisotropy of the gap, however, because the gap possesses the full point group symmetry of the crystal.

The energy gap Δ is clearly evident in tunneling measurements into conventional superconductors. An exponentially-vanishing (at low temperatures) tunnel current is found for voltages $V < \frac{\Delta}{e}$, with a sharp increase in the conductance at $V = \frac{\Delta}{e}$. In the cuprates, there is strong evidence that the energy gap is not fully

formed even at low temperatures ($\Delta_{min} \cong 0$), as shown in many tunneling measurements that find a large sub-gap density of states even at zero voltage bias.

The maximum gap is very anisotropic in the cuprates. As reviewed in Annett *et al.* (1990) and Hirata and Asada (1991), tunneling into the *c*-axis direction leads to a gap of $\frac{2\Delta}{k_B T_c} \sim 3.5$, in contrast to tunneling into the *a-b* plane direction, in which the gap ($\frac{2\Delta}{k_B T_c} \sim 6$) is much larger. Coffey (1993) has reviewed a considerable number of tunneling experiments and finds evidence for features at 2Δ in superconductor-insulator-normal metal (S-I-N) junctions and 3Δ in superconductor-insulator-superconductor (S-I-S) junctions, as well as dip features in angle-resolved photoemission spectroscopy (ARPES) data, that are consistent with predictions for a unconventional *d*-wave superconductor.

In an unconventional superconductor, symmetry considerations often require that $\Delta_{min} = 0$. If a real (not complex) gap changes sign as a function of $\mathbf{k}$, there are necessarily nodes where $\Delta(\mathbf{k}) = 0$ and thus $\Delta_{min} = 0$. Depending on the particular symmetry and the Fermi surface, the gap can have point, line and surface nodes. The presence of nodes allows there to be low energy excitations even at low temperatures, leading to power law temperature dependences in measured quantities instead of exponential temperature dependences. Unfortunately, it is experimentally difficult to measure Δ_{min} with enough resolution to establish the presence of a true node, as opposed to a large gap anisotropy. In addition, impurities can mask the intrinsic

properties of the cuprates, making it difficult to determine the symmetry of the gap from measurements of the magnitude alone.

One of the most sensitive measurements of the anisotropic gap is the measurement of the temperature dependence of the penetration depth, $\lambda(T)$. Early experiments claimed that the temperature dependence was exponential, consistent with isotropic s-wave pairing. Upon closer examination by Annett *et al.* (1990) the measurements were shown to have a power law temperature dependence, indicating that the gap was anisotropic. Using high-quality single crystals of YBCO, Hardy *et al.* (1993) carefully measured the change in penetration depth, $\Delta\lambda(T) = \lambda(T) - \lambda(0)$, using a superconducting microwave resonator. They found that $\Delta\lambda(T)$ was linear in temperature from 3 K to 25 K, implying a very anisotropic gap with line nodes and a Δ_{min} that was at most 2% of the full gap (Hardy *et al.*, 1993). By deliberately introducing impurities, they recovered the T^2 dependence seen in lesser-quality crystals and thin films and predicted for dirty d-wave superconductors (Hirschfeld and Goldenfeld, 1993). Thus a linear penetration depth is a key indication of sample quality, and the experiments in this thesis have been done on equivalent high-quality crystals.

Measurements of the nuclear relaxation rate, $\frac{1}{T_1(T)}$, in YBCO by Nuclear Magnetic Resonance (NMR) (reviewed by Slichter, 1994) had provided earlier evidence for $\Delta_{min} = 0$. If $\Delta_{min} > 0$ (as in conventional superconductors), at low temperatures the nuclear relaxation rate has an exponential temperature dependence

$\frac{1}{T_1(T)} \sim \exp\left(\frac{-\Delta_{min}}{k_B T}\right)$ that is not observed experimentally in the cuprates. If the gap has nodes on the Fermi surface with $\Delta_{min} = 0$, then $\frac{1}{T_1(T)}$ follows a power law temperature dependence of $\frac{1}{T_1(T)} \sim T, T^3, T^5$ for surface, line or point nodes, respectively (Annett *et al.*, 1990). The observed power law dependence for the cuprates is T^3, evidence for a superconducting gap with line nodes (Imai *et al.*, 1988; Annett *et al.*, 1990).

NMR measurements (reviewed in Slichter, 1994) of $\frac{1}{T_1(T)}$ also show the absence of a Hebel-Slichter coherence peak. In conventional superconductors there is a rapid rise in $\frac{1}{T_1(T)}$ just below T_c, due to coherence effects and the build-up of the density of states near the Fermi level just as the gap opens up. The explanation of the Hebel-Slichter peak was one of the greatest successes of the BCS model, and its absence in the cuprates is another possible indication of unconventional pairing.

Other experiments are also consistent with an excess of low energy excitations and have been interpreted as supporting an energy gap with line nodes. Raman scattering experiments (as reviewed in Annett *et al.*, 1990) do not show a minimum gap and have been found to be in experimental agreement with predictions of pairing in a *d*-wave symmetric state with line nodes (Devereaux *et al.*, 1994). Measurements of the low temperature specific heat (reviewed in Annett *et al.*, 1990) show a linear

temperature dependence and not the exponential dependence expected for isotropic *s*-wave superconductors. In addition, Yu. *et al.* (1992) found a large enhancement of the thermal conductivity in an untwinned single crystal of YBCO in the superconducting state, which they interpreted as resulting from a strong suppression of the quasiparticle scattering rate by spin fluctuations in an unconventional *d*-wave superconductor. More recently, Moler *et al.* (1994) have measured the electronic specific heat of high-quality YBCO single crystals in a magnetic field. They found a field-dependent linear term signifying a density of states $N \propto \sqrt{\left(\frac{H}{H_{c2}}\right)}$, in agreement with the prediction of Volovik (1993) for a *d*-wave symmetric pairing state with line nodes in the gap.

There are also direct experimental measurements of the angular momentum dependence of the gap. Using angle-resolved photoemission spectroscopy (ARPES), Shen *et al.* (1993) found the gap in $Bi_2Sr_2CaCu_2O_8$ (BSCCO) to be four-fold symmetric with a maximum value of 18 ± 1 meV in the k_x and k_y directions and 1 ± 1 meV along the diagonal $k_x^2 = k_y^2$. The angular dependence of the gap in YBCO has recently been probed by Yu *et al.* (1995) through a measurement of the field-dependent off-diagonal elements of the thermal conductivity tensor. They found that Andreev scattering of quasiparticles by screening currents caused heat flow normal to an applied temperature gradient, and could be explained with a *d*-wave symmetric gap function having nodes near $\langle 110 \rangle$.

Chapter 3

PROPOSED THEORIES OF THE CUPRATES

There have been a multitude of theories advanced to explain high T_c superconductivity. It would be impossible to provide even a cursory description of all of them, so I will limit this discussion to a short list of leading theories, while still trying to get some representation of the wide variety of theoretical approaches. One convenient way to categorize these theories is whether they start from Fermi liquid theory or not.

In Fermi liquid theory, a one-to-one correspondence is established between the excitations of a free electron gas and the excitations of interacting conduction electrons in metal. A quasiparticle is a low-energy elementary excitation of a Fermi liquid with all the properties of a real electron, but with a modified velocity, mass, and other properties. Quasiparticles incorporate all of the high-energy effects of the interaction, and quasiparticle motions are the only low-frequency electronic excitations. Therefore, all low-frequency dynamic properties of a Fermi liquid show universal behavior for energies and temperatures much less than the Fermi energy. This is in contrast to the cuprates, which deviate experimentally from the expected Fermi liquid universal behavior in the normal state.

The question of Fermi liquid or non-Fermi liquid behavior is partially motivated by the two-dimensional character of the CuO_2 planes that are the unifying structural feature of the cuprates. In three dimensions, Fermi liquid theory is quite

successful in describing the normal state properties of conventional metals. Superconductivity is understood as an instability to pairing within a Fermi liquid as described in the BCS theory of superconductivity. In one dimension, however, it is well known that Fermi liquid theory breaks down and a suitable description of low energy excitations for short-range repulsive interactions is that of a Luttinger liquid. Whether the same breakdown of Fermi liquid theory occurs in the two-dimensional CuO_2 planes of the cuprates is not yet known, and will prove to be crucial in understanding both the normal and superconducting states of the cuprates.

In the previous chapter, I outlined how the cuprates deviate experimentally from a conventional Fermi liquid picture. Whether some modification of Fermi liquid theory can be successfully applied to two-dimensional systems with strong electronic correlations is still a very controversial question. The theoretical starting point (Fermi liquid or non-Fermi liquid) provides a convenient way to differentiate between the different theories, as is clearly demonstrated by quoting from a dialogue between two prominent theorists, Philip Anderson and Robert Schrieffer, that was published in *Physics Today* in 1991. Although this article is a few years old, it still accurately reflects the essential ingredients of the proposed theories of Anderson and Schrieffer. In their own words, Anderson has focused "on a non-Fermi-liquid normal state with separate spin and charge excitations, and deconfinement by interlayer Josephson tunneling as the driving force for superconductivity," while Schrieffer has examined "the interplay between antiferromagnetism and superconductivity, extending the pairing theory

beyond the Fermi liquid regime in terms of spin polarons or 'bags' (Anderson and Schrieffer, 1991)."

I will begin with the "exotic" non-Fermi liquid approach of Philip Anderson and colleagues. In Anderson's theory of the cuprates, there still exists a well-defined Fermi surface for neutral, spin $\frac{1}{2}$ fermions called "spinons." Anderson points out that a Fermi surface can exist in a non-Fermi liquid, as demonstrated in one-dimensional Luttinger liquid models (Anderson, 1992). Since spinons do not carry charge, "holons" that are charged and spinless were proposed to accompany the spinons. Thus, in Anderson's theory, the charge and spin of a bare hole are separated into spinons and holons, two independent elementary excitations. The interaction between spinons and holons is weak and they are not bound together, and the two excitations can have different Fermi velocities as well as different statistics.

In normal Fermi liquid metals, a hole quasiparticle with a definite energy is created when an electron is removed. In Anderson's theory, removing an electron creates at least one spinon excitation and one holon excitation as well as many soft collective excitations. The resulting spectrum has a cusp at the spinon energy which Anderson argues is consistent with angle-resolved photoemission experiments (Anderson and Schrieffer, 1991; Anderson, 1994a).

In Anderson's model, transport current is only weakly scattered by charge fluctuations (such as phonons or impurities) because transport involves a collective displacement of the entire spinon Fermi surface, while spin impurities cause residual resistivity (Anderson and Schrieffer, 1991). In addition, there is "confinement" of the

proposed Luttinger liquid in the two-dimensional CuO_2 planes (Anderson, 1991; Clarke *et al.*, 1995). There is no coherent transport along the *c*-axis, because only real electrons can move coherently from plane to plane, and they break up incoherently into spinons and holons. Confinement increases the kinetic energy in the planes and drives the high T_c of the cuprates. Pairs of electrons can tunnel coherently between planes beginning at a temperature $T_c \propto \frac{t_\perp^2}{J}$, where $t_\perp$ is the interlayer matrix element and J is the width of the spinon energy band (Anderson and Schrieffer, 1991; Chakravarty *et al.*, 1993). There is a crossover from two- to three-dimensional behavior at T_c.

Anderson believes that the mechanism for superconductivity is not the main problem to be solved, but that the mechanism will follow easily once the normal metal above T_c is understood. In addition, Anderson believes that the correct theoretical model to describe the cuprates is the one-band Hubbard model (Anderson and Schrieffer, 1991). Only the antibonding band formed by hybridization of the Cu $d_{x^2-y^2}$ orbitals and the O $2p_\sigma$ orbitals is important for low energy properties (on an energy scale of ~ 1 eV), with the degree of hybridization controlled by charge and spin polarization effects upon doping (Anderson, 1992). The interaction between electrons is repulsive, with a Hubbard gap, U, between states having two holes and one hole per Cu site.

In contrast to Anderson, Schrieffer is not ready to totally abandon Fermi liquid theory. He points out that the BCS pairing theory can be generalized beyond simple

Fermi liquid theory, as evidenced by the ability to systematically include the strong damping of normal-state excitations in strong-coupling superconductors (Anderson and Schrieffer, 1991). Therefore, he believes that it is possible for some field theoretic approach to succeed in describing high T_c superconductivity.

In the *Physics Today* article (Anderson and Schrieffer, 1991) mentioned above, Schrieffer provided a excellent summary of his research efforts, which have focused on whether spin bags are the dominant elementary excitations in the single-band Hubbard model. A spin bag has a charge +e and spin 1/2 but is surrounded by a region of decreased spin order and spin twist, forming a "bag" that moves with the hole. The attraction between spin bags comes from the lower exchange energy needed to make a shared bag as opposed to two separate bags. This attraction only occurs for momentum transfer q smaller than the inverse bag size (about 2-3 lattice spacings), while the interaction is repulsive for larger q (Schrieffer, 1992).

Another theory of the cuprates describes the normal state of the cuprates as a marginal Fermi liquid, as proposed by Varma *et al.* (1989). In their phenomenological model, they assume that the spectral function for spin and charge fluctuations has an anomalous frequency dependence, such that the imaginary part of the spin susceptibility is proportional to $\frac{\omega}{T}$ for $\omega << T$ but equal to a constant for $T << \omega << \omega_c$, where ω_c is a cutoff frequency. With this spin spectrum, marginal Fermi liquid theory can account for many of the anomalous normal state properties of the cuprates, including the linear temperature dependence of the resistivity, thermal

conductivity, and optical conductivity in optimally doped cuprates, as well as the crossover to ordinary Fermi liquid behavior that is seen in overdoped cuprates (Varma, 1995a; Sire, 1994 and references therein). In this model, superconductivity results from an interaction based on charge transfer fluctuations. As will be discussed in the next chapter, the pairing state is predicted to have an extended s-wave symmetry, in which the gap function may or may not have nodes on the Fermi surface.

A different approach has been taken by David Pines and others in their development of a phenomenological theory of the normal and superconducting states of the cuprates. Instead of following a "top-down" approach in which a particular Hamiltonian is selected and then studied, Pines elected to begin with a "bottom-up" phenomenological description of the anomalous low frequency magnetic behavior (Pines, 1995 and references therein). NMR experiments showed that there are strong temperature-dependent antiferromagnetic correlations between the nearly localized Cu^{2+} spins in the planes, and that these correlations are present into the superconducting state (experiments reviewed by Slichter, 1994). This led Millis, Monien, and Pines (MMP, 1990) to propose a phenomenological low frequency spin-spin correlation function peaked for wavevectors near (π,π) in momentum space.

This magnetic interaction scenario led to a description of the normal state as a nearly antiferromagnetic Fermi liquid, with a magnetic interaction between quasiparticles providing the pairing interaction for superconductivity at high transition temperatures (Pines, 1991 and references therein). In addition, the peaking of the effective interaction at (π,π) leads uniquely to a superconducting pairing state with

$d_{x^2-y^2}$ symmetry (Pines, 1995 and references therein). The precise meaning and experimental ramifications of $d_{x^2-y^2}$ pairing symmetry will be explained in the next chapter.

The $d_{x^2-y^2}$ pairing state symmetry was first suggested for the cuprates by Scalapino and co-workers (Bickers *et al.*, 1989) based on calculations of the exchange of antiferromagnetic spin fluctuations in a Hubbard model. At that time, they concluded that the mechanism could not produce transition temperatures as high as 90 K. Weak coupling calculations carried out independently in Tokyo (Moriya *et al.*, 1990) and Urbana (Monthoux, Balatsky and Pines, 1992, hereafter MBP) showed that high transition temperatures were possible and that the superconducting pairing state symmetry was $d_{x^2-y^2}$. MBP showed that quantitative results could be obtained only by including the full structure of the interaction, and that calculations (such as those done by the Tokyo group) which "put everything on the Fermi surface" led to misleading results. Strong-coupling calculations showed that quasiparticle lifetime effects suppressed T_c but that high transition temperatures could still be obtained (Monthoux and Pines, 1993, 1994; Ueda *et al.*, 1992). In addition, lifetime effects caused by scattering from non-magnetic impurities (which can result in significant pair-breaking effects in a *d*-wave superconductor) were shown to be smaller than the lifetime effects already included in the strong-coupling calculations.

The antiferromagnetic spin-fluctuation model successfully explains the linear dependence of the planar resistivity on temperature, optical properties, and the high

transition temperatures using the same spin-fluctuation spectrum and coupling constants. The maximum gap is predicted to be quite large ($\frac{2\Delta(0)}{k_B T_c} \sim 10$) and to open up rapidly below T_c (Pines, 1994a and references therein). Because a $d_{x^2-y^2}$ symmetric pairing state contains nodes (along the 45° direction), it naturally explains the following experiments which were discussed in Chapter 2 and are listed below: linear dependence of penetration depth on temperature, NMR relaxation rates, Raman scattering, and angle resolved photoemission. The absence of a Hebel-Slichter peak can also be explained with a $d_{x^2-y^2}$ symmetric pairing state (Scalapino, 1995 and references therein). Several groups (Barzykin and Pines *et al.* (1994); Maki and Wan (1994); and Quinlan and Scalapino (1995)) have recently begun to obtain agreement between $d_{x^2-y^2}$ pairing theory and neutron scattering experiments for the underdoped cuprates.

The spin-fluctuation model has also been used to explain the effects of impurities on superconducting properties, particularly the substitution of Zn and Ni for planar Cu atoms in YBCO. Monthoux and Pines (1994) found that the effect of impurities on T_c in a *d*-wave superconductor to be $\frac{\Delta T_c}{T_c} \sim 9 n_i$ in the unitary limit, where n_i is the percent concentration of the impurity. In the *d*-wave pairing state, Zn impurities have a larger effect on both T_c (with $\frac{\Delta T_c}{T_c} \sim 12.6 n_{Zn}$ seen experimentally) and NMR measurements of $^{63}T_1(T)$ because Zn is non-magnetic (closed-shell

electronic configuration), destroys the local magnetic order in the planes, and thus alters the spin fluctuation spectrum (Pines, 1994 and references therein). This is in contrast to the much smaller effect of Ni substitution, which does not affect measurements of $^{63}T_1(T)$ and changes T_c by only one-third as much as Zn (Pines, 1994 and references therein). Ni is magnetic and acts as a sub-unitary potential scatterer as it does not affect the local magnetic order. The influence of impurities on resistivity and T_c has also been calculated by Radtke *et al.* (1993a) using Eliashberg theory.

Pines (1994a) has argued that the experimental difference between Zn and Ni substitution is a "smoking gun" that provides strong support for the spin-fluctuation mechanism and a $d_{x^2-y^2}$ pairing state. Furthermore, the suppression of T_c by Zn provides evidence against Anderson's interlayer coupling mechanism, as pointed out by Lance Cooper (referenced in Pines and Monthoux, 1995). Zn substitution in YBCO has only a minor effect on the *c*-axis resistivity and optical properties and thus does not reduce the strength of interlayer coupling even though T_c is substantially reduced. In addition, Pines argues that charge and spin are not separated in the normal state, as required for Anderson's theory. This can be seen by the opening up of a temperature-dependent pseudo-gap in the spin spectrum (observed in NMR measurements) that is accompanied by changes in the resistivity in underdoped cuprates (Pines, 1994a).

There are also important differences between the antiferromagnetic spin fluctuation theory and both Schrieffer's spin fluctuation theory and the marginal Fermi liquid theory. Schrieffer believes that the coupling between the quasiparticles and spin fluctuations is so strong that the normal state excitations are spin bags. Schrieffer and co-workers then focus on second order spin fluctuation exchange terms to obtain *s*-wave superconductivity, while Pines uses the first order term to get *d*-wave pairing (Pines, 1991). In the marginal Fermi liquid theory, the momentum dependence of the spin spectrum is assumed to be smooth, unlike the spin spectrum in the antiferromagnetic Fermi liquid theory.

Another exotic theory that has been advanced to explain high T_c superconductivity is "anyon superconductivity." Anyons are fractionally charged particles that were originally proposed by Robert Laughlin (1986) in the context of the fractional quantum Hall effect. An exchange of anyons results in a phase factor $e^{i\theta}$, with θ not limited to the usual $\theta = 0$ (bosons) or $\theta = \pi$ (fermions), but instead able to take on any value. For the cuprates, Laughlin has argued that $\theta = \frac{\pi}{2}$ and that the pairing state breaks time-reversal symmetry.

Another proposed explanation is that high T_c superconductivity results from conventional electron-phonon coupling, despite early calculations that found the maximum T_c for a phonon mechanism to be of order 40 K, far below the high T_c's of the cuprates (Schrieffer, 1992). A strong isotope effect is the classic indication of the importance of the electron-phonon interaction for superconductivity. Experimentally,

the isotope effect is very small for optimally doped cuprates and has been taken as evidence against a phonon-based mechanism for superconductivity. The lack of an isotope effect does not immediately rule out phonon-based superconductivity, however, as the isotope effect can be very small or have the opposite sign for strong-coupling BCS superconductors.

There is experimental evidence that phonons are modified in the superconducting state. This is found in differential conductance curves ($\frac{dI}{dV}(V)$) of superconductor-normal metal tunnel junctions, which contain structure at energies that can be related to phonon modes. Below the transition temperature, some of these phonon modes soften (move to lower energies), other phonon modes harden (move to higher energies), and some are unaffected (Yagil *et al.*, 1995 and references therein). Thus, the electron-phonon interaction in the cuprates is very selective, unlike that in conventional BCS superconductors. The structure in the tunneling data is also too strong to be explained with the ordinary electron-phonon interaction, but this could imply that additional excitations are coupled to the phonons (Yagil *et al.*, 1995). Although a phonon-based mechanism has not been ruled out entirely, it is unlikely to explain high T_c superconductivity in the cuprates. That general opinion has not dissuaded theorists such as Richard Klemm (1994) from questioning all anomalous experimental results, including our own, and attempting to explain them using conventional theory.

Alexandrov and Mott (1993, and references therein) believe that the cuprates can be described as a charged Bose-liquid of bipolarons. Using a microscopic Hamiltonian, they arrive at the same ground state as the phenomenological model of preformed local pairs (Ogg, R. A., Jr, 1946; and Schafroth, M. R., 1955). In the local pair model, electron pairs with short coherence lengths (on the order of $\xi \sim a$) are formed above T_c. A subsequent Bose-Einstein condensation (at T_c) then leads to superconductivity. In the theory of Alexandrov and Mott (1993, and references therein), the local pairs are composed of bipolarons (bosons with charge 2e and spin 0 or 1). The formation of mobile bipolarons (two electrons plus accompanying lattice polarization) reduces the large kinetic energy of the electrons in the two-dimensional CuO_2 planes. Alexandrov and Mott (1993, and references therein) claim to explain many of the unusual and characteristic normal state properties of the cuprates with their charged bipolarons (which are different from Schrieffer's spin polarons). Polarons involve lattice polarizations and thus phonons, and the same arguments against a phonon mechanism for superconductivity also apply to this theory.

The final theories that I want to consider are based on van Hove singularities. Van Hove singularities occur at cusps in the electronic (or phonon) density of states (DOS) where the slope $\frac{d(DOS)}{dE}$ diverges, and can lead to anomalies in low temperature properties. In agreement with band structure calculations, angle-resolved photoemission experiments on several cuprates (for example, Dessau *et al.*, 1993) show the existence of a saddle point close to the Fermi energy in the cuprates, corresponding

to a weak (logarithmic) van Hove singularity. The proposed theories (Tsuei *et al.*, 1990; Markiewicz, 1990; Newns *et al.*, 1991; Radtke *et al.*, 1993b) focus on whether the close proximity of the Fermi surface to the van Hove singularity can explain the enhanced T_c and other anomalous properties of the cuprates. Recently, Dagotto *et al.* (1995) proposed a theory in which the antiferromagnetic spin fluctuation (AF) scenario is combined with the van Hove singularity (vH) scenario. In this AFvH model, both the pairing mechanism and the van Hove singularity are caused by antiferromagnetic correlations. Like the antiferromagnetic spin fluctuation theory, the AFvH model predicts a $d_{x^2-y^2}$ pairing state symmetry. In addition, the AFvH model shows that an optimal doping exists at which T_c is maximized (as is experimentally observed), and that at this optimal doping the quasiparticle lifetime is linear with energy.

Chapter 4

SYMMETRY OF THE SUPERCONDUCTING PAIRING STATE

In the previous chapter, I described in general some (but certainly not all) of the theories that have been proposed for the cuprates. The large number and variety of theories give some indication of the immense effort that has gone into understanding the cuprates, as well as the complexity of the materials in question. Part of the initial confusion was due to a large amount of conflicting and sometimes misleading initial experimental data. Experimentalists repeated the standard measurements and analyzed the results using the BCS theory of superconductivity. As discrepancies with the standard theory were uncovered, experimentalists discovered the importance of materials issues in the cuprates. Only with the availability of exceptionally pure materials have we been able to accurately measure intrinsic physical properties, as described in Chapter 2.

During this time, many theorists focused on understanding only a small subset of the experimental data, without attempting to show comprehensive agreement with all experiments. Historically, successful theories have not only explained all known experimental results, but have also provided a deeper understanding that allows new experiments to be proposed. Unfortunately, this insight has been lacking in many of the proposed theories of the cuprates.

Some theories have progressed to the point where definite predictions could be made and tested. One of the first such predictions was the assertion of David Pines

and co-workers (Monthoux *et al.*, 1992) that the superconducting pairing state must have $d_{x^2-y^2}$ symmetry if superconductivity results from the exchange of antiferromagnetic spin fluctuations. This challenge to the experimental community attracted much attention, as it provided a specific theoretical prediction that could be experimentally tested. We will now examine the predictions for the symmetry of the pairing state for many of the theories described in the previous chapter, and then consider how the pairing state symmetry can be experimentally determined.

Predicted symmetries. First of all, it is necessary to define what is meant when a pairing state is said to have a certain symmetry (e.g., $d_{x^2-y^2}$ symmetry). Specifically, we want to determine the symmetry of the Cooper pair wave function, which can be written as the product of a relative coordinate wave function $\varphi(x_1 - x_2)$ and a spin function (following the discussion and notation of Scalapino, 1995). At this point, we can simplify matters by noting that measurements of the Knight shift (Barrett *et al.*, 1991) not only rule out spin triplet pairing ($S = 1$), but also imply that the pairs are spin singlet ($S = 0$) (Annett *et al.*, 1990). For spin singlet pairing, the simplest allowed orbital symmetries of $\varphi(x_1 - x_2)$ are *s*-wave ($L = 0$) and *d*-wave ($L = 2$).

In momentum space, $\varphi(x_1 - x_2)$ can be expanded as $\varphi(x_1 - x_2) = \sum_k \varphi_k e^{i\mathbf{k}\cdot(\mathbf{x}_1 - \mathbf{x}_2)}$ where the φ_k's are basis functions of the irreducible representations of the symmetry group of the crystal. A detailed catalogue of the possible symmetries for the cuprates is found in Annett *et al.* (1990). It is common to

discuss the symmetry classification of the cuprates in terms of a tetragonal lattice (D_{4h} symmetry), even though some of the cuprates (e.g. YBCO) have a slight orthorhombic distortion (D_{2h} symmetry) that removes some of the allowed symmetry operations. For D_{4h} symmetry, there are five even parity (corresponding to spin singlet) irreducible representations that are listed in Table I (taken from Scalapino, 1995). Several of these symmetries have been proposed to be the symmetry of the pairing state, as will be discussed below. For example, the pair wave function is said to have extended *s*-wave symmetry if $\varphi_k \sim (\cos(k_x a) + \cos(k_y a))$, and $d_{x^2-y^2}$ symmetry if $\varphi_k \sim (\cos(k_x a) - \cos(k_y a))$.

Irreducible representation	Symmetry	Basis function examples
Γ_1^+	extended *s*-wave	$1,\ \cos(k_x a) + \cos(k_y a)$
Γ_2^+		$\sin(k_x a)\sin(k_y a)(\cos(k_x a) - \cos(k_y a))$
Γ_3^+	$d_{x^2-y^2}$	$\cos(k_x a) - \cos(k_y a)$
Γ_4^+	d_{xy}	$\sin(k_x a)\sin(k_y a)$
Γ_5^+		$\sin(k_x a)\sin(k_z a),\ \sin(k_y a)\sin(k_z a)$

Table I. Even parity irreducible representations of D_{4h} (from Scalapino, 1995)

In a tetragonal structure, we can define a generalized *s*-wave or *d*-wave symmetry based on in-plane rotations about the *c*-axis. The pairing state has *d*-wave symmetry if it changes sign under a rotation of $\frac{\pi}{2}$, and *s*-wave symmetry if it does not. In an orthorhombic structure, this classification breaks down as linear combinations of *s*-wave and *d*-wave states are allowed by symmetry, although there will exist states of

predominantly *s*-wave or *d*-wave character if the orthorhombic distortion is small. This is particularly useful since superconductivity arises from the nearly square CuO_2 planes.

One of the remarkable aspects of superconductivity is that a single wavefunction, with a magnitude and phase, can describe the superconducting condensate formed by the Cooper pairs. In the absence of current flow, all of the pairs in the superconductor have the same phase, a property called macroscopic phase coherence. We will use this phase coherence to experimentally determine the symmetry of the pair wave function through the symmetry of the superconducting order parameter or gap, Δ_k. In BCS theory, the two are directly related by $\varphi_k = \frac{\Delta_k}{E_k}$, where $E_k = \sqrt{(\varepsilon_k^2 + \Delta_k^2)}$ and $\Delta_k = -\sum_{k'} \frac{V_{kk'}\Delta_{k'}}{2E_{k'}}$, with $V_{kk'}$ being the effective interaction (Scalapino, 1995). The physical picture is that the quasiparticles (mixtures of electron and hole states) interact with the pair condensate, leading to an energy gap, Δ_k, in the quasiparticle excitation spectrum that reflects the symmetry of the pair wave function.

The energy gap is experimentally accessible, and measurements of the gap provide a key experimental insight into the mechanism of superconductivity. As the gap is directly related to the pair wave function, it is also described by a complex number with a magnitude and phase, and is principally responsible for many superconducting properties. Before describing our measurements of the relative phase

of the gap in YBCO, I will first discuss the predictions for the gap symmetry made by some of the leading theories described in the last chapter.

Anderson, Chakravarty and colleagues (Chakravarty *et al.*, 1993) have proposed an anisotropic *s*-wave pairing state based on their interlayer tunneling mechanism. Interlayer pairing mixes an *s*-wave pair function with higher angular momentum states, leading to a gap that is suppressed in magnitude along the 45° diagonals but remains positive and finite. The anisotropic *s*-wave gap has the mathematical form

$$[\text{anisotropic } s\text{-wave}] \quad \Delta(\mathbf{k}) = \Delta_0[\cos(k_x a) - \cos(k_y a)]^4 + \Delta_1 ,$$

where Δ_1 is the minimum value of the gap. The gap is real and does not change sign, and the phase of the gap is constant.

In the marginal Fermi liquid of Varma and others, charge-transfer fluctuations provide the attraction necessary for superconductivity (Varma, 1995a and references therein). The large inter-electronic repulsion on the Cu sites implies that the pair wavefunction amplitude on the Cu ions must be zero (Varma, preprint, 1995b). This can be written as $\psi(r = 0) = \sum_{\sigma} \langle c_{\sigma}(0) c_{-\sigma}(0) \rangle = 0$, and after Fourier transformation $\sum_{\mathbf{k}} \psi(\mathbf{k}) = \sum_{\sigma} \langle c_{\sigma}(\mathbf{k}) c_{-\sigma}(-\mathbf{k}) \rangle = 0$. Therefore, the pair wavefunction must be both positive and negative for different parts of the Brillouin zone, vanishing at lines or points in between regions (Varma, preprint, 1995b). The gap function $\Delta(\mathbf{k}) = \psi(\mathbf{k}) E(\mathbf{k})$ has nodes where the pair wavefunction does, but Varma (preprint, 1995b) stresses that it is not necessary for $\sum_{\mathbf{k}} \Delta(\mathbf{k}) = 0$, as in $d_{x^2-y^2}$ pairing. In

addition, the Fermi surface may or may not intersect the surface where $\Delta(\mathbf{k}) = 0$ (Varma, 1995a) and thus the gap may or may not have nodes, depending on the particular cuprate material in question. The symmetry of Varma's proposed gap function is extended *s*-wave (actually $s + g$ in strict symmetry terms, where *g* is a state with angular momentum $L = 4$), and the corresponding mathematical form of the gap function (not normalized) in *k*-space is

$$[\text{extended } s\text{-wave}] \quad \Delta(\mathbf{k}) = \Delta_0\{(1+\gamma^2)[\cos(k_x a) - \cos(k_y a)]^2 - \gamma^2\}.$$

This describes a gap with eight lobes of alternating sign and eight nodes split by approximately $\pm\gamma\frac{\pi}{2}$ from the (110) or 45° direction. A similar gap is also predicted for the valence-fluctuation theory of Baird Brandow (1993).

As mentioned in the previous chapter, superconductivity based on the exchange of antiferromagnetic spin fluctuations in Pines' magnetic scenario leads uniquely to a pairing state with $d_{x^2-y^2}$ symmetry. The proposed gap function for this pairing state is

$$[d_{x^2-y^2}] \quad \Delta(\mathbf{k}) = \Delta_0(\cos(k_x a) - \cos(k_y a)).$$

The $d_{x^2-y^2}$ gap has four lobes that are assumed to align with the *a*- and *b*-axes of the crystal as seen in angle-resolved photoemission experiments. The lobes alternate in sign, with four nodes in the (110) or 45° directions. The sign change of the gap between orthogonal directions is equivalent to a relative phase change of π, because $-1 = e^{i\pi}$. The gap takes the form of the difference of two cosine terms due to the

Fermi surface having the shape of a square. Another term that has been used to describe this symmetry is $k_x^2 - k_y^2$ symmetry, which can be shown to be equivalent by expanding the cosines in the gap function. In the limit of small k_x and k_y, the gap function becomes $\Delta(\mathbf{k}) \propto [(1 - k_x^2 a^2) - (1 - k_y^2 a^2)] \propto k_x^2 - k_y^2$.

It is instructive to provide a physical basis for $d_{x^2-y^2}$ pairing based on a configuration space description, following Pines (1995). Consider the spin-fluctuation interaction between quasiparticles that are almost localized on a 2D lattice. There is a large on-site Coulomb repulsion and the interaction at the four nearest-neighbor sites is attractive. The interaction at neighbor sites at progressively greater distances weakens while alternating between attraction and repulsion, with the interaction always being repulsive along the 45° diagonals where $x^2 = y^2$. Electrons can pair if they can spatially arrange themselves in a $d_{x^2-y^2}$ orbit (with angular momentum $L = 2$) to avoid the Coulomb interaction at the origin, while taking advantage of the attraction at the four nearest neighbors. The $d_{x^2-y^2}$ pairing state is favored over other d-wave states (e.g., the d_{xy} state) because the $d_{x^2-y^2}$ state naturally avoids the net repulsion of the interaction along the 45° diagonals, with the nodes of its gap function located there.

In the $d_{x^2-y^2}$ pairing state, the gap changes sign as a function of momentum. This can be understood by examining the BCS gap equation, $\Delta_k = -\sum_{k'} \frac{V_{kk'}\Delta_{k'}}{2E_{k'}}$,

where k and k' are both near the Fermi surface. Since the spin-fluctuation-based interaction $V_{kk'}$ is positive and large for large momentum transfers, the only way to take advantage of this is for the gap, Δ_k, to change sign as a function of k.

It is also useful to compare the spin-fluctuation interaction mechanism with the conventional electron-phonon interaction responsible for BCS superconductivity. Following a discussion by Scalapino (1995), the effective pairing interaction for conventional superconductors can be written as the sum of an attractive phonon exchange interaction and a repulsive screened Coulomb interaction. The Coulomb term is dominant, making the effective interaction repulsive. A examination of the interaction in time, however, reveals that the Coulomb interaction is limited to short times, while the attractive electron-phonon interaction is retarded by the slower lattice response. To take advantage of the attractive interaction, the electrons in the Cooper pairs must be correlated in time to avoid the short-time Coulomb repulsion. In this way the time average of the effective pairing interaction is attractive. The time correlations can be clearly seen in the frequency dependence of the gap, in which $\mathrm{Re}\,\Delta(\omega)$ changes sign and goes negative at the typical phonon energy, ω_0. Similarly, the sign change of the $d_{x^2-y^2}$ gap as a function of direction in momentum space shows that the pairing state is avoiding the repulsive part of a net attractive interaction in configuration space.

Complex mixture symmetry states are also allowed by symmetry and have been proposed. The $s+id$ state was suggested by Kotliar (1988) to appear at low

temperatures in a theory based on Anderson's resonating-valence-bond mechanism. The gap for this state can be written as

$$[s+id] \quad \Delta(\mathbf{k}) = \Delta_0\{\varepsilon + i(1-\varepsilon)[\cos(k_x a) - \cos(k_y a)]\},$$

where ε depends on the relative strength of the *s* and *d* components. Based on his anyon superconductivity theory, Laughlin and others (Rokhsar, 1993; Beasley *et al.*, 1994) have argued that the symmetry is $d_{x^2-y^2} + i\,\varepsilon\, d_{xy}$, where ε in this case is a small parameter. For this state, the gap takes the mathematical form

$$[d+id] \quad \Delta(\mathbf{k}) = \Delta_0\{(1-\varepsilon)[\cos(k_x a) - \cos(k_y a)] + i\varepsilon[2\sin(k_x a)\sin(k_y a)]\}.$$

Because the order parameter is complex, these mixture states break time-reversal symmetry and have double transition temperatures, both of which have not been observed experimentally.

To differentiate between the proposed theories, the symmetry of the superconducting gap must be experimentally determined by measuring the gap as a function of momentum space direction. As the gap $\Delta(\mathbf{k})$ is a complex number, experiments can probe its symmetry by measuring its magnitude or its phase. Most experiments are sensitive only to the magnitude of the gap, and only a few techniques (for example, angle-resolved photoemission) can directly probe the momentum dependence of the gap magnitude. These measurements were discussed in Chapter 2, and show that the magnitude of the gap is very anisotropic and has a four-fold rotational symmetry. The minimum gap is located along the (110) or 45° direction (the node direction in a $d_{x^2-y^2}$ symmetry) and is less than 20% of the maximum gap

value (located along the *a*- and *b*-axis directions). Some measurements, such as the linear dependence of the penetration depth on temperature, suggest that the minimum gap is $\Delta_{min} = 0$ to a few percent uncertainty. Unfortunately, this is not enough to unambiguously establish the presence of true nodes (as predicted by $d_{x^2-y^2}$ symmetry) as opposed to a large suppression of the gap but without nodes (as predicted by anisotropic *s*-wave pairing), and so other measurements are needed to distinguish between the proposed theories.

By plotting the magnitude and phase of the gap for the leading candidate states described above, it is easy to see that measurements of the relative phase provide a much clearer distinction between proposed theories, as shown in Figure 4.1. The relative phase of the gap is defined with respect to $\theta = 0$, where θ specifies the direction in momentum space and $\theta = 0$ corresponds to momentum along, e.g., the positive *a*-axis direction. The isotropic and anisotropic *s*-wave states are both real and positive, with a constant relative phase of zero. This is in contrast to the relative phase of the $d_{x^2-y^2}$ state, which has four discontinuous jumps of π at the (110) nodes ($\theta = 45°$, 135°, 225°, and 315°) where the gap changes sign. There are eight π-jumps in the relative phase of the extended *s*-wave state, which is invariant under a 90° rotation with the four largest magnitude lobes all having the same (positive) sign. The nodes in the extended *s*-wave state are split away from 45° by a variable amount that depends on the different cuprate materials. Finally, the relative phase varies continuously with angle for the two mixed symmetry states, the $s+id$ state and the $d+id$ state.

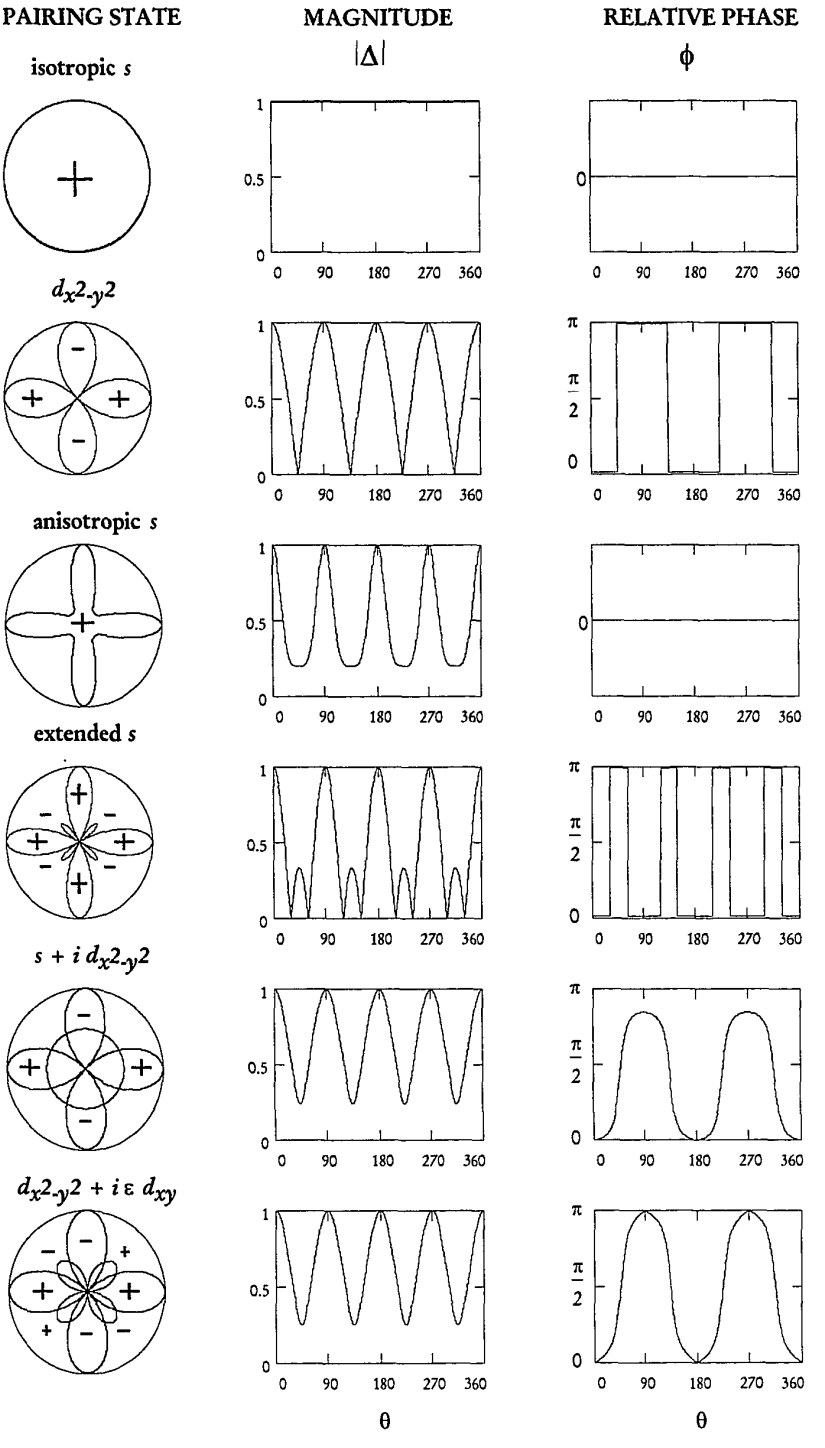

Figure 4.1. Magnitude and relative phase of the gap as a function of angle in momentum space for the primary pairing state symmetry candidates.

In general, it would be desirable to measure the relative phase between arbitrary angles in momentum space to completely map out the relative phase of the gap and thus determine its symmetry. The cuprates are ceramics and hard to cleave in desired directions, making a full mapping very difficult. On the other hand, single crystals of YBCO can be grown with flat growth faces and good corners, allowing us to probe the superconducting condensate along the *a*-axis and *b*-axis directions using Josephson tunnel junctions. By simply measuring the relative phase of the order parameter between these two directions (separated by $\Delta\theta = 90°$) it is possible to distinguish between many of the leading candidate pairing states described above.

The most likely pairing states are the anisotropic *s*-wave state, the extended *s*-wave state, and the $d_{x^2-y^2}$ state, based on the discussion above and in previous chapters. A measurement of the relative phase of the gap between the *a*-axis direction and the *b*-axis direction, δ_{ab}, immediately establishes whether or not the pairing state has $d_{x^2-y^2}$ symmetry. A gap with $d_{x^2-y^2}$ symmetry changes sign at a true node between these two directions, equivalent to a relative phase change of $\delta_{ab} = \pi$. This is in striking contrast to the relative phase change of $\delta_{ab} = 0$ that is predicted for both anisotropic *s*-wave and extended *s*-wave pairing, as well as the conventional isotropic *s*-wave pairing. For the $s+id$ mixture state with a fraction ε of *s*-wave component, the relative phase change is $\delta_{ab} = (1-\varepsilon)\pi$. For an equal mixture of *s* and *d* components, $\delta_{ab} = \frac{\pi}{2}$. Finally, a phase shift of $\delta_{ab} = \pi$ is expected for a $d+id$ pairing state, the

same as for $d_{x^2-y^2}$ symmetry, because the imaginary d_{xy} component has nodes along the *a* and *b* directions.

Experimental determination of symmetry. Measurements of the relative phase δ_{ab} are possible using a dc SQUID as an interferometer to compare the phases in the orthogonal *a*-axis and *b*-axis directions. The basic experimental design is shown in Figure 4.2, in which Josephson tunnel junctions are fabricated on the orthogonal *a*- and *b*-faces of a single crystal of YBCO and connected by a loop of a conventional *s*-wave superconductor, Pb, to form a bimetallic ring. The resulting device is a two-junction interferometer, or dc SQUID, in which the dependence of the electrical properties on magnetic flux is used to measure the relative phase δ_{ab}, an intrinsic phase shift between pairs tunneling into the YBCO crystal in the *a*-axis and *b*-axis directions. The basic idea for these measurements was suggested to us by A. J. Leggett (private communication, 1992), based on a test for axial *p*-wave symmetry in the heavy-fermion superconductors proposed by Geshkenbein, Larkin, and Barone (1987). Sigrist and Rice (1992) independently proposed the same scheme in an explanation of the paramagnetic Meissner effect (a description of this experiment can be found in Chapter 8) based on *d*-wave pairing.

Most SQUIDs are used as ultra-sensitive, nearly quantum-limited detectors in real-life applications to measure magnetic flux, current, or voltage. In this thesis, however, the dc SQUID will be used as self-measuring sample to obtain the relative phase of the superconducting gap between orthogonal directions in YBCO, δ_{ab}.

SQUIDs have been extensively studied for many years, and are ideal macroscopic systems for testing fundamental properties of quantum mechanics. As an introduction to SQUIDs for the non-expert, I recommend a popular article in *Scientific American* by John Clarke (1994).

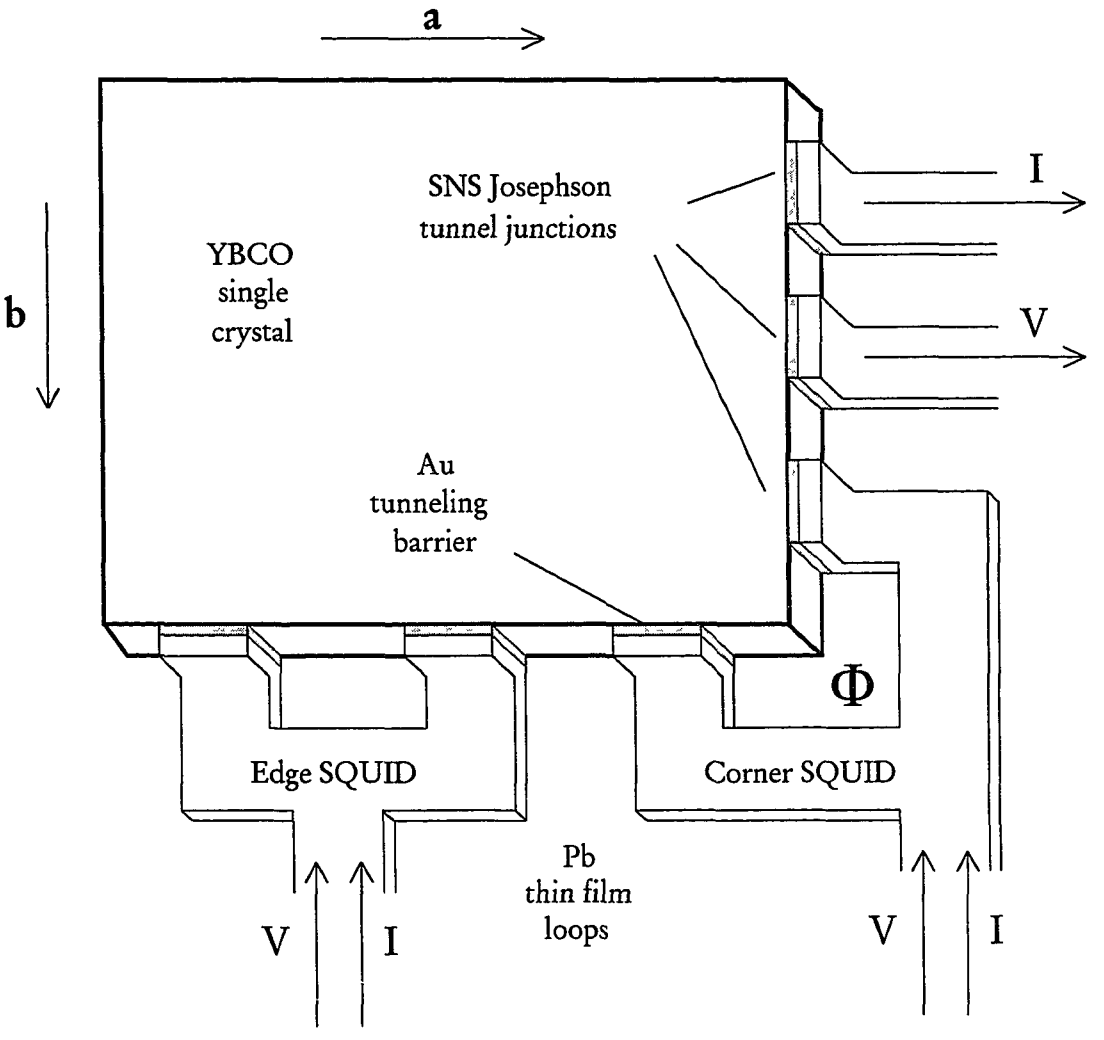

Figure 4.2. Design of the SQUID experiments. The corner SQUID interferometer is used to determine the relative phase between orthogonal directions. The edge SQUID is used as a control sample, in which both junctions are on the same crystal face. Additional single junctions are used as current and voltage (I, V) leads.

There are two key properties of a dc SQUID that are essential to the successful determination of the symmetry of the pairing state in YBCO. The first involves the ability to probe directionally the phase of the superconducting condensate using Josephson junctions. The supercurrent in a single Josephson junction is given by $I = I_c \sin(\phi)$, where ϕ is the gauge-invariant phase difference between the two superconductors and I_c is the critical current, the maximum supercurrent that can be supported by the junction. Since the tunneling probability in a Josephson tunnel junction depends exponentially on the barrier thickness and is strongly peaked for wavevectors perpendicular to the face of the junction, the Josephson supercurrent in the individual junctions on the orthogonal *a* and *b* faces samples the phase of the YBCO gap in the direction orthogonal to that junction. Leggett (private communication, 1993) has shown that the argument for the directionality of pair tunneling is also valid for other Josephson weak links, such as the SNS (superconductor-normal metal-superconductor) or SNIS (superconductor-normal metal-insulator-superconductor) junctions we have used in these experiments.

The second key property is that a dc SQUID is an interferometer that can be used to compare the phases of the YBCO gap in orthogonal directions. This property comes from the multiply connected geometry of a dc SQUID, in which two Josephson junctions are connected in parallel to form a loop. The phase coherence of the superconducting order parameter must be maintained around the loop in order for the superconducting condensate wave function to be single valued. This makes the dc

SQUID sensitive to any intrinsic phase shifts inside the superconducting materials that may result from the symmetry of the pairing state.

The ability to measure intrinsic phase shifts can be seen by examining the equations for a dc SQUID with junction critical currents I_{ca} and I_{cb}. When the SQUID is in the supercurrent state, an applied bias current I is divided between the two junctions such that

$$I = I_{ca} \sin(\phi_a) + I_{cb} \sin(\phi_b),$$

where ϕ_a and ϕ_b are the gauge-invariant phase differences across the junctions on the *a* and *b* faces of the YBCO crystal. Phase coherence and flux quantization force the constraint

$$\phi_a - \phi_b + 2\pi \frac{\Phi}{\Phi_0} + \delta_{ab} = 0$$

on ϕ_a and ϕ_b. Here, $\Phi = \Phi_{ext} + L\,J$ is the magnetic flux (product of magnetic field and area) in the loop, and is the sum of an externally-applied flux Φ_{ext} and the flux from a net circulating current J around the SQUID loop, which has self-inductance L. The extra term δ_{ab} is the predicted intrinsic phase shift inside the YBCO crystal between pairs tunneling into the crystal in the *a* and *b* directions. There is no corresponding intrinsic phase shift for the other half of the SQUID loop, which is made from the conventional *s*-wave superconductor, Pb. Using a bimetallic dc SQUID makes it possible to experimentally determine δ_{ab} in YBCO, the primary focus of this thesis.

A magnetic field applied to the dc SQUID changes the quantum-mechanical phase differences across each of the two junctions, which in turn affects the critical current that the SQUID is able to support. A progressive increase or decrease of the magnetic flux through the SQUID causes the critical current to modulate between a maximum and minimum value with a periodicity of one flux quantum, Φ_0. For the special case of zero loop inductance and a symmetric dc SQUID, with equal critical currents $I_{ca} = I_{cb} = I_0$, the critical current modulates with applied flux from a maximum of $2I_0$ to a minimum of zero, according to

$$I_c(\Phi_{ext}) = 2I_0\left|\cos(\pi \frac{\Phi_{ext}}{\Phi_0} + \delta_{ab})\right|.$$

Including the SQUID self-inductance through finite values of the screening parameter $\beta = \frac{2I_0 L}{\Phi_0} = \frac{I_c L}{\Phi_0}$ leads to the introduction of circulating currents around the SQUID, which generate a flux contribution $L J$ and reduce the modulation depth of the critical current. For large β, $\frac{\Delta I_c}{I_c} \sim \frac{1}{\beta}$.

The two principal cases for a corner SQUID geometry are shown in Figure 4.3. If the YBCO has *s*-wave symmetry (isotropic, anisotropic, or extended), the phase of the YBCO order parameter is the same at each junction, so that $\delta_{ab} = 0$ and the circuit will behave as an ordinary dc SQUID. In particular, this means that the critical current is a maximum at zero applied field, with no circulating current. For $d_{x^2-y^2}$ symmetry, $\delta_{ab} = \pi$ and the junctions start out of phase at zero flux, forcing a

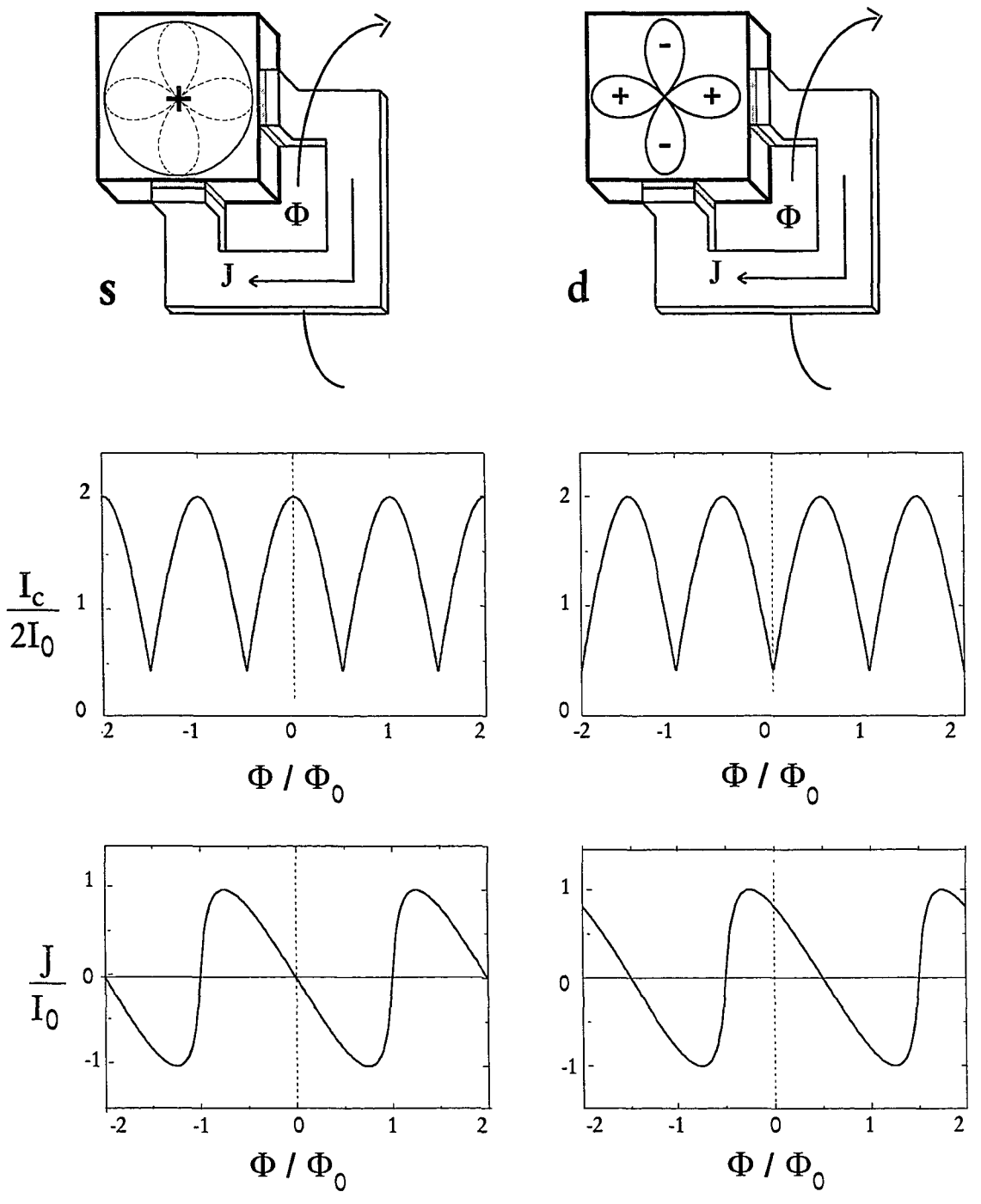

Figure 4.3. Modulation of the critical current and circulating supercurrent *vs.* applied magnetic flux for corner SQUIDs with *s*-wave and *d*-wave symmetry.

circulating current to be established (at zero applied flux) to maintain phase coherence around the SQUID loop, assuming that the SQUID inductance L is sufficiently large. The circulating current produces an amount of flux equal to $\frac{1}{2}\Phi_0$ to compensate for the intrinsic π phase shift inside the YBCO crystal. This circulating current shifts the modulation pattern of critical current vs. applied flux as shown in Figure 4.3, such that the critical current for a corner SQUID has a minimum at zero applied flux instead of the usual maximum. In the case of an edge SQUID, for any of the possible pairing states, $\delta_{aa} = 0$ and no phase shift would be observed. Edge SQUIDs thus serve as control samples for this experiment.

By measuring the flux modulation of the bimetallic SQUID, we can obtain δ_{ab} and deduce the symmetry of the pairing state of the YBCO sample. The beauty of this experiment is that it depends only on the relative phases of the order parameter and is not sensitive to the type, size, or critical currents of the junctions.

The experimental challenge is therefore clear: fabricate and measure a bimetallic dc SQUID in which the two orthogonal *a*- and *b*-faces of the single crystal of YBCO are connected by a conventional *s*-wave superconductor, Pb. The next chapter describes the growth of the single crystals of YBCO, the fabrication of the dc SQUIDs, and the experimental set-up used to measure the completed SQUIDs. In the following chapters, I present experimental data from Pb-Au-YBCO dc SQUIDs and Josephson junctions showing strong evidence for a relative phase change $\delta_{ab} = \pi$, equivalent to a sign change of the gap between orthogonal directions in YBCO. The sign change of

the gap is consistent with a $d_{x^2-y^2}$ pairing state symmetry, and is the primary result of this thesis.

Chapter 5

EXPERIMENTAL TECHNIQUES

Crystal growth. The YBCO crystals used in this thesis were grown in Don Ginsberg's laboratory using a flux-melt technique described in Joe Rice's thesis (1992) and the references therein. $BaCO_3$, CuO, and Y_2O_3 were mixed with Y, Ba, and Cu in a molar ratio of 1 : 4 : 10 and ground with an agate mortar and pestle. The resulting powder was put into an yttria-stabilized zirconia crucible. To allow a cavity for crystal growth to develop during heating, it was necessary to avoid packing the powder in the crucible. The crucible was heated in a box furnace to 980°C to melt the flux, and then was slowly cooled to 830°C. During cooling, stoichiometric single crystals of YBCO grow out from the flux into a cavity that is thought to be formed by released CO_2 in the flux. At room temperature, the crucible was crushed in a hydraulic press, cracking open the cavity. During this process, many YBCO crystals broke away from the flux and were easily harvested. Others were carefully removed from the flux with tweezers. The crystals grow in a characteristic platelet shape with dimensions as large as 2 x 2 x 0.05 mm, although most are much smaller. These as-grown crystals were placed on a pressed pellet of YBCO and oxygenated for about a week in a quartz tube furnace with flowing oxygen at 400°C.

After oxygenation, crystals were selected on the basis of size, sharp corners, flat growth faces, and twinning. I used crystals that were roughly 0.5 x 0.5 mm in the *a-b* plane with a thickness of 20 - 40 μm. YBCO crystals much thicker than 50 μm are generally lower in quality, and are often composed of different crystals that have

grown together with flux and other impurities trapped in the middle. I was usually able to place a total of five to six SQUIDs and junctions on the *a* and *b* faces of each crystal. Sharp 90° corners insure that only orthogonal directions are sampled in a corner SQUID or Josephson junction, and also help to minimize the SQUID inductance. Flat growth faces are necessary so that tunneling is directional and capable of probing the *k*-dependence of the order parameter. A SEM photograph of the corner of a YBCO crystal showing a sharp corner and flat growth faces is shown in Figure 5.1. Finally, I used both twinned and untwinned crystals with no difference in the phase shift measured, as will be discussed later.

Twinning is a ubiquitous defect related to the orthorhombic structure of fully-oxygenated YBCO, in which the in-plane lattice constants are a = 3.82Å and b=3.89Å, while the out-of-plane lattice constant is c=11.68Å. During the growth process, as the crystals cool through an "oxygenation window" from 675°C to 400°C, they take up oxygen and change structure from tetragonal to orthorhombic (Rice, 1992). The differential thermal contraction between the CuO-rich flux and YBCO crystals creates non-uniform stresses in the YBCO crystals. These stresses are relieved by twinning, in which the *a*- and *b*- axes interchange across a (110) twin plane that extends the entire way through thin crystals in the *c*-axis direction. Structurally, this disrupts the CuO chains that lie along the *b*-axis, but this disruption is minor compared to the disorder present in defects such as grain boundaries.

A crystal can have many alternating twin domains, where each domain is separated by a twin plane and has the opposite orientation of *a*- and *b*-axes. The typical

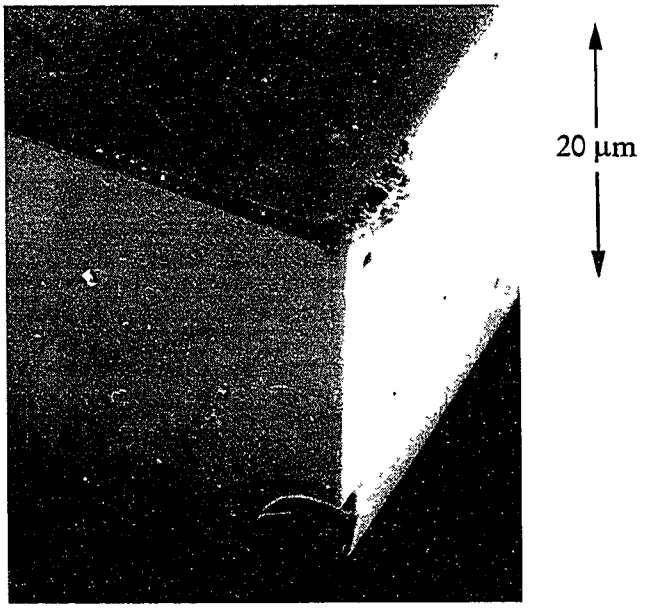

Figure 5.1. SEM photograph of a YBCO single crystal showing a sharp corner and flat natural growth faces.

Figure 5.2. Polarizing optical microscope photograph of a YBCO single crystal showing twin domains.

spacing of twin planes in a heavily twinned crystal is roughly 1000Å, but crystals can grow with much larger domains, up to the size of the crystal (Rice, 1992). It is possible to view twin domains using a polarizing optical microscope. By crossing the polarizer and analyzer with the polarizer oriented along the (110) direction, one can identify the different single domain regions by a change in color contrast (Rice, 1992). An example of a crystal with twin domains is shown in the optical microscope photograph of Figure 5.2. By comparing with a reference crystal that has been characterized by x-ray diffraction it is possible to determine the axes directions in a given domain, as indicated in the photograph. This allowed me to fabricate junctions on specific single domain regions of the crystal.

Twinning is undesirable for separating and measuring anisotropic properties such as the resistivity that differ in the *a* and *b* directions. As will be discussed in Chapter 6, tunneling is also a potential concern for the determination of the symmetry of the superconducting order parameter, and so both twinned and untwinned crystals were used in these experiments.

It is possible to obtain untwinned crystals by either thermomechanical detwinning or a special growth process. In the thermomechanical detwinning method, a twinned crystal is heated to 400°C and subjected to mechanical stress applied along one of the twinned *a/b*-axes to push the twins out of the sample. This method works best with thicker crystals that have been cleaved into the shape of a rectangle to uniformly apply stress. In the special growth method implemented by Joe Rice, the YBCO crystals are rapidly cooled to room temperature, quenching in the tetragonal phase. Then the crystals are harvested and annealed in flowing oxygen as described

above, but without any non-uniform stress. Therefore twins are less likely to form and the untwinned domains in a thin crystal will be correspondingly larger, and completely untwinned crystals have been grown using this method.

I have been fortunate to have had access to some of the best YBCO crystals in the world, as characterized by any method used to determine sample quality (for example, the width of the specific heat peak, normal state resistivity, linear penetration depth at low temperatures, and many others). The crystals have very few impurities as opposed to crystals grown in other groups with gold and alumina crucibles. I have received crystals from several crystal growers in Don Ginsberg's group; Joe Rice (at the start of the project), Wonchoon Lee, and John Giapintzakis. My appreciation for their efforts increased dramatically after making two batches of YBCO crystals myself, under the supervision of Regina Dudley. Although perfectly usable, my crystals were all heavily twinned. I relied on the 'professional' growers for large untwinned crystals as well as sample characterization. This includes such techniques as SQUID magnetometry, used to determine the onset and sharpness of the superconducting transition.

Junction fabrication. After selecting YBCO crystals based on the criteria outlined above, I flash-evaporated 1000Å - 2000Å of Au in stripes on the *a-c* and *b-c* faces of the crystal. The Au stripes were approximately 50 μm wide. This was done to control the current distribution in the completed junctions. At the start of the project, I had evaporated Au to cover the entire *a-c* and *b-c* faces, and only used a mask to define the Pb junctions and contacts. As a result, the junctions were shorted to each

other by the Au, and the current would move along the continuous Au layer to find the lowest resistance contact to the YBCO crystal. This did not necessarily occur at the junction being tested, and made it impossible to insure that the supercurrent was probing the correct directions in *k*-space. Limiting the Au to discrete stripes resolved this problem.

The YBCO crystals with the Au stripes were then annealed at 400°C in flowing oxygen for a few hours, typically 2-4 hours. This allowed the Au to diffuse a short distance into the 'dead region' at the surface of the crystal, presumably a region of oxygen-deficient YBCO. SIMS and Auger analysis revealed that Au diffused 1000Å in the *c*-axis direction and 8000Å laterally along the surface after annealing at 410°C for 12 hours (J.-T. Kim, private communication, 1995). Au diffuses faster in the *a-b* plane than along the *c*-axis, and so I estimate that the extent of the Au diffusion inside the crystal in the *a* and *b* directions to be at most a few thousand Angstroms, for the much shorter annealing time of 2-4 hours. The annealing step was necessary to lower the (otherwise large) contact resistance between the Au and YBCO, allowing the observation of supercurrent in the completed devices.

The problem then became connecting the Au stripes with a Pb loop to make a bimetallic Pb-Au-YBCO SQUID as well as to make electrical contacts to the device. Macroscopic contact pads (consisting of 20Å Cr, 1500Å Ag, and 500Å In) were fabricated on a glass slide using photolithography, a standard process that is described in the thesis of Ron Wakai (1987), a former Dale Van Harlingen (DVH) group member. The YBCO crystal must be held securely so that a thin film of Pb can be evaporated through a mechanical mask up onto its edges to make both the SQUID and

the connections to contact pads. Both requirements, holding the crystal without covering its edges and constructing a flexible mechanical mask for the Pb evaporation, proved to be much more difficult than I had imagined. In fact, my most important experimental contributions involved finding new ways to accomplish these goals, and will be described below.

Experimentalists use many adhesive materials to hold samples, such as 5-minute epoxy, Duco cement, rubber cement, and GE (General Electric) varnish. I tried a large assortment of the usual adhesives before I discovered polyamide (Dupont, Pyralin Polyimide P.I. 2555), a spin-on glass that is used in lithography. Polyamide is very viscous, dries slowly, and has very good low temperature properties. I placed a fairly large (1 mm diameter) thin circular drop of polyamide at the center of contact pads on a glass slide. The drop was prepared by loading the end of a capillary tube with a small amount of polyamide, dabbing it on a glass slide to remove excess liquid, and gently touching the glass slide.

The crucial step of this procedure involved placing the YBCO crystal in the polyamide at the right moment. The bottom face of the crystal must be held securely without allowing the polyamide to completely cover the Au on the *a*-*c* and *b*-*c* faces. To do this, it was necessary to monitor and control the viscosity of the drop using the heated stage and large-working-distance zoom microscope of a lead bonder (Hybond, model 572-17). The YBCO crystal was suspended (with the *c*-axis vertical) from the end of a flat syringe tip by means of a small vacuum pump (Air Cadet, model 7530-40, Cole-Parmer Instruments Co.) and rubber hose, and was moved into position above the drop by an x-y-z mechanical positioner. The polyamide was heated to 40°C using

the hot stage until it was sufficiently viscous to support the weight of the YBCO crystal, but not so long that the drop developed a skin that prevented adhesion. At the correct moment, the vacuum suspending the YBCO crystal was released. The crystal fell into position and partially submerged into the polyamide drop, leaving most of the *a-c* and *b-c* faces exposed. To cure the polyamide so that it would not crack at low temperatures, the crystal and polyamide were then heated in an oven for 30 minutes at 170°C.

Next came the equally difficult step of preparing a mask for the Pb evaporation to define the SQUIDs and junctions and connect to the contact pads. I first tried to use the same standard photolithographic techniques that were used to make the contact pads. This was unfeasible since standard photolithography works with a flat mask in contact with a flat substrate, while the YBCO crystal had significant thickness and was sitting on a three-dimensional drop of polyamide above the contact pads.

I then tried projection lithography, in which the image of a mask is focused (demagnified) onto the sample using the optics of an ordinary microscope. In this method there is no contact between the mask and sample, but the three dimensional nature of the problem still made it unworkable. The photoresist (Shipley, AZ 1350J) did not spin onto the sample with a uniform thickness, but instead was thicker near the edges of the YBCO crystal. The thickness variation made it difficult to expose the photoresist uniformly and obtain the sharp profile needed to lift-off the Pb after evaporation to make a completed device. In addition, I found that at least 6000Å - 7000Å of Pb were needed to ensure that the Pb was continuous from the polyamide up

onto the edges of the YBCO crystal. This large thickness of Pb made any lithography-based fabrication impractical.

An alternative to lithography was to use a mechanical mask to define the Pb junctions. In the standard technique, the desired pattern is cut out of a rigid metal foil. However, this type of mechanical mask could not be pressed up against both the YBCO crystal and contact pads on the glass slide without leaving a gap next to the crystal. Evaporated metal would not be well defined and would feather out, connecting to other devices, particularly when the evaporation is at an angle to metalize the vertical *a-c* and *b-c* faces of the YBCO crystal.

To solve this problem, I developed a flexible mechanical mask made of a roll-on resist (Dupont, Riston 4615). Riston is a green, flexible material about 100 μm thick and is usually used in lithography when a very thick photoresist layer is needed. The plastic films that surround the green material must be peeled away before it can be stretched out on a glass slide. Looking through a zoom microscope and using a clean razor blade, I carefully cut small thin strips of the roll-on resist and placed them against the YBCO crystal to shield those regions during evaporation. The strips were usually 30 - 100 μm in width and a millimeter long. I picked up the strips using old STM (Scanning Tunneling Microscope) tips attached to the end of a pencil vise. By padding my hands and wrists, I was able to place the strips with an accuracy of 10 μm or less (using the zoom microscope), fixing one end of the strip before laying the rest into position. Thus, I could define the areas to be coated with Pb to make SQUIDs and junctions as well as the connections to the contact pads. I pushed the flexible strips up

against the edges of the crystal to avoid the large separations that cause feathering during evaporation.

The Pb evaporation was done with a Commonwealth Scientific ion mill evaporator. The glass slide with the crystal, mask, and contact pads was placed on a water-cooled sample stage using vacuum grease. The stage could be continuously rotated to face either the ion mill or the boats holding the metal for evaporation. Ion milling (500 V beam voltage, 100 V accelerator voltage, and beam current of 80 mA) was used to clean and thin the Au layer. The Pb (or Pb-In) was evaporated at a 30°-40° angle at a rate of 30Å/sec to a final thickness of almost 1 μm. The flexible mask and the angled evaporation allowed me to make the junctions on the vertical edges of the YBCO crystal. A photograph of a sample with the flexible mask, taken after the Pb evaporation, is shown in Figure 5.3.

The flexible mechanical mask was removed after the evaporation was completed, as shown in Figure 5.4. Occasionally a piece of the roll-on resist would shift during evaporation and allow the Pb lines to overlap, but this could be fixed by carefully scraping the unwanted Pb with a STM tip. The large contact pads were connected to twisted Cu wire pairs by first pressing a small piece of In to bond to the contact pad, then sandwiching the Cu wire (tinned with solder) with another In pad to hold it securely as well as to make electrical contact. Each device had at least two independent connections to the contact pads, as shown in Figure 5.5.

Measurement setup. Because SQUIDs are so sensitive, our measurements required careful attention to shielding. All measurements were performed in a rf-

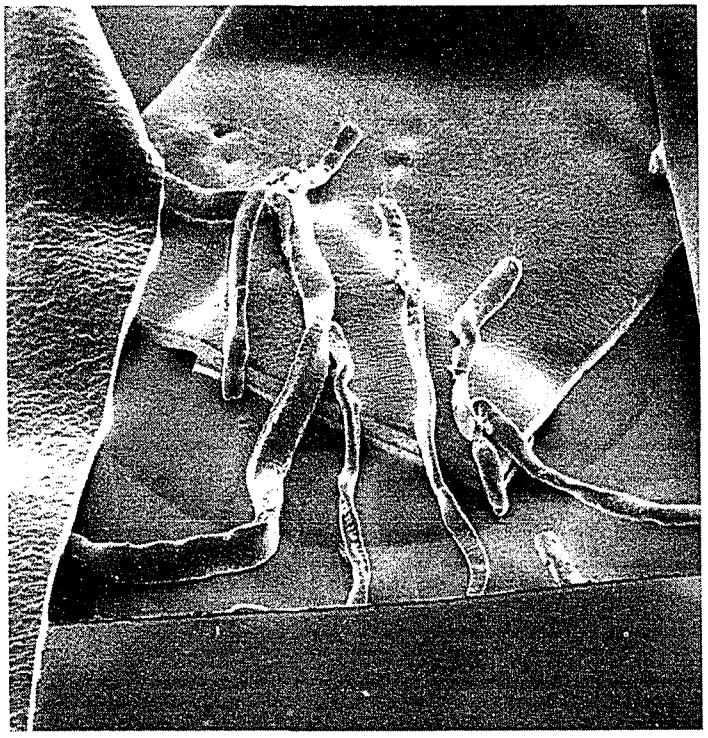

Figure 5.3. Sample after Pb evaporation with flexible mask still in place.

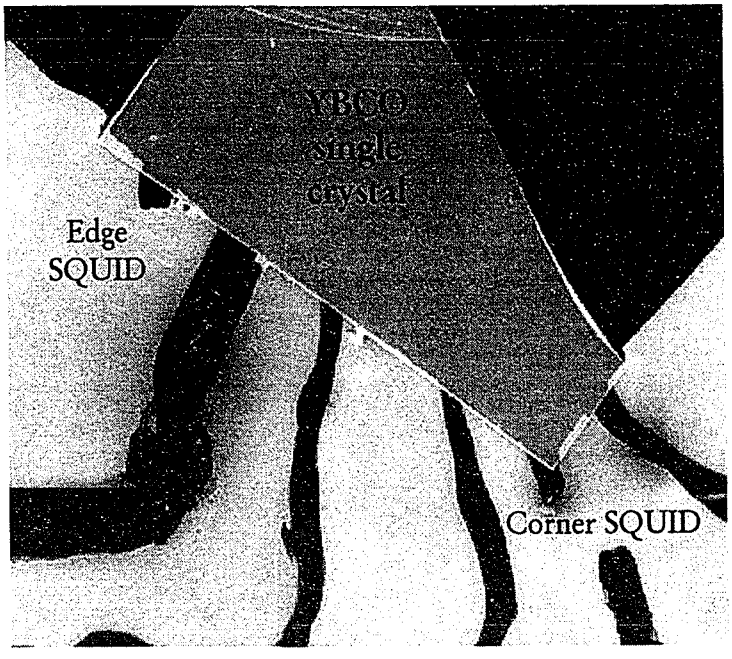

Figure 5.4. Completed sample with flexible mask removed.

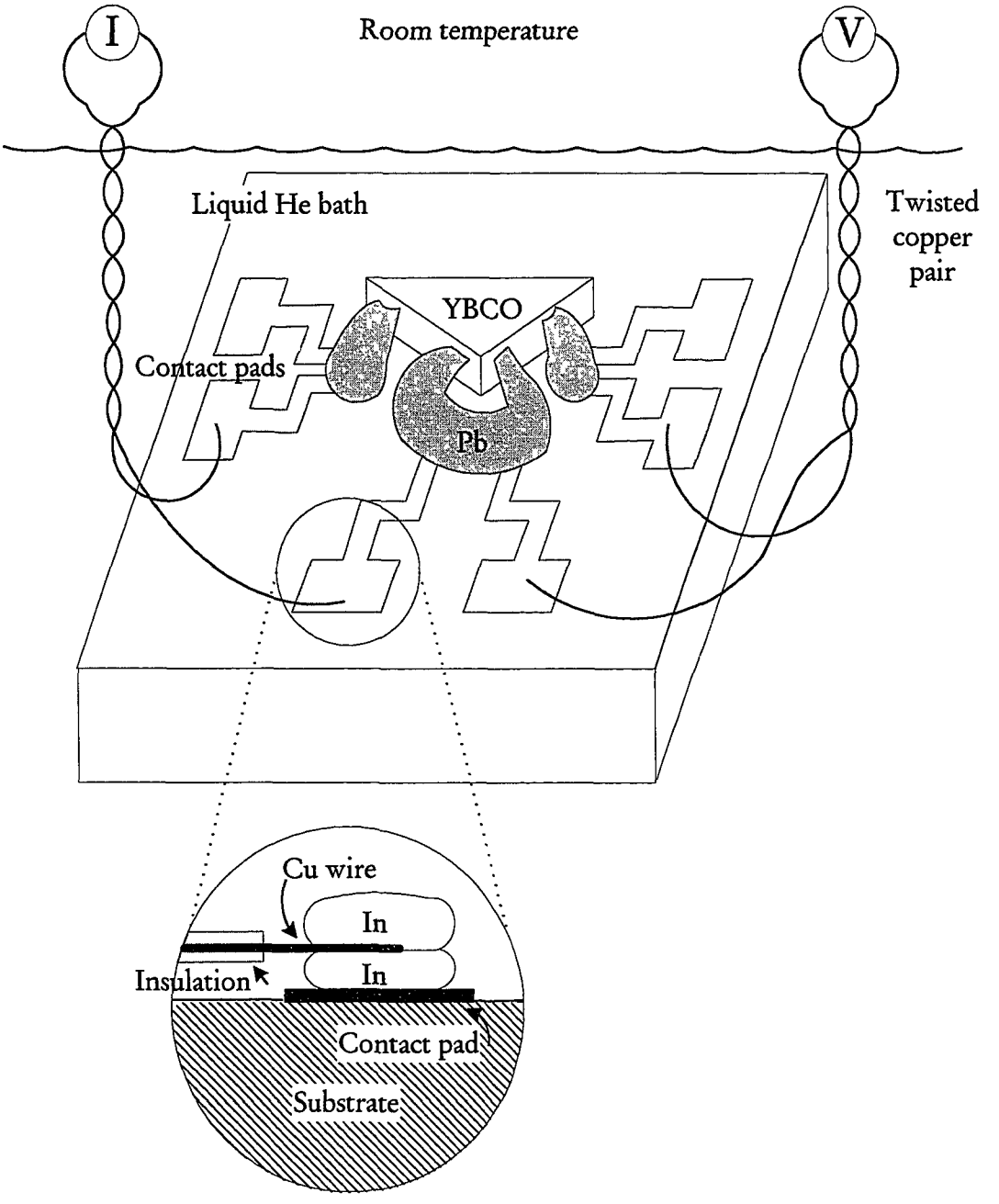

Figure 5.5. The electrical connections to a bimetallic corner SQUID. Twisted copper pairs are used to minimize electrical noise. The inset shows a side view of the indium sandwich used to connect the copper wire and the contact pads.

shielded room to reduce the effects of noise. Double-walled μ -metal shielding was used to reduce the residual magnetic field of the earth (0.5 Gauss) to less than 1 milligauss, as determined using conventional SQUIDs. For the SQUID measurements, the leads were filtered to further reduce the effect of noise.

The experience and home-built equipment of many former DVH group members were invaluable to the success of these experiments. For much of this work, I used a SQUID-testing insert built by Lan Vu. The insert had a modulation coil for the application of a magnetic field, and the samples were mounted vertically (field applied horizontally) to most effectively take advantage of the μ-metal shielding. A can made of superconducting Pb provided additional shielding. In addition, the insert and sample were lowered directly into a liquid He^4 bath, providing excellent temperature control. By pumping on the bath, its temperature could be regulated anywhere in the range of 4.2 K to 1.5 K. This was accomplished using a system of pumping lines, valves, and a pressure regulator that had been built previously by many former DVH students. The temperature was measured after data collection was completed, using either a liquid He^4 pressure-temperature conversion table or a silicon diode thermometer and temperature controller (Lakeshore Temperature Controller, DRC-91C). I used a voltage-controlled current-box built by Kendall Springer for current biasing the SQUIDs. The computer program used for data acquisition was originally written by Joe Walko, which I later modified (with Joe's help) for this project.

The measurements involved standard techniques. Diagrams of the electrical connections to the SQUID are shown in Figure 5.5 and Figure 5.6. Each Pb line is connected to at least two independent contact pad lines to avoid measuring the resistance of the leads in a four terminal configuration. Current-voltage characteristics (I-V's) were obtained using the current box mentioned above. The bias current through the SQUID was controlled with an output voltage (-10V to 10V) of a 12-bit D/A card (National Instruments) that was set by the data acquisition program. The voltage leads were connected to a preamplifier having a gain of $100-1000$ and a low-pass filter set to 10 kHz (Ithaco Low Noise Preamplifier, model 1201). The output was carried out of the rf-screened room.

A current 'twiddle' was added to the bias current at a frequency of 211 Hz, using the sine-wave output of a lock-in amplifier, to allow the simultaneous measurement of dynamic resistance and voltage as a function of bias current. The output voltage then consisted of a dc voltage (from the dc current bias) and ac voltage (from the current 'twiddle') that were measured using a digital voltmeter (Keithley Digital Multimeter, model 195, or a Keithley Sensitive Digital Voltmeter, model 182) and lock-in amplifier (Stanford Research Systems, models SR510 and SR530), respectively. This data was then sent to the computer (and data-acquisition program) either as a voltage digitized by the A/D card or through an IEEE bus. In addition, microwaves were applied to the junctions (using a Hewlett-Packard Sweep Oscillator, model 8350B) to induce Shapiro steps, which were observed in I-Vs displayed on an oscilloscope (Tektronix, model 5110).

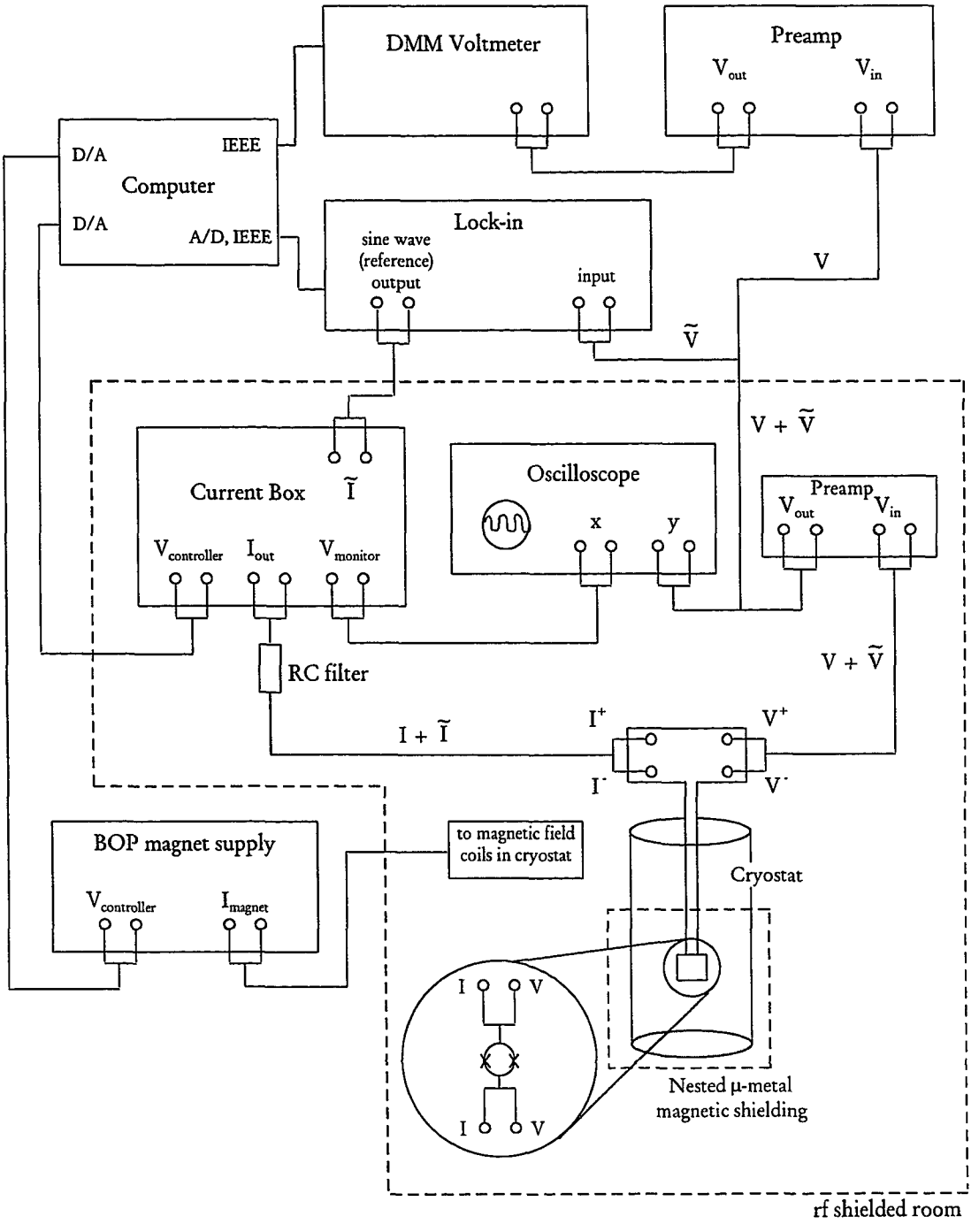

Figure 5.6. Schematic of experimental set-up.

I measured the response of the SQUIDs or junctions to magnetic flux (magnetic field times the area of SQUID loop) by monitoring the voltage and dynamic resistance of the SQUID biased at a set current. Magnetic field was applied using a bipolar op-amp power supply (Kepco, model BOP 50-4M) controlled by the data acquisition program. Exceptional care was taken to accurately and precisely zero the current through the modulation coil or Helmholtz coils before cooling slowly from 120 K to 4.2 K and below. The data acquisition program set the bias current through the SQUID and then recorded the voltage and dynamic resistance as it slowly swept the magnetic field in both polarities. A double trace was taken to insure repeatability of the data, and to detect the occurrence of flux trapping, which could be correlated with an abrupt shift in the trace of voltage or dynamic resistance versus magnetic field. This was done for many values of bias current (to allow for the extrapolation to zero bias current that was required to account for a bias-current dependent flux contribution, as will be discussed in Chapter 6), and repeated for many separate cool-downs.

The depth of the critical current modulation of the SQUIDs was only a few percent (due to the large value of β, as was explained in Chapter 4), and so measurements of critical current versus field were very difficult and not regularly done. The single junction measurements, however, exhibited a strong critical current modulation with field, and were recorded using a different program logic. For a set magnetic field, the bias current was slowly stepped up while the voltage (or dynamic resistance) was monitored. When the voltage (or dynamic resistance) climbed above a set threshold (corresponding to onset of the resistive state), the value of the bias current was recorded as the critical current. The dependence of the measured critical current

on this voltage (or dynamic resistance) threshold was checked and optimized by modeling complete I-V's with noise rounding for select field values.

Chapter 6

DC SQUIDS: EXPERIMENTAL RESULTS AND ANALYSIS

The motivation and basic experimental scheme for measuring the relative phase of the superconducting order parameter in YBCO between the *a*-axis and *b*-axis directions were introduced in Chapter 4. In this chapter, I will discuss the experimental dc SQUID results and some of the complicating issues that could impact the results and interpretation of our experiment. This chapter is based on work that has been published previously (Wollman *et al.*, 1993; 1994a; 1994b; Van Harlingen *et al.*, 1994a; 1994b; Van Harlingen, 1995).

Much theoretical and experimental has been done on dc SQUIDs and related Josephson tunneling phenomena, with entire textbooks devoted to these subjects. A short list of relevant texts that I have found useful follows: Barone and Paternò (1982), DeGennes (1989), Parks (1969), Solymar (1972), Tinkham (1975), and Van Duzer and Turner (1981). I will assume some basic results from these and other texts in the following discussions and in Chapter 7.

Before presenting the experimental results, I want to discuss some potentially complicating issues that we considered at the beginning of this work. Since dc SQUIDs are very sensitive to magnetic field, it is important to properly shield the SQUIDs so that the Earth's residual magnetic field does not produce a significant phase shift in the experiment. As described in the last chapter, we have used nested μ-metal and superconducting shielding to reduce the ambient magnetic field to a level estimated

to be on the order of a few tenths of a milligauss, based on measurements of conventional SQUIDs and Josephson-junction arrays. Because of the flux focusing of the superconducting crystal and films, the field in our SQUID loop can actually be much greater, on the order of 1 mG. For a typical SQUID area of $30 \times 30\ \mu m^2$, this corresponds to a flux in the loop of order $0.05\ \Phi_0$. This is not negligible, but is less than the spread in experimental results due to trapped flux effects (described later in the chapter), and is much less than the observed phase shift of order $0.5\ \Phi_0$.

Another consideration was the possibility that domains might form in a single crystal of YBCO, such that the superconducting order parameter might be, *e.g.*, rotated with respect to the order parameter of a different region. This could happen in a twinned or partially twinned crystal, assuming that the positive and negative lobes of a $d_{x^2-y^2}$ symmetric gap function locked onto the *a*- and *b*-axis directions, respectively. In this scenario, if a corner SQUID connected two (or a multiple of two) adjacent twin-domain regions in which the positive and negative lobes were reversed along with the crystalline axes, no intrinsic phase shift would be measured because the SQUID would sample the same signs of the order parameter in the two orthogonal directions.

With this reasoning, we initially thought that we could only use untwinned single crystals of YBCO for the experiment. However, we realized that there are experimental and theoretical arguments that the order parameter maintains its phase orientation across twin boundaries. The consequence of order parameter domain wall at a twin boundary (with a change in sign of the gap) is the formation of a Josephson

junction. The domain wall energy is of the order of the Josephson coupling energy across the twin boundary, $E_J \approx \frac{\hbar I_b}{2e}$, where I_b is the twin-boundary critical current. Experimentally, I_b is very large ($I_b \sim 10\,A$) because both the critical current densities of the twin boundaries and the twin surface areas are very large. This implies that order parameter domains are energetically unfavorable and a single order parameter domain is favored even in twinned samples. In addition, we see little difference between the critical currents of junctions prepared on twinned and untwinned regions of the same YBCO crystal. If the order parameter changed sign at twin boundaries, the critical current of junctions on heavily twinned regions would be reduced by averaging over twin regions of opposite polarity, a result that is not observed experimentally. Finally, we have obtained the same phase shift results for SQUID experiments on twinned and untwinned crystals, as will be described later in this chapter.

Another initial consideration was the orthorhombicity of YBCO, as the symmetry classifications in Chapter 4 are strictly valid only for a tetragonal crystal structure. In addition to the complication of mixed symmetry states (of predominantly *s*-wave or *d*-wave character if the orthorhombic distortion is small), it is possible that a *d*-wave state in an orthorhombic material would have order parameter lobes of different size, *e.g.*, the positive lobes might be larger than the negative lobes. This should not affect the phase coherence experiments unless one set of lobes was significantly larger than the other, such that the coupling to the smaller lobe was

overwhelmed by the larger lobe. In this case, the SQUID would again sample the same sign of the order parameter, and no intrinsic phase shift would be measured. This situation is unlikely, according to Leggett (private communication, 1993), since we use a normal metal (Au) for the barrier layer in a SNS (superconductor-normal metal-superconductor) junction, which reduces the coupling to any non-desired lobes of the order parameter along directions other than the one being probed.

It is important to note that the previous two concerns involve obtaining an *s*-wave experimental result for a $d_{x^2-y^2}$ pairing state symmetry. A general observation is that it is much easier to devise a theoretical scenario in which the effects of a *d*-wave order parameter are masked, resulting in an experimental *s*-wave result, than the opposite situation of an *s*-wave order parameter leading to a *d*-wave experimental result. This makes our eventual determination of a sign change of the order parameter between orthogonal directions a much stronger indicator of $d_{x^2-y^2}$ pairing.

With these initial considerations out of the way, I now present our experimental results. One of our first achievements in this work was the successful fabrication of superconducting junctions on YBCO single crystals, an important prerequisite to making SQUIDs. The Pb-Au-YBCO junctions of the bimetallic dc SQUIDs are SNS (superconductor-normal metal-superconductor) junctions or SNIS (superconductor-normal metal-insulator-superconductor) junctions, as determined by theoretical modeling of the temperature dependence of the critical currents. It is difficult to make reproducible junctions having a specified critical current, a

consequence of the complex fabrication procedure described in the previous chapter. The critical currents typically range from 10 μA-500 μA at 2 K.

The superconducting junctions in this work exhibit noise-rounded resistively-shunted-junction (RSJ) current-voltage ($I-V$) characteristics. Figure 6.1(a) shows the $I-V$ curve for a junction fabricated on the edge of a single crystal of YBCO. The observed noise-rounding of the $I-V$ is much greater than that calculated for thermal noise-rounding, and may be intrinsic to our junctions. Noise rounding can be quantified in terms of the noise parameter, $\Gamma = \frac{\pi k_B T}{I_c \Phi_0}$. At typical operating temperatures of 2 K - 4 K, the thermal noise rounding is expected to be $\Gamma = 0.05$, compared to the experimental value of $\Gamma \geq 0.2$ for our bimetallic dc SQUIDs. Additional noise rounding is introduced by the ac current modulation used to measure the dynamic resistance simultaneously with the $I-V$.

To extract the intrinsic phase shift δ_{ab} inside the YBCO crystal, we must determine the phase at zero flux of the critical current *vs.* applied flux (I_c *vs.* Φ) curves for corner Pb-Au-YBCO dc SQUIDs, as described in Chapter 4. The critical currents of our bimetallic SQUIDs modulate by only a few percent with applied flux, making it difficult and time-consuming to obtain sufficient data to accurately measure phase shifts.

An alternative method was devised, in which the SQUID modulation is detected by biasing the SQUID at a constant current and measuring the dynamic resistance *vs.* applied magnetic flux. For all measurements reported here, the SQUIDs

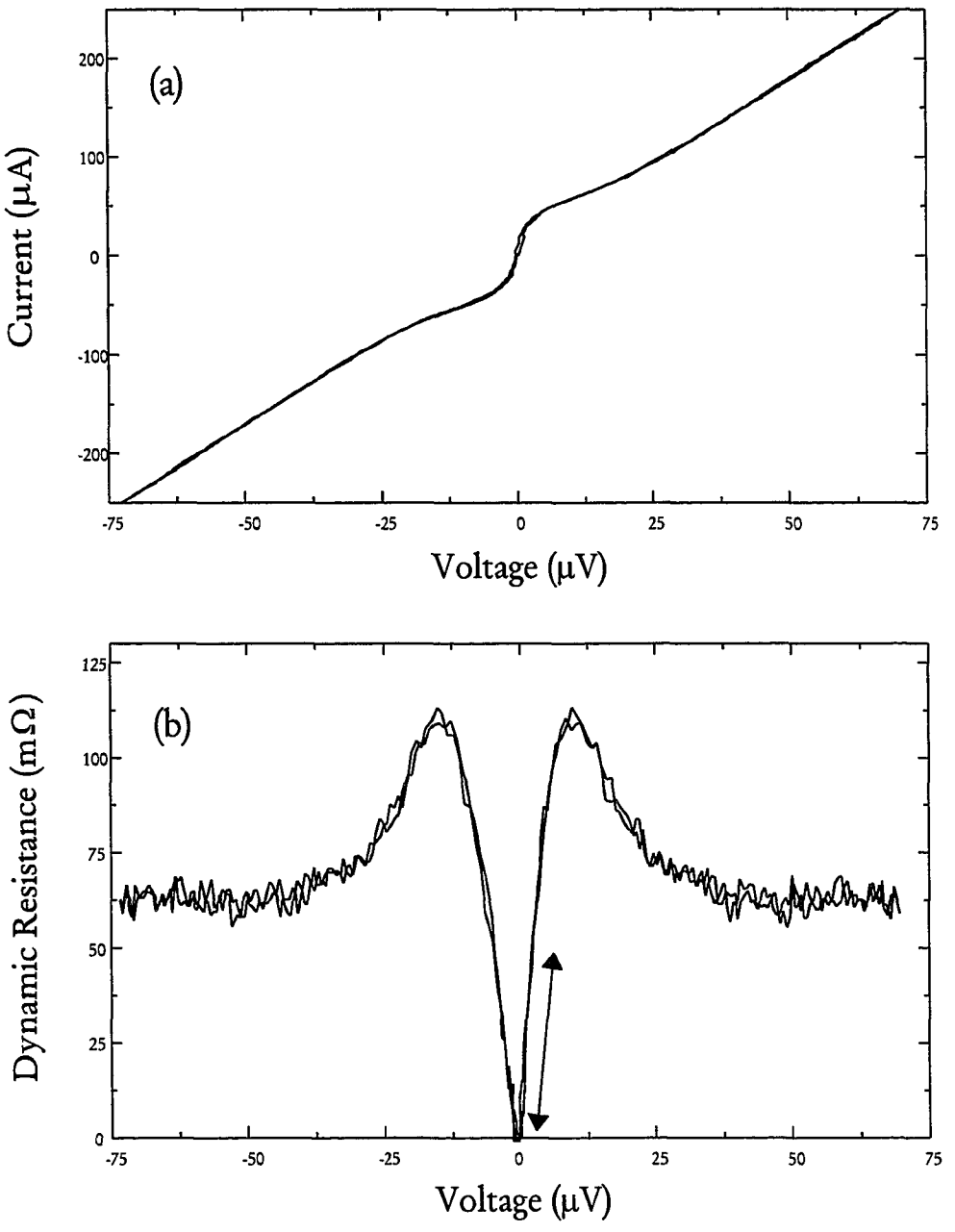

Figure 6.1. (a) Current *vs.* voltage for a junction fabricated on the edge of a YBCO single crystal. (b) Dynamic resistance *vs.* voltage. The arrows indicate the noise-rounded, finite-voltage region below the resistance maximum where the SQUID measurements were made.

are biased in the noise-rounded finite-voltage region below the resistance maximum, as indicated in Figure 6.1(b). In this region, an increase of the dynamic resistance corresponds to an decrease in the critical current. A minimum in the resistance at zero flux therefore corresponds to a maximum in the critical current and a phase shift of $\delta_{ab} = 0$, while a maximum in the resistance corresponds to a phase shift of $\delta_{ab} = \pi$.

The dynamic resistance *vs.* applied flux curve (R *vs.* Φ) for a Pb-Au-YBCO corner SQUID is shown in Figure 6.2 for several values of bias current. Besides the expected periodic modulation, there is a bias current-dependent phase shift that must be accounted for in order to measure the intrinsic phase shift δ_{ab}. This bias current-dependent phase shift is one of the major complications of the experiment, and is caused by the asymmetric division of the bias current through the two parallel branches of the SQUID which generates a net flux in the SQUID loop.

A detailed discussion of this effect can be found in De Waele and De Bruyn Ouboter (1969) and Tesche and Clarke (1977). Asymmetries in the critical currents (and normal state resistances) of the junctions and the inductances of the branches contribute to this effect. Consider an asymmetric SQUID with junction critical currents $I_{ca} = (1+\alpha)\frac{I_c}{2}$ and $I_{cb} = (1-\alpha)\frac{I_c}{2}$ and branch inductances $L_a = (1+\eta)\frac{L}{2}$ and $L_b = (1-\eta)\frac{L}{2}$, where $\alpha = \frac{I_{ca} - I_{cb}}{I_c}$ is the fractional critical current asymmetry and $\eta = \frac{L_a - L_b}{L}$ is the corresponding inductance asymmetry. Compared to the symmetric SQUID discussed in Chapter 4, the depth of the critical current modulation

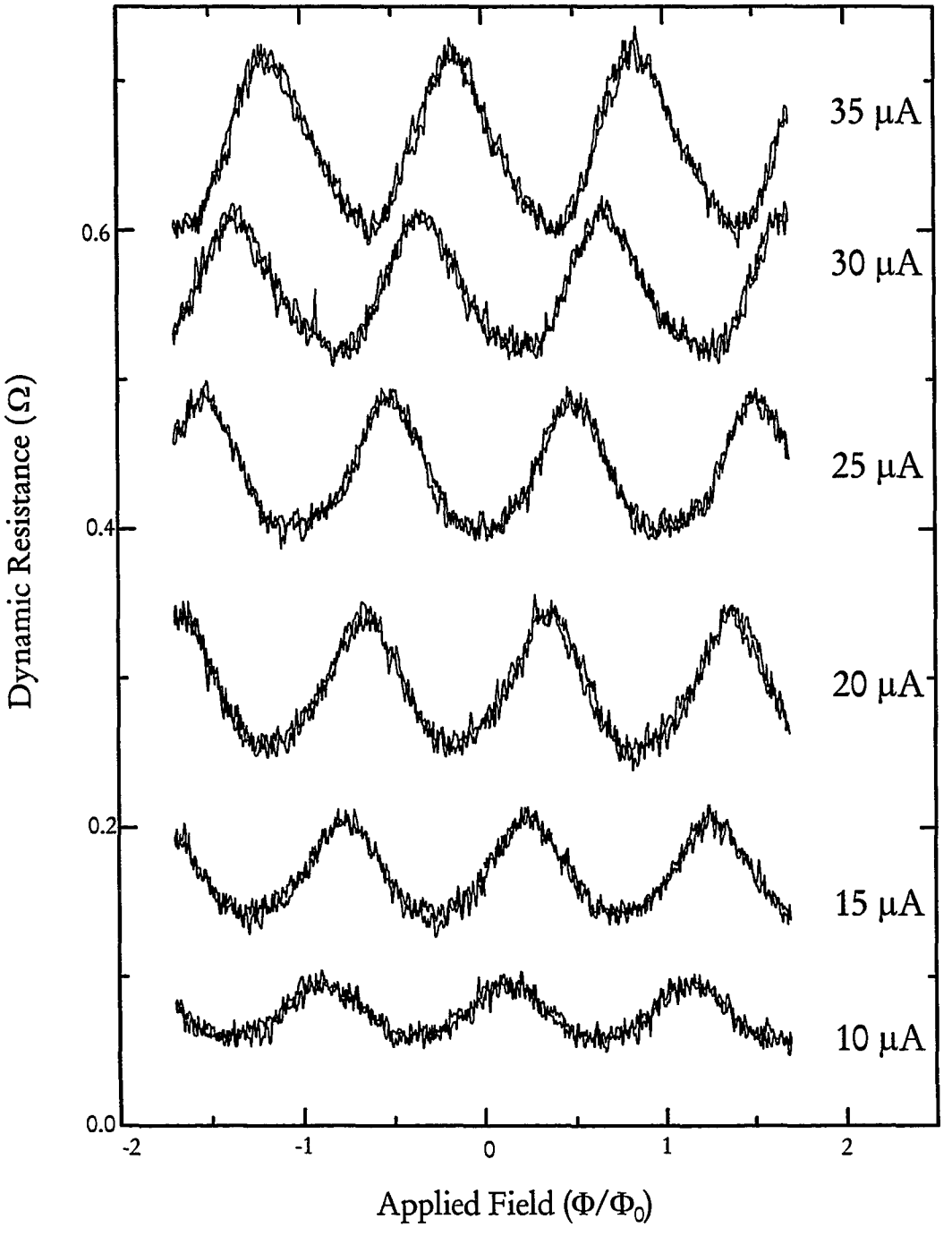

Figure 6.2. Modulation of the dynamic resistance *vs.* applied magnetic flux for different bias currents in a corner SQUID, showing the expected periodicity and a bias current-dependent phase shift arising from SQUID asymmetries. Because of noise rounding, the modulations can be measured for currents well below the thermodynamic critical current, which was approximately 50 μA for this device.

in an asymmetric SQUID is reduced by a factor of $(1-\alpha)$ in the limit of zero inductance. For a SQUID with finite inductance that is biased near the critical current, the additional flux contribution, $\Delta\Phi$, linking the SQUID loop varies linearly with the bias current I, approximately as

$$\Delta\Phi = \frac{1}{2}(\alpha+\eta)\,L\,I = \frac{1}{2}(\alpha+\eta)\,\beta\,\Phi_0\,\frac{I}{I_c},$$

which can be substantial if the inductance and asymmetry are large. This asymmetry is also responsible for the resistance oscillations visible at currents greater than the critical current as shown in Figure 6.3 (with no applied magnetic flux), caused by the self-modulation of the SQUID with bias current.

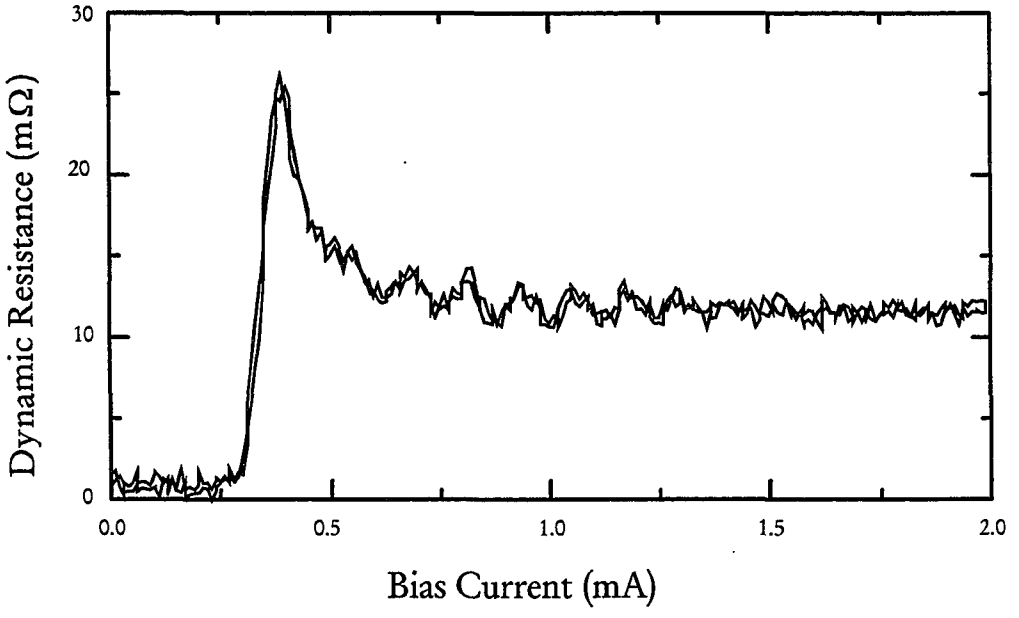

Figure 6.3. Dynamic resistance *vs.* bias current for a Pb-Au-YBCO SQUID. The resistance oscillations are caused by the self-modulation of the SQUID with increasing bias current.

The best way to obtain δ_{ab} is to reduce any asymmetries until there is no additional phase shift caused by the bias current and the intrinsic phase shift can be directly obtained from phase of the R *vs.* Φ curves at zero applied flux. In light of the fabrication procedure described in Chapter 5, it is not easy to completely eliminate the critical current asymmetry. The major difficulty involves the Au and Pb evaporations, which must be done at a compound angle to coat the vertical (and orthogonal) *a*- and *b*-faces of the YBCO crystal as well make connections to the contact pads, making it difficult to ensure that identical thicknesses of Au are evaporated onto the two orthogonal faces. This can lead to critical current asymmetry, since the critical current of an SNS junction is a sensitive function of the thickness of the normal metal layer.

Another way to obtain δ_{ab} is to devise a scheme to extrapolate the R *vs.* Φ curves to zero bias current, where there the self-generated magnetic flux is negligible. The simplest procedure is to plot the value of applied flux at which the resistance is a minimum (corresponding to a maximum in the critical current) *vs.* the bias current and extrapolate linearly to zero current, as shown in Figure 6.4 for the SQUID modulations in Figure 6.2. For a corner SQUID, an *s*-wave state (isotropic, anisotropic, or extended) would have an intercept at $\Phi = 0$; a $d_{x^2-y^2}$ state would have an intercept at $\Phi = \frac{\Phi_0}{2}$. For each extrapolation, we can determine the zero bias flux intercept to an statistical uncertainty (based on a least squares fit) of roughly $\pm 0.1\,\Phi_0$, depending on the asymmetry of the SQUID (which controls the slope) and on the magnitude of the critical current (which controls the extent of the extrapolation). As

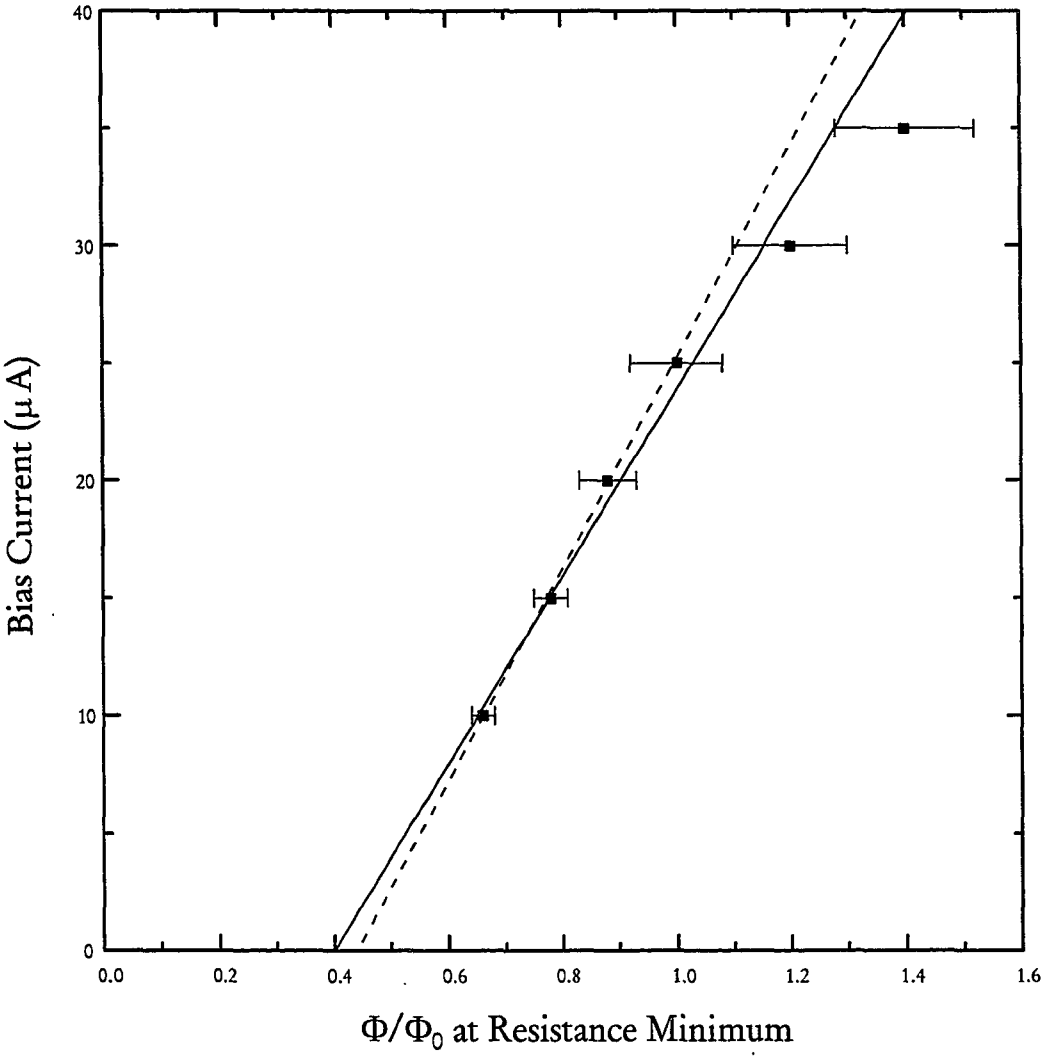

Figure 6.4. Linear extrapolation to zero bias current of the applied flux corresponding to resistance minima for the corner SQUID data shown in Figure 6.2. The solid line is a least-squares fit to the data points, with a zero bias current intercept of (0.40 ± 0.06) and a correlation of 0.988. The increased error bars at the larger bias currents reflect the difficulty in extracting phase information from increasingly non-sinusoidal SQUID modulations, introducing significant systematic errors. Excluding the upper two data points from the analysis results in the dashed line least-squares fit, with an intercept of (0.45 ± 0.01) and a correlation of 0.999. Although we believe we are justified in removing these data points, we have chosen to include all data points (and error bars) in our extrapolation procedure, yielding an intercept of $(0.41\ ^{+0.04}_{-0.02})$ for this particular extrapolation.

will be discussed below, the statistical uncertainty in the intercept from the extrapolation procedure is less than the variation due to the presence of trapped flux, and so a full statistical treatment of all extrapolations will not be presented.

Before presenting the extrapolation results for our corner and edge SQUIDs, I want to address the validity of this extrapolation procedure. I emphasize that this procedure is only valid in the noise-rounded finite-voltage region of the $I-V$ curve, as demonstrated by theoretical modeling and computer simulations (Van Harlingen, private communication, 1993). It is experimentally verified by the results of the edge SQUIDs, which always extrapolate to zero flux as required independent of the pairing state. Additionally, we have been able to measure corner SQUID modulations in the limit of zero bias current, where there is no effect due to asymmetry, and find that the measured phase shift is the same as for the other corner SQUIDs with more extensive extrapolations.

Some questions have been raised about this procedure by F. Wellstood and co-workers (Mathai *et al.*, 1995 and references therein), who state (correctly) that the extrapolation procedure is not valid for their SQUIDs with large critical currents and $I-V$ characteristics that can be accurately described by the RSJ model. In their experiment, which will be described in greater detail in Chapter 8, screening currents of SQUIDs at zero current bias are measured using a Scanning SQUID Microscope and are found to be linear with applied field. The validity of the extrapolations depends on the response of the SQUID as the bias current is increased. For the case of zero dissipation (no noise-rounding) far below the critical current, there is a lag in the

circulating current as the bias current is increased from zero, which can not be accounted for by the extrapolation procedure. In the presence of dissipation (noise-rounding), however, there is a experimentally relevant region in which the extrapolations are valid. This problem has recently been studied by Rzchowski and Hinaus (1995), who have developed a rigorous extrapolation procedure.

Measurements and linear extrapolations for all 7 corner SQUIDs are shown in Figure 6.5, each cooled slowly in zero field. In particular, note the reduced bias current scale (on the left side, for the open symbols) for the two corner SQUIDs that have modulations even at zero bias current. One of these two samples was untwinned, and the other was partially twinned. The corner SQUID intercepts vary from $0.3 - 0.6\,\Phi_0$, limiting our ability to unambiguously identify the pairing state symmetry. Each corner SQUID, however, does exhibit a significant phase shift of order π consistent with a $d_{x^2-y^2}$ or $s+id$ pairing state symmetry.

The variation in the intercept is likely due to trapping of magnetic flux vortices. Flux trapped near one of the Josephson junctions can reduce its critical current and modify the SQUID asymmetry, causing a change in the slope of the current-dependent phase shift. A vortex can also be trapped near the SQUID loop, linking flux to the SQUID and inducing a parallel shift in the curves. This is demonstrated in Figure 6.6 which shows a series of measurements taken on a corner SQUID and an edge SQUID from the same (partially untwinned) crystal in successive cooldowns of the sample after warming to above the transition temperature of YBCO. The corner SQUID

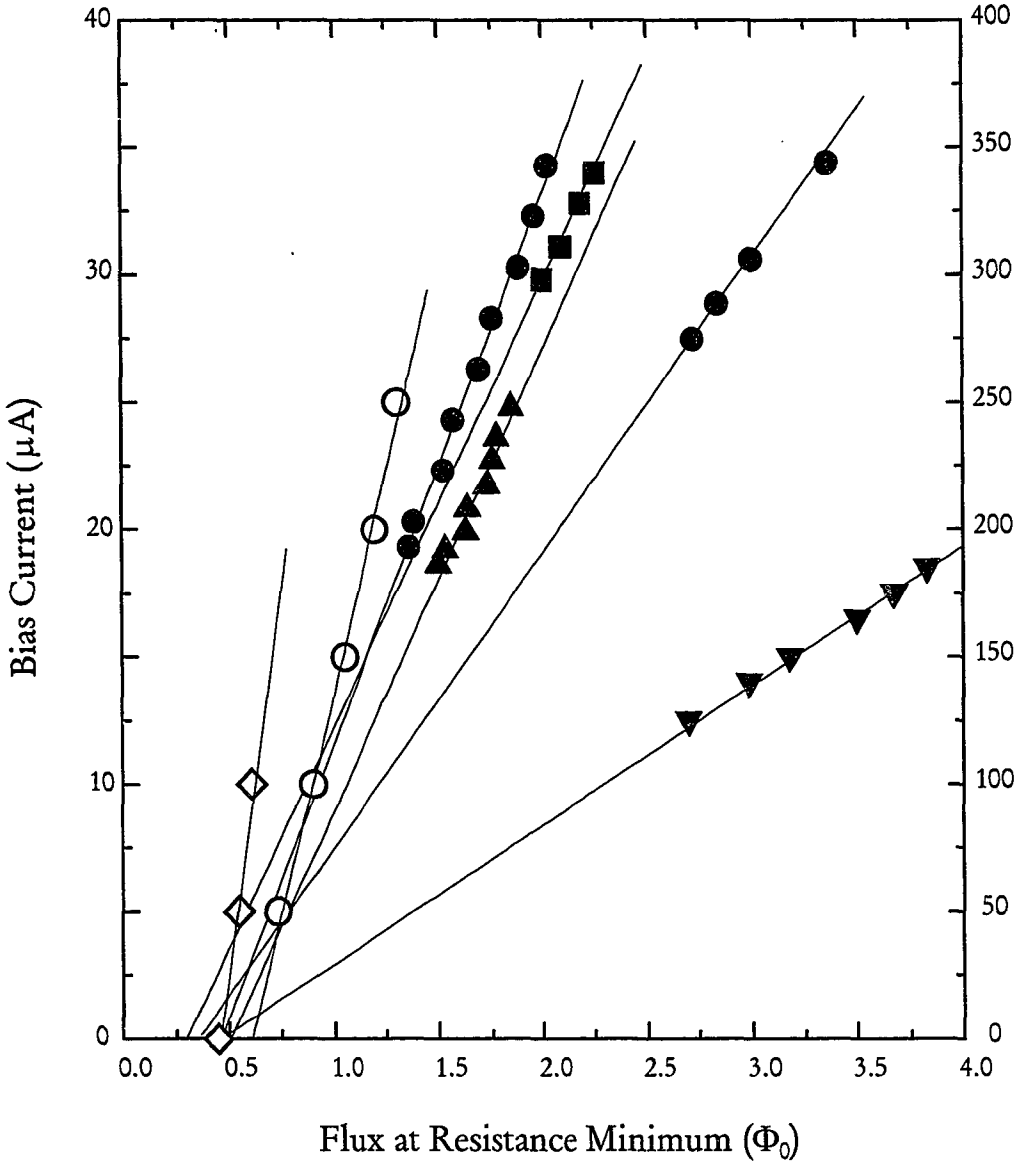

Figure 6.5. Linear extrapolations to zero bias current of the applied flux corresponding to resistance minima for all seven corner SQUIDs. The open symbols are scaled to the left axis. An intercept of 0 would occur for *s*-wave pairing; the observed intercept is of order $\Phi_0/2$ and corresponds to a phase shift of $\delta_{ab} = \pi$, consistent with a $d_{x^2-y^2}$ pairing state symmetry. The distribution of the intercepts is due to magnetic vortices trapped near the SQUID.

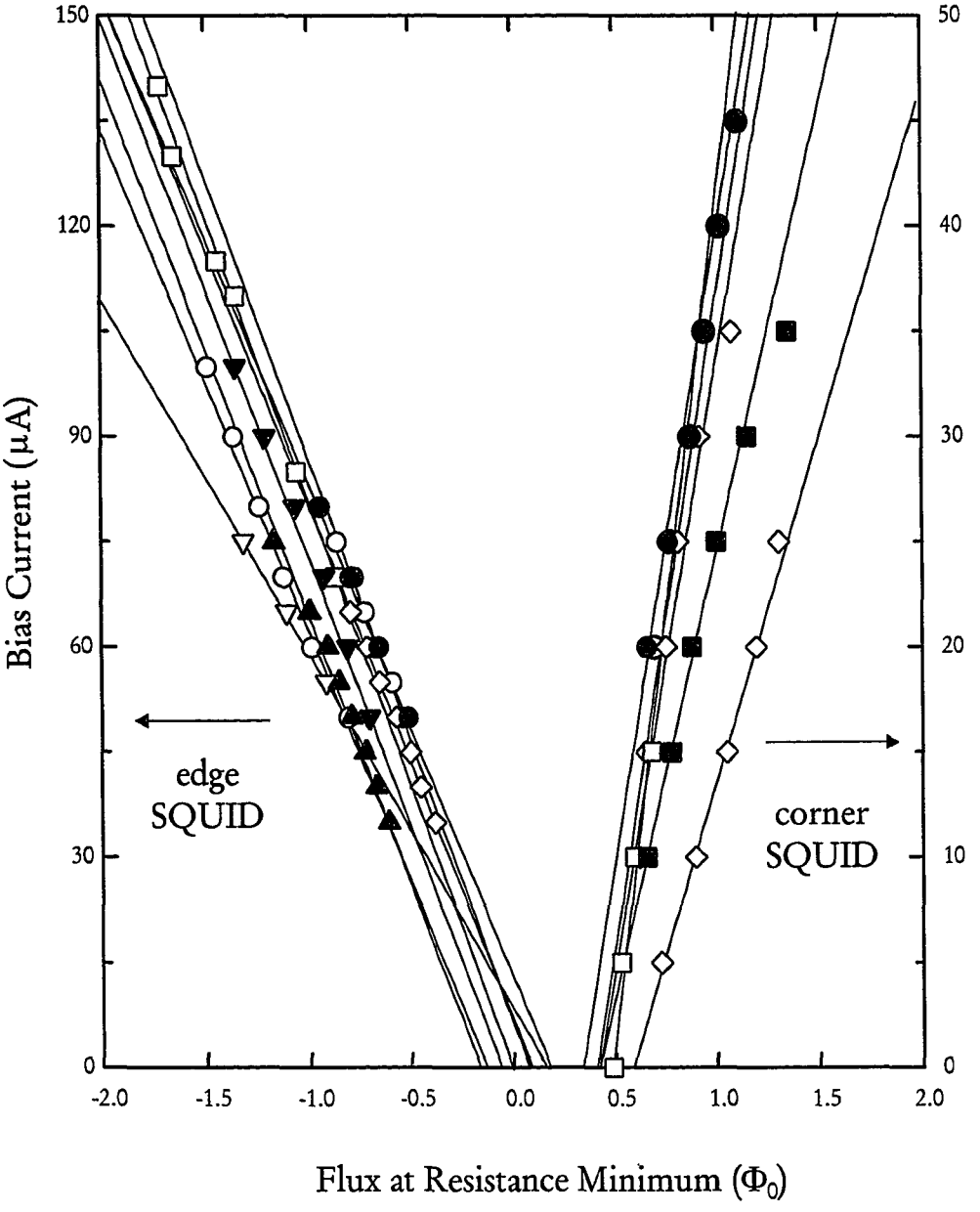

Figure 6.6. Linear extrapolations for a corner SQUID and an edge SQUID fabricated on the same crystal. Each curve represents a different cooldown of the sample. The edge SQUID extrapolates to zero, as it must regardless of the pairing state. On the other hand, the corner SQUID shows clear evidence for a relative phase shift of $\delta_{ab} = \pi$, consistent with a sign change of the order parameter between orthogonal directions in the YBCO. The distribution of the intercepts is due to magnetic vortices trapped near the SQUID.

intercepts cluster around $\frac{\Phi_0}{2}$, suggesting a statistical distribution of trapped configurations about the intrinsic (zero flux) result. In support of this is the data from the edge SQUID for which the intercepts are distributed about zero, as is expected independent of the pairing state.

An additional concern that was raised involves the obvious difference between our corner and edge SQUIDs, that is, the presence of a corner. Klemm (1994) argued that there may be a singularity in the supercurrent flow at the corner, or a preferential trapping of flux at the corner, that could be responsible for the π phase shift that we observe. We find no evidence for either of these effects (Wollman *et al.*, 1994a). The current flow at the corners is smooth, even for perfectly sharp corners, and any singularity would be removed by the rounding of the corner found in a real sample. In addition, flux trapping is not expected to be different at the corners, which are substantially rounded on the relevant length scale of the penetration depth, and most of the relevant flux trapping is in the Pb films rather than in the bulk crystals. Therefore, the corner plays no significant role, as confirmed by many measurements on conventional SQUIDs having corners.

The final topics that I want to discuss are the limitations of this experiment and the potential improvements that can be made. The SQUID fabrication was very difficult and time-consuming with a small success ratio, keeping us from measuring as many SQUIDs as we would have liked. The experimental results were complicated by SQUID asymmetries and the need for an extrapolation procedure. The relatively large

areas of the SQUIDs (which were unavoidable, given the described fabrication procedure) made the measurements sensitive to trapped flux. With these complications, we can conclude only that the intrinsic phase shift between orthogonal directions in YBCO is of order π, consistent with a $d_{x^2-y^2}$ or $s+id$ pairing state symmetry.

An alternative (and more direct) way to show the existence of the π phase shift in a *d*-wave material is to measure the half-integer flux ($\frac{1}{2}\Phi_0$) that is spontaneously generated in the bimetallic SQUID loop at zero applied magnetic field. Indeed, this was the original experiment that Tony Leggett suggested to us as a way to determine the pairing state symmetry. At that time, our research group was already developing a Scanning SQUID Microscope (SSM) that would give us the capability to do this proposed experiment. We hoped to eventually use this approach in addition to measuring the transport properties of the bimetallic SQUIDs. A working SSM was completed shortly afterwards, but delays in the development of subsequent versions of our SSM kept us from doing this experiment. This is unfortunate, because the SSM would have eliminated the complications of flux trapping and the need for extrapolations. Measurements of the spontaneously-generated half-integer flux have recently been carried out for thin-film versions of our experiment by other researchers, and will be reviewed in Chapter 8.

Chapter 7

JOSEPHSON JUNCTIONS: EXPERIMENTAL RESULTS AND ANALYSIS

In the dc SQUID experiment described in the last chapter, we observed a dual modulation of the critical current with applied magnetic field that inspired a new set of measurements to determine the pairing state symmetry. Superimposed on the low-field periodic SQUID modulation was a critical current modulation envelope with a much larger characteristic field scale. In this well-known effect, magnetic field that is applied to the SQUID loop also threads the barrier regions of the two individual Josephson junctions that make up the SQUID, causing them to modulate and introducing a single-junction modulation envelope in the SQUID response. The much larger characteristic magnetic field scale of the envelope is determined by the ratio of the area of the SQUID loop to the area of the individual junctions (perpendicular to the applied field).

From this observation, we realized that measurements of the magnetic field modulation of the critical current of single Pb-YBCO Josephson junctions could be used to determine the pairing state symmetry. This is accomplished by comparing diffraction patterns obtained on junctions fabricated on *a* and *b* faces to those obtained for junctions straddling the *a* - *b* corners of YBCO single crystals. For a *d*-wave pairing state symmetry, the corner junction samples both signs of the order parameter and has a modified diffraction pattern compared to the edge junctions. The experimental results reported in this chapter have been published previously (Wollman

et al., 1995). In agreement with the SQUID measurements, we find that the order parameter of YBCO has a phase shift of π between the *a* and *b* directions as required for $d_{x^2-y^2}$ symmetry.

The effects of an applied magnetic field on the critical current of Josephson tunnel junctions have been extensively studied. The magnetic field penetrating through the barrier region transverse to the tunneling direction creates a phase gradient across the width of the junction, resulting in a variation of the local current density and a reduction in the total critical current. For a rectangular junction of area A, width w, magnetic barrier thickness t, and uniform critical current density J_0, low enough that self-field effects are negligible, the critical current has the usual Fraunhofer diffraction form

$$I_c(\Phi) = J_0 A \left| \frac{\sin(\pi\Phi / \Phi_0)}{(\pi\Phi / \Phi_0)} \right|$$

where $\Phi = B\,w\,t$ is the magnetic flux through the junction for applied magnetic field B. The geometry and expected flux modulation are shown in Figure 7.1(a).

To test the symmetry of the pairing state of the YBCO crystal, we measure the critical current of a junction fabricated on the corner of the crystal as shown in Figure 7.1(b). In this geometry, part of the tunneling is into the *a*-*c* face of the crystal and part is into the *b*-*c* face. A magnetic field applied along the *c*-axis penetrates through each segment of the junction barrier. For an *s*-wave material (isotropic, extended *s*, or anisotropic *s*), each face would see the same phase and the critical current would have the usual Fraunhofer diffraction pattern. However, for a *d*-wave superconductor, the

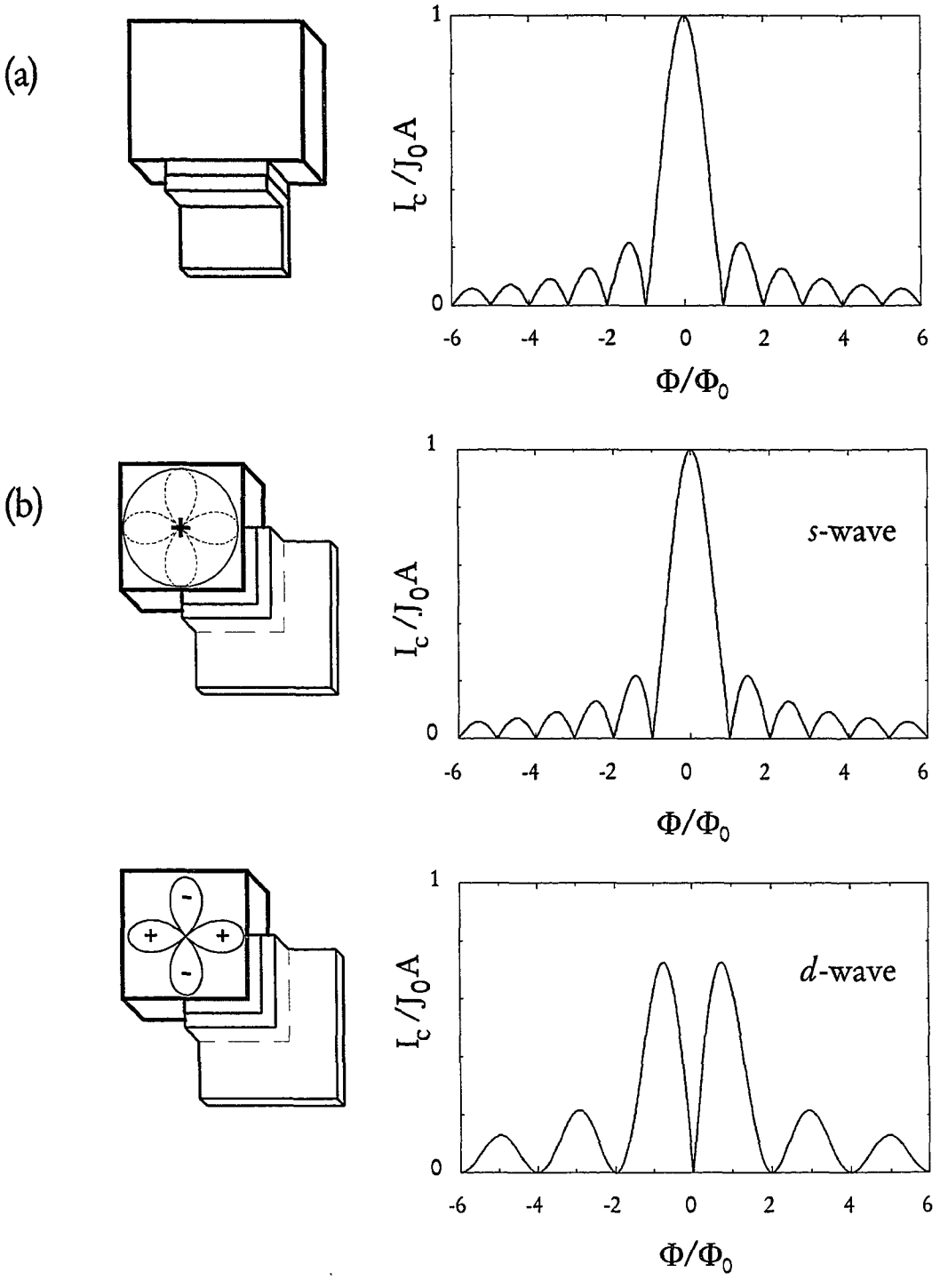

Figure 7.1. (a) Fraunhofer diffraction pattern for the critical current *vs.* magnetic flux threading the junction barrier that is characteristic of a single Josephson tunnel junction. (b) Diffraction pattern expected for a single corner junction with *s*-wave (isotropic, anisotropic, or extended) and *d*-wave pairing symmetry.

order parameter in the *a* and *b* directions would have the opposite sign, significantly modifying the single junction diffraction pattern. In a symmetric corner junction (with equal-area junctions on the *a* and *b* faces) and uniform critical current density, the critical current modulates according to

$$I_c(\Phi) = J_0 A \left| \frac{\sin^2(\pi\Phi / 2\Phi_0)}{(\pi\Phi / 2\Phi_0)} \right|.$$

At zero applied field, the current through the two orthogonal faces cancel exactly and the critical current vanishes. Applying a field in either direction increases the critical current, with a maximum value at $\frac{\Phi}{\Phi_0} = 0.74$ of roughly 72% of the maximum current for an *s*-wave junction. The critical current vanishes only when an integer number of flux quanta thread each half of the junction separately, giving a flux modulation period twice that for the edge junction Fraunhofer diffraction pattern. The modulation *vs.* applied flux threading the junction for the s-wave and d-wave cases is shown in Figure 7.1(b).

We have measured the single junction modulation characteristics of Josephson junctions fabricated on the edges and corners of YBCO single crystals. A typical sample is shown in Figure 7.2. As described in Chapter 5, the junctions are formed by depositing Pb thin films onto the *a-c* and *b-c* faces of a crystal which had been previously coated with a Au overlayer; a drop of polyamide holds the crystal to the substrate, providing a smooth ramp from the substrate surface to the crystal face so that the Pb film remains continuous. The YBCO-Au-Pb junctions exhibit resistively-

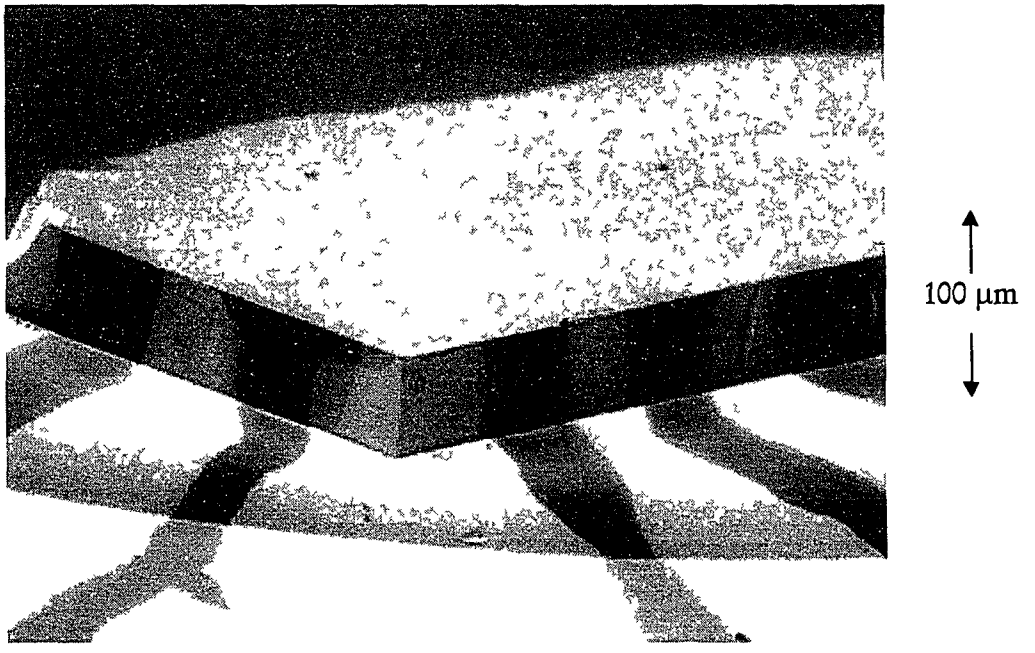

Figure 7.2. SEM photograph of a YBCO single crystal with junctions fabricated on the *a-b* corner and along the *a* and *b* edges.

shunted junction (RSJ) current-voltage characteristics with additional noise-rounding. Typical dimensions are 100 μm wide x 20 μm (the crystal thickness), with critical currents at 2.0 K of $20-100\,\mu A$ and resistances of $200-500\,m\Omega$. For these critical current densities ($<5\,A/cm^2$), the Josephson penetration depth is greater than 100 μm, so the junction may be considered to be in the small junction limit.

We determine the critical current by ramping up the bias current until a dynamic resistance of $\sim 100\,m\Omega$ appears across the junction, as measured by lock-in amplifier detection of the voltage generated by a drive current of order 1 μA rms. For very low critical currents ($<5\,\mu A$), it is necessary instead to measure the flux-induced modulation of the dynamic resistance and deduce a value for the critical current. A

magnetic field is applied perpendicular to the *a-b* plane of the crystal. Typically, the magnetic coupling area is about $2 \cdot 10^{-7}$ cm^2 so that a magnetic field of order 1 G is required to put a single flux quantum of magnetic flux through the junction.

The measured magnetic field modulation of a single junction on the edge face of a crystal is shown in Fig. 7.3(a). The critical current exhibits a Fraunhofer diffraction pattern with a maximum at zero applied field. In contrast, the modulation for a corner junction plotted in Fig. 7.3(b) is strikingly different, exhibiting a pronounced dip at zero applied field as expected for the *d*-wave case. The flux periodicity of the corner junction is also different, with all peaks being the same width; the edge junction shows a central peak with a width twice that of the sidelobes, as expected for the Fraunhofer pattern. We have observed this behavior in approximately ten junctions of each type. Unfortunately, because of uncertainties in the effective junction area and magnetic flux-focusing due to the superconducting crystal and films, we are not able to determine the actual amount of magnetic flux threading the tunnel junctions. As a result, we cannot determine if the separation of minima in the corner junctions is twice that in the edge devices as predicted for *d*-wave pairing.

Another example of a corner junction is shown in Figure 7.4(a). Here, we plot the current-voltage characteristic for two values of magnetic flux, showing an increase in I_c as the field is increased. The flux modulation patterns for both polarities of bias current are plotted in Figure 7.4(b). Again, there is a sharp dip in the critical current at zero field, falling to less than 25% of its peak value and to only about 15% of what we

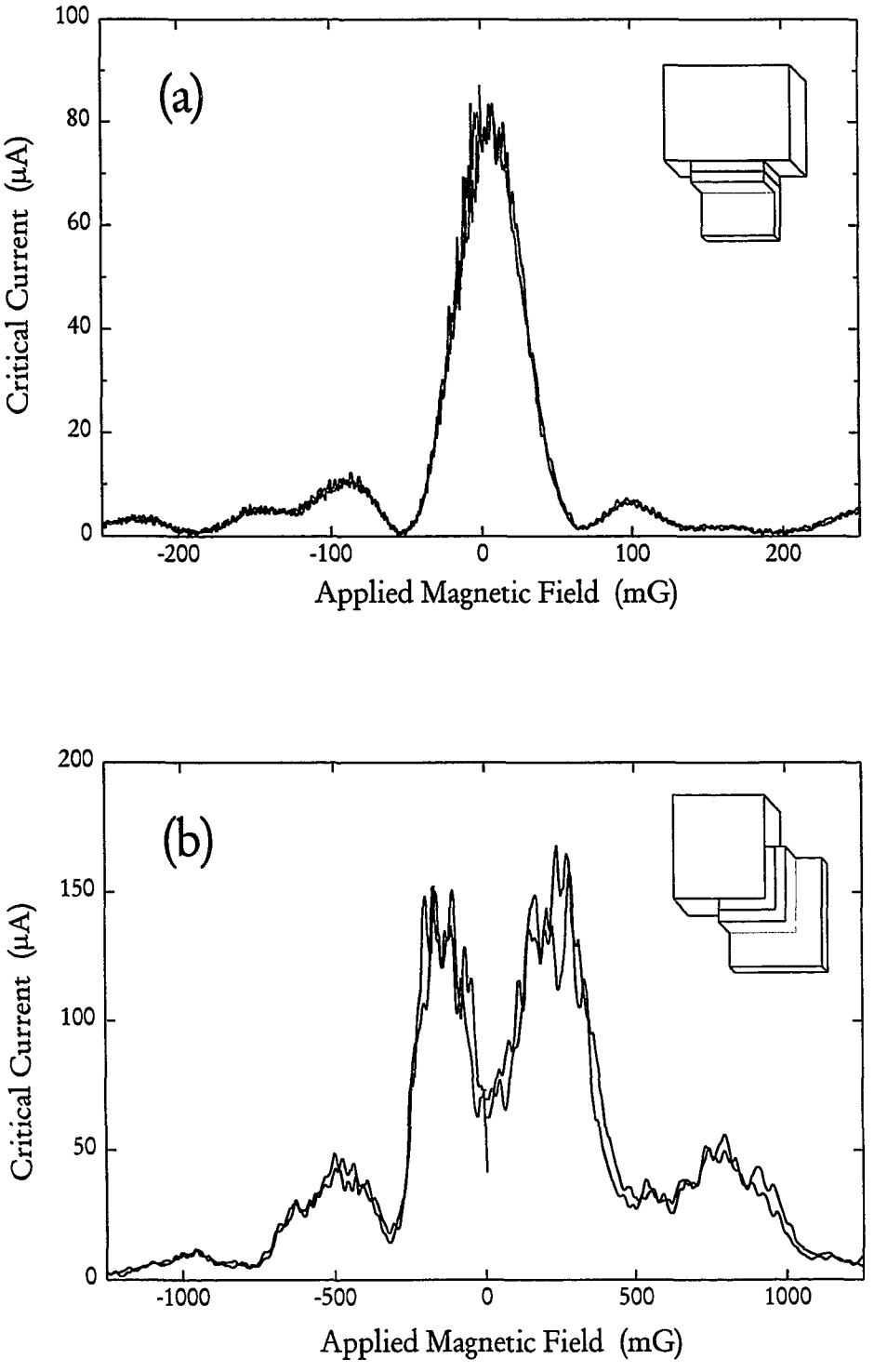

Figure 7.3. Modulation patterns measured on (a) an edge junction and (b) a corner junction. The dip at zero field in the critical current of the corner junction is strong evidence for *d*-wave pairing.

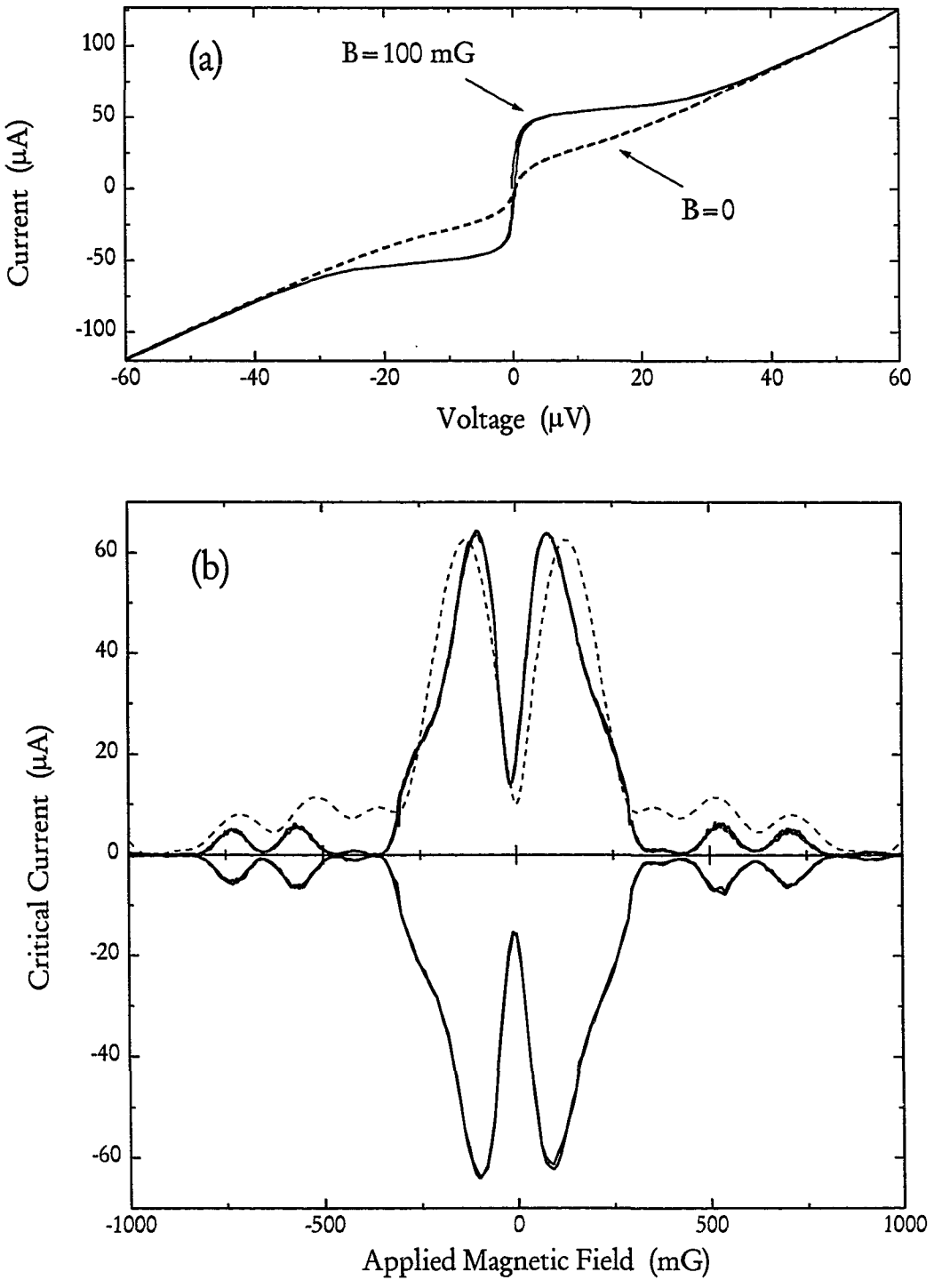

Figure 7.4. (a) Current *vs.* voltage for a corner junction showing the increase of the critical current as field is applied in either direction. (b) Corresponding critical current modulation for both bias current polarities showing symmetry with respect to both current and field directions. The dashed curve is calculated for a *d*-wave corner junction with a 15% asymmetry in the junction areas on the *a* and *b* faces.

estimate the critical current would be for an *s*-wave junction. At higher fields, the critical current decays sharply and exhibits several side lobes.

The detailed shape of the diffraction pattern is largely governed by the asymmetry of the corner junction. As an example, we consider a junction with uniform current density and barrier thickness and widths w_a and w_b of the junction segments on the two faces. The critical current for a *d*-wave crystal then depends on the relative asymmetry parameter $\gamma = \frac{w_a - w_b}{w_a + w_b}$ according to

$$I_c(\Phi,\gamma) = J_0 A \left| \frac{\sqrt{\sin^2(\gamma\pi\Phi/\Phi_0) + [\cos(\pi\Phi/\Phi_0) - \cos(\gamma\pi\Phi/\Phi_0)]^2}}{\pi(\Phi/\Phi_0)} \right|.$$

In particular, the cancellation of the critical current at zero flux will not be complete if the widths are unequal; the residual critical current at zero field is a fraction γ of the peak current expected for a uniform s-wave junction. In Figure 7.5(a), we show diffraction patterns calculated for several values of γ, where $\gamma = 0$ corresponds to a perfectly symmetric corner junction and $\gamma = 1$ corresponds to a junction fabricated on one edge. Note that although I_c is increased at zero field by asymmetry, the mirror symmetry with respect to applied field is always maintained. In Figure 7.4(b), the dashed curve is the critical current calculated from this expression for a junction asymmetry $\gamma = 0.15$, which fits the observed dip in the critical current at zero field. Note that the shape of the side lobes is also accurately modeled; in particular the suppression of the first and fourth side lobes is reproduced.

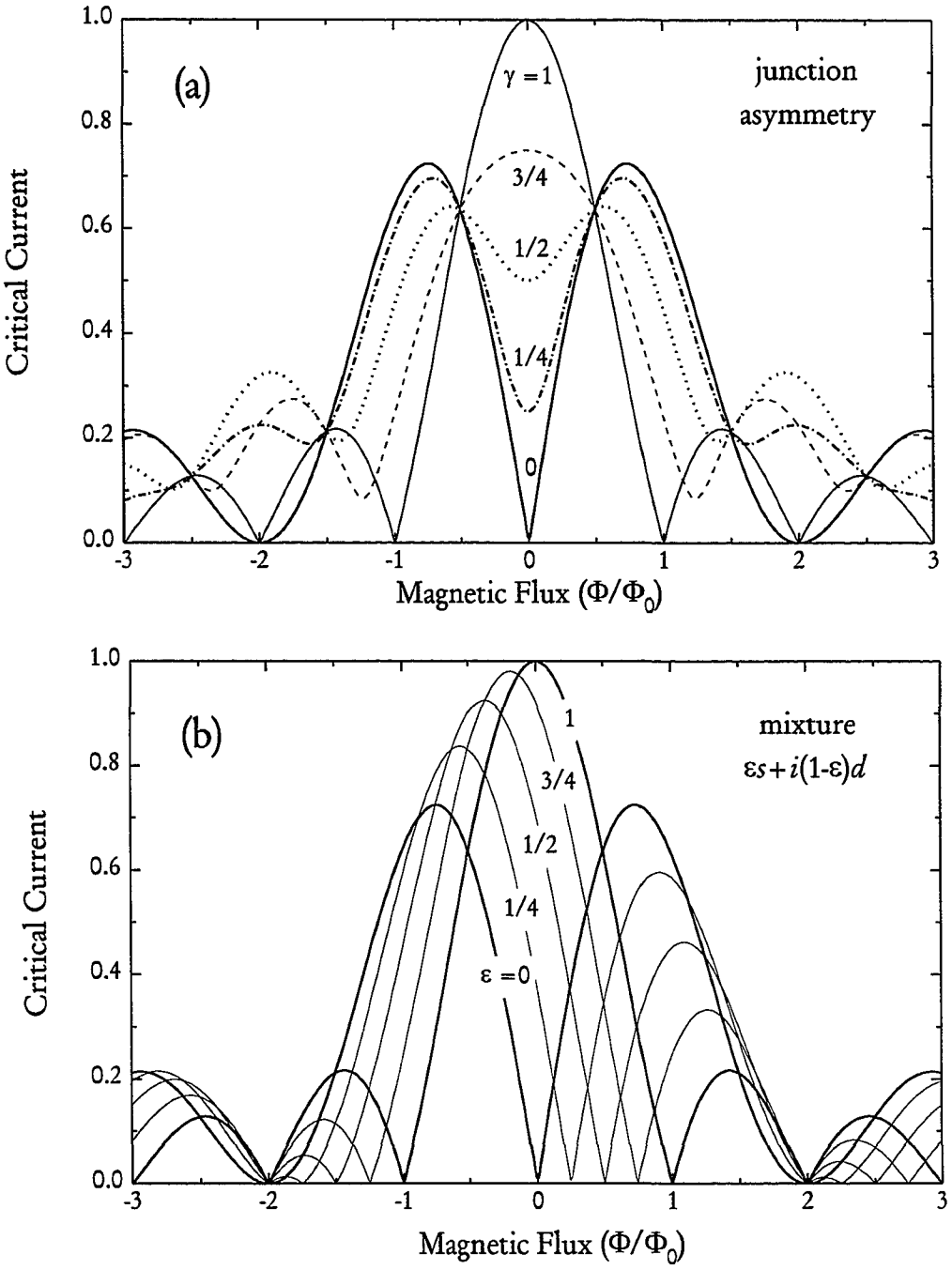

Figure 7.5. (a) Effect of geometric asymmetry on the single-junction modulation of a corner junction for *d*-wave symmetry, showing the residual critical current at zero field. There would be no effect for *s*-wave symmetry. (b) Single-junction modulation patterns calculated for the $s + id$ state with a fraction ε of *s*-wave component, showing the shift in the dip position from zero field and the imbalancing of the peak heights as ε increases.

The observed corner junction diffraction pattern also provides strong evidence against the proposed $s+id$ state. The critical current modulation of a symmetric corner junction for an $s+id$ state, with a fraction ε of s-wave pairing, is given by

$$I_c(\Phi,\varepsilon) = J_0 A \left| \frac{\sqrt{[1-\cos(\pi\Phi/\Phi_0)][1-\cos(\pi\Phi/\Phi_0)-\pi\varepsilon]}}{\pi(\Phi/\Phi_0)} \right|,$$

which reduces to the symmetric *d*-wave diffraction pattern for $\varepsilon = 0$ and to the usual *s*-wave Fraunhofer diffraction pattern for $\varepsilon = 1$, as shown in Figure 7.5(b). Miller *et al.* (1995) have given an analytical expression for the combined case of $s+id$ pairing and junction asymmetry. The first key point is that the critical current dip for *d*-wave pairing is not suppressed by an (imaginary) *s*-wave component, but rather the dip is shifted linearly in flux by $\varepsilon\Phi_0$. The second key point is that the fractional imbalance in the peak heights for small ε is roughly equal to ε, allowing us to place an upper limit of about 5% (from all of our corner junction measurements) on the amount of *s*-wave component in a $s+id$ pairing state.

These single junction measurements have several distinct advantages over the dc SQUID measurements described in the last chapter. First, the single junction coupling area is substantially smaller (typically by a factor of 100) than the dc SQUID loops. As a result, the magnetic field scale for coupling a flux quantum to the junction is much larger, rendering residual fields relatively unimportant. The smaller area also substantially reduces the probability of flux trapping near the junction. Perhaps the most significant advantage is that the shape of the diffraction pattern indicates where the zero for magnetic flux in the junction occurs. For both the *s*-wave and *d*-wave

cases, the diffraction pattern is symmetric around zero field in the absence of trapped magnetic flux near the junction. The effect of trapped flux is to skew the diffraction pattern significantly, destroying the mirror symmetry about zero flux. This behavior is shown in Figure 7.6(a), which shows a measured diffraction pattern for a trapped corner junction. To demonstrate the effects of flux trapping, we have calculated the modulation of the critical current with field for junctions with a magnetic vortex trapped near the junction. We model the vortex by assuming a non-uniform magnetic field through the junction barrier, consisting of the uniform applied field plus a Gaussian-distributed flux contribution localized in the junction. For both the *s*-wave and *d*-wave cases, the diffraction pattern is significantly distorted, giving a clear signature when a trapped vortex is present. In Figure 7.6(b), we show the critical current modulation for a corner junction on a *d*-wave crystal with a vortex of width 10% of the junction width and total integrated flux $\frac{\Phi_0}{2}$, located halfway between the corner and one edge of the junction; the diffraction pattern closely models the experimental pattern of Figure 7.6(a). The critical current modulation for *s*-wave and *d*-wave corner junctions with the vortex trapped at several different positions along the junction is shown in Figure 7.7, demonstrating that any flux trapping destroys the mirror symmetry of the diffraction patterns.

The key point is that for the single junction measurements, symmetry in the diffraction pattern is a strong indication that there is no flux trapping in the junction. This is in sharp contrast to the SQUID measurements in which trapped flux only shifts

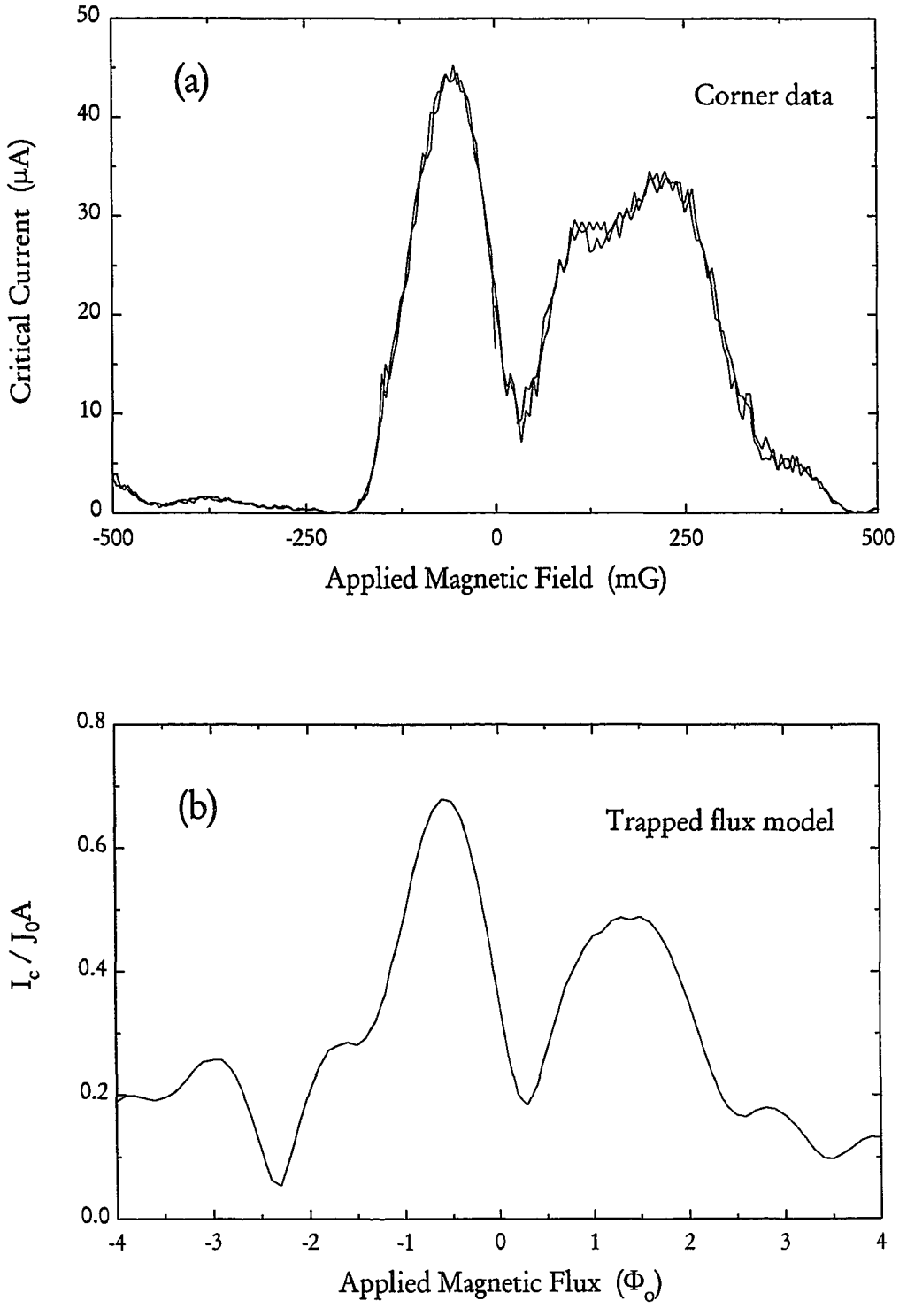

Figure 7.6. (a) Measured critical current modulation with applied field for a corner junction showing asymmetry arising from trapped magnetic flux near the junction. (b) Calculated modulation pattern for a vortex located halfway between the corner and edge of a corner Josephson junction, assuming a *d*-wave pairing state.

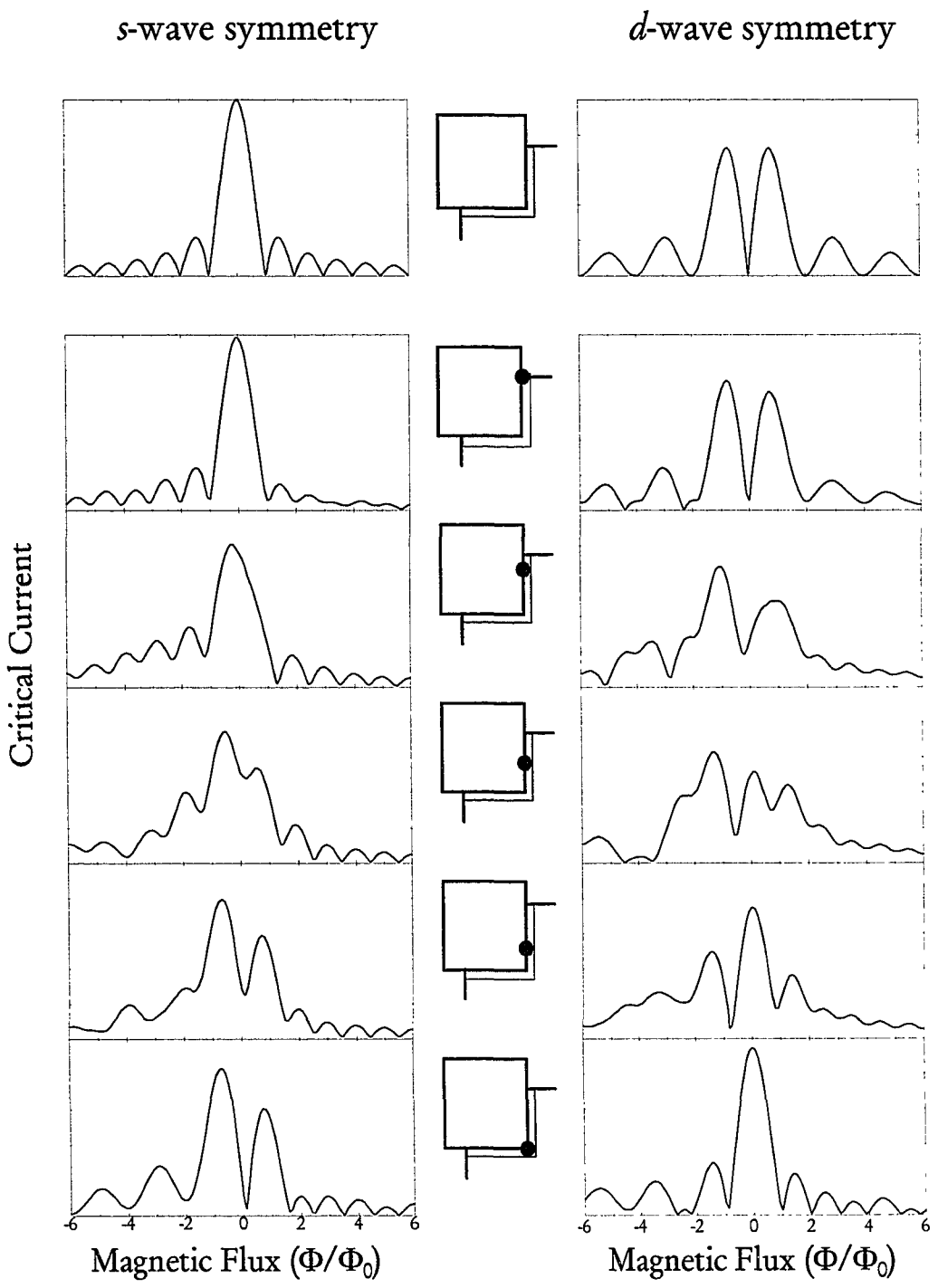

Figure 7.7. Effect of trapped magnetic vortices on the single junction modulation patterns for corner junctions with *s*-wave and *d*-wave symmetry for different vortex locations. Note that the presence of the vortex always breaks the polarity symmetry of the diffraction pattern, providing a clear test for the presence of trapped flux.

the periodic flux modulation and is virtually indistinguishable from an intrinsic phase shift. Finally, we emphasize that the symmetrical dip observed in the critical current is not easily explained nor mimicked by any other mechanism; to our knowledge such behavior has rarely if ever been reported in the extensive literature on diffraction patterns in single Josephson junctions.

In summary, we find strong evidence for a sign change of the order parameter between orthogonal directions in YBCO, consistent with a $d_{x^2-y^2}$ pairing state symmetry. The primary indication is a cusp-like suppression of the critical current near zero applied field in junctions that tunnel partially into the *a* and *b* directions at the corner of the crystal. Junctions on the *a* or *b* edges exhibit conventional Fraunhofer diffraction patterns as expected. These measurements are largely impervious to junction asymmetries and trapped magnetic flux in the junction.

Chapter 8

OTHER PHASE-SENSITIVE EXPERIMENTS

An experimental result in physics is not widely accepted until it has been reproduced elsewhere. Our initial observation of a π phase shift between orthogonal directions in YBCO in bimetallic dc SQUIDs sparked many additional phase-sensitive experimental tests of the pairing state symmetry. At a fundamental level, all of these experiments measure the relative phase of the order parameter using a dc SQUID or multiply-connected loop geometry. Most, but not all, find strong evidence for the π phase change between orthogonal directions in YBCO. I refer the reader to Barone (1994) for an independent review of these experiments.

Brawner and Ott (1994) have reproduced our experiment in the most direct way using a bimetallic Nb-YBCO dc SQUID. The SQUID was made by pressing a YBCO single crystal against a edges of a semicircle machined in a solid Nb body, connecting two YBCO-Nb point contact junctions in a SQUID geometry. Instead of trying to reduce the effects of trapped flux and residual field on the SQUID with magnetic shielding, they used identical Nb-Nb SQUIDs on either side of the Nb-YBCO SQUID for a relative phase comparison. Phase shift information was obtained from the bias-current dependence of an ac voltage across the SQUID that was produced by an ac flux modulation of $\frac{1}{2}\Phi_0$. The magnetic flux threading the three SQUIDs was assumed to be the same if the outer two Nb-Nb SQUIDs were in phase

with each other, with the relative phase of the Nb-YBCO SQUID obtained in comparison to the other two. They found a relative phase shift of $160° \pm 30°$ between the Nb-YBCO and Nb-Nb SQUIDs, in agreement with our measurements.

Using a scanning SQUID microscope, Tsuei, Kirtley and others (Tsuei *et al.*, 1994; and Kirtley *et al.*, 1995) at IBM have measured flux quantization in superconducting YBCO rings with zero, two, and three grain boundary junctions. If the order parameter changes sign an odd number of times around a ring, there is a cumulative π phase shift. Screening currents are generated (for a sufficiently large loop inductance) to make up the extra π phase shift as required by phase coherence and flux quantization. This results in a spontaneous magnetization (at zero applied magnetic field) equivalent to a half-integer flux quantum, which can be measured using a scanning SQUID microscope.

To fabricate the rings, Tsuei *et al.* (1994) deposited an epitaxial thin film of YBCO (*c*-axis normal) onto a $SrTiO_3$ tricrystal, with grain boundary junctions formed at the interfaces between the three sections. The grain boundary angles were controlled by the relative crystalline orientation of the underlying tricrystal, with the *a*- and *b*-axes of the YBCO aligned along the (100) and (010) axes of the $SrTiO_3$ substrate in each section.

The YBCO rings were defined using ion milling, with rings containing zero, two, or three grain boundary junctions. The tricrystal was designed so that the order parameter would change sign an even number of times around a zero or two junction ring, and an odd number of times for a three junction ring. Thus a zero or two

junction ring would not be frustrated, while a three junction ring would be frustrated and have a spontaneous magnetization equivalent to a half-integer flux quantum. This is exactly what was seen in the experiment, with the three junction ring always having a half-integer flux quantum of trapped flux, compared to the zero and two junction rings which only had whole-integer flux quantum. In addition, by using a tricrystal with slightly different grain boundary angles, Tsuei *et al.* were able to determine that the nodes where the order parameter changed sign were within 10° of a 45° angle, ruling out extended *s*-wave pairing and providing further strong evidence for $d_{x^2-y^2}$ pairing.

A scanning SQUID microscope was also used to scan bimetallic thin film YBCO-Ag-Pb(In) dc SQUIDs by Mathai, Wellstood and others (1995) at the University of Maryland. As in our experiment, half of the SQUID was made of YBCO, and the other half was made from an *s*-wave superconductor Pb(In). Two geometries were used for the SQUIDs: one with junctions oriented both normal and parallel to the *a*-axis of the YBCO (equivalent to our corner SQUID), and another with both junctions oriented normal to the *a*-axis (equivalent to our edge SQUID). As in the IBM experiment, they observed spontaneous magnetization of a half-integer flux quantum in the corner SQUID geometry, and only whole-integer flux quantization in the edge SQUID geometry. In addition, they checked for time-reversal symmetry in the current-flux SQUID characteristics by reversing all fields and currents, including those in the SQUID used to scan the bimetallic SQUIDs. They concluded that the

order parameter was time-reversal-invariant with a phase shift of $(0.98 \pm 0.05)\pi$ between the orthogonal *a*- and *b*-axes of YBCO.

Both of the scanning SQUID experiments have found evidence for a π phase shift between orthogonal direction in thin films of YBCO. Since they are capable of probing the phase anisotropy, this implies that tunneling in grain boundary and edge junctions is directional even though the interfaces are rough on the scale of the coherence length (Van Harlingen, 1995).

The π phase shift is not seen in all such thin film experiments with rough interfaces. Chaudari and Lin (1994) measured the critical current from an included hexagon region of a YBCO thin film across a continuous grain boundary junction to the surrounding region. The *a*- and *b*-axes of the hexagon were misaligned by 45° with respect to the surrounding film. In a $d_{x^2-y^2}$ symmetry the different faces were predicted to carry different critical currents (two with a positive sign, two with a negative sign, and two close to zero). A uniform monotonic decrease in critical current was observed as successive edges of the hexagon were excluded from the measurement. Each edge contributed equally to the total critical current (opposite to what was predicted for *d*-wave symmetry); this was taken as evidence for *s*-wave pairing.

Since the circumference of the hexagon was much larger than the penetration depth (by a factor of order 1000), the grain boundary junction was in the long junction limit. In addition, the lithographically defined interface was considerably rough. Under these conditions, Millis (1994) showed that it was energetically favorable for

Josephson vortices to form along the interface and allow each face of the hexagon to carry the same maximum critical current. Thus, the experiment of Chaudari and Lin is inconclusive with respect to the pairing state symmetry.

The long junction limit has also been studied systematically by Miller *et al.* (1995) using a tricrystal substrate similar to that of the IBM group led by Tsuei. Instead of rings, a single frustrated YBCO grain boundary junction (conceptually equivalent to our corner junction) was fabricated where the different sections of the tricrystal meet. The width of the junction (and its critical current density) was varied to explore both the short and long junction limits. In the short junction limit, a pronounced dip in the critical current was seen at zero magnetic flux, although the diffraction patterns had complicated structure that was likely due to junction roughness and critical current inhomogeneities. In the long junction limit, however, only a peak in the critical current was observed. This agreed with their theoretical analysis showing that both *s*- and *d*-wave junctions should have the same *s*-wave-like behavior in the long junction limit.

Another phase-sensitive experiment in which frustration may be a consequence of $d_{x^2-y^2}$ pairing is the paramagnetic Meissner effect or Wohlleben effect (Braunisch *et al.*, 1993). In this experiment, a field-cooled paramagnetic magnetization is observed in certain BSCCO samples. A review of this experiment in the context of *d*-wave symmetry has been recently completed (Sigrist and Rice, 1995). Sigrist and Rice (1994) suggested that a possible explanation for this phenomena was the existence of spontaneous supercurrents between multiply-connected *d*-wave superconducting

islands. At zero magnetic field, the spontaneous currents (created to balance intrinsic π phase shifts due to *d*-wave pairing in frustrated multiply-connected loops) would be randomly oriented and the usual Meissner effect would be observed. A small magnetic field applied during cooling, however, would polarize the spontaneous currents, leading to the paramagnetic magnetization that is seen experimentally. The theoretical interpretation of this experiment is not completely resolved, as Thompson *et al.* (1995) have recently reported a similar effect in disks of Nb, a conventional *s*-wave superconductor.

A different class of phase-sensitive experiments involves Josephson tunneling in the *c*-axis direction between YBCO and a conventional *s*-wave superconductor. While it is relatively easy to obtain supercurrent into the *a-b* plane directions, that is not the case in the *c*-axis direction. One explanation is that the extremely short *c*-axis coherence length and surface contamination (or de-oxygenation) suppresses Josephson coupling. Another explanation is derived from a $d_{x^2-y^2}$ pairing symmetry. Since it is generally believed that YBCO has a cylindrical Fermi surface and thus no density of states in the *c* direction, it is likely that the tunneling process must involve some component of transverse momentum. Assuming that Josephson tunneling samples the in-plane order parameter according to this small transverse momentum, the angular average of a $d_{x^2-y^2}$ order parameter (with positive and negative lobes of equal magnitude) is zero. Thus, to first order, no supercurrent would be expected in a *c*-axis junction between an *s*-wave and tetragonal *d*-wave superconductor. There could be

supercurrent with an orthogonal *d*-wave superconductor such as YBCO, however, since the magnitudes of the positive and negative lobes would likely be different and thus lead to a non-zero angular average.

Two groups have reported supercurrent in c-axis YBCO-Pb tunnel junctions and have obtained diffraction patterns of critical current versus magnetic field. Iguchi and Wen (1994) found a dip in the diffraction pattern, which they modeled as a mixture of tunneling into exposed *a* and *b* faces and *a-b* corners of micrograins formed during the growth of the *c*-axis-oriented YBCO thin film. They neglected to account for the global phase coherence between the many physically separated tunneling regions, thereby weakening the conclusion that *d*-wave symmetry was responsible for their diffraction patterns.

In contrast, the group at San Diego led by Bob Dynes observed nearly ideal Fraunhofer diffraction patterns in *c*-axis YBCO-I-Pb tunnel junctions fabricated on chemically etched single crystals (Sun *et al.*, 1994). They recovered the accepted YBCO penetration depth in the *c*-axis from the modulation period and geometric widths of the junctions, giving support to their claim of tunneling only in the *c*-axis direction. The magnitude of the I_cR_n product (where I_c is the critical current and R_n is the normal state junction resistance) was typically reduced from the usual Ambegoakar-Baratoff value by a factor of order 10 for crystals, and by a factor of order 100 for heavily twinned *c*-axis-oriented thin films (Katz, 1995). They concluded that it was difficult to explain their results with simple *d*-wave symmetry. Explaining this experiment is one of the most interesting challenges for the $d_{x^2-y^2}$ pairing scenario;

our own attempts to understand supercurrent in *c*-axis tunnel junctions will be presented in the next chapter.

In summary, a compilation of the key experiments designed to determine the symmetry of the pairing state is shown in Table 2. A star indicates that the results of an experiment (listed in left column) are consistent with a particular pairing state symmetry (listed along the top). The question marks indicate that an alternative explanation has been proposed, suggesting that the experimental results may in fact be consistent with a particular pairing state symmetry. Many of the experiments finding evidence for $d_{x^2-y^2}$ pairing can place limits on the maximum fraction of *s*-wave component in a $s+id$ mixture state; this maximum fraction is listed as a percentage in the $s+id$ column.

Experiment	Research Group	Isotropic *s*-wave	Anisotropic *s*-wave	Extended *s*-wave	Pure $d_{x^2-y^2}$	Mixture $s+id$
Magnitude measurements	many		★	★	★	★
Penetration depth	U. of British Columbia (Hardy, Bonn, ...)		★	★	★	2%
ARPES	Stanford U. (Z.-X. Shen, Dessau, ...)		★	?	★	20%
dc SQUID interferometry	U. of Illinois (Wollman, Van Harlingen, ...)				★	15%
dc SQUID interferometry	ETH (Brawner and Ott)				★	10%
dc SQUID magnetometry	U. of Maryland (Mathai, Wellstood, ...)				★	5%
Tricrystal ring magnetometry	IBM (Tsuei, Kirtley, ...)				★	3%
Biepitaxial junctions	IBM (Chaudari, Lin, ...)	★	?	?	?	?
Single-junction modulation	U. of Illinois (Wollman, Van Harlingen, ...)				★	5%
Single-junction modulation	U. of Houston (Miller, *et al.*)				★	25%
c-axis junction modulation	U. of California, San Diego (Sun, Dynes, ...)	★	★	★	?	★
c-axis (*a*-*b* steps) junction modulation	U. of Tsukuba, Japan (Iguchi and Wen)				★	25%

Table 2. Compilation of key experiments designed to determine the symmetry of the superconducting pairing state.

Chapter 9

UNFINISHED BUSINESS

Experimentalists tend to focus solely on experiments that have produced exciting new results and often do not report on failures or unfinished projects. This is understandable given human nature and the current funding situation, in which it is simply not enough to do good, basic work. The funding agencies preferentially award money to projects that appear guaranteed to produce results. Thus, experimentalists must start out in new directions before they receive the funding to do so. This project was a example of post-funding, in which a new avenue of research is started (using research funds technically designated for something else) to insure that the new direction is promising enough to merit funding. The whole system places failure in such a negative light that unproductive scientific forays may simply go unreported, lest they be held against the applicant in the next grant award/renewal cycle. The problem is that withholding such information makes it more difficult for the next researcher to accomplish similar goals.

It is often said that a third-base coach in baseball is not doing his job unless he occasionally gets a runner thrown out at home plate. The same holds for scientists, who must most effectively spend the resources the nation chooses to invest in science. This involves taking risks and exploring new possibilities, and recognizing the simple truth that experiments do not always work the way we want them to work. In this

spirit I will discuss several of our unfinished experiments, as well as our motivation for attempting them.

Other cuprates. The major thrust of our follow-up experiments has been to extend our measurements to cuprates other than YBCO. All of the direct phase-sensitive measurements of the π phase shift between orthogonal directions have been done on crystals or thin films of YBCO. The obvious question that must be addressed is whether *d*-wave pairing symmetry is a general property of the cuprates or simply unique to YBCO.

One of the other cuprates that we chose was $Nd_{1.85}Ce_{0.15}CuO_4$ (NCCO). There are many indications that the electron-doped Nd family is very different from the rest of the hole-doped cuprates. NCCO has different normal state dependences on temperature that other cuprates: the resistance goes as T^2 (compared to T in YBCO) and the Hall angle as T^4 (compared to T^2 in YBCO). Unlike other cuprates, measurements of the temperature dependence of the surface impedance and penetration depth of NCCO crystals and films can be accurately modeled with an *s*-wave symmetric gap (Anlage *et al.*, 1994). Point contact tunneling spectroscopy was used by Huang *et al.* (1990) to extract the $\alpha^2 F(\omega)$ Eliashberg function, which compared favorably to the phonon density of states and led to a theoretical T_c value consistent with experiment. This suggests that conventional *s*-wave (phonon-mediated) pairing may be important.

I tried to measure phase shifts in NCCO using single crystals provided by R.L. Greene's group at the University of Maryland. Following the same procedure as previously described for YBCO, I obtained substantially different results in making junctions on NCCO crystals. The junctions were higher in resistance that those made on YBCO crystals and did not support supercurrent. Thus, no phase measurements could be made.

We believe that the surface of NCCO is significantly harder to tunnel into than YBCO. Others have also had difficulty making good contacts to NCCO crystals (R. L. Greene, private communication, 1995). Z. X. Shen and co-workers were able to prepare clean surfaces for angle-resolved photoemission studies of NCCO crystals by cleaving the crystals in-situ (in vacuum) perpendicular to the *c*-axis. That option is not possible for our experiment as we found that cleaving NCCO parallel to the *a* and *b* faces created rough surfaces. We are in the process of trying to etch the as-grown surface before evaporating Au, which may remove a particularly tough "dead layer" and provide suitable contacts to the crystal.

In addition to NCCO, we have also attempted to obtain Thallium-based crystals suitable for SQUID measurements. Our motivation comes from a recent theoretical explanation by Kathy Levin and co-workers (Liu *et al.*, 1995) of the π phase shift observed in corner SQUID experiments, an explanation that applies only to cuprates with more than one CuO_2 plane per unit cell. They point out the existence of in-phase and out-of-phase states associated with each of the subbands that are generated when the single-layer problem is transformed to a bilayer problem. An in-

phase gap results from the intralayer interaction being dominant, and out of phase behavior when the interlayer interaction is dominant. Depending on whether the respective interactions are attractive or repulsive, the predicted phase shift in a corner SQUID experiment can be either zero or π. This suggests that the observed π phase shift can be consistent with *s*-wave symmetry in a bilayer cuprate.

To test this proposal, we have tried to do our phase-sensitive SQUID experiment on Tl 2212, which only has one CuO_2 plane and should not show the π phase shift. Unfortunately, the crystals of Thallium material that we have received have not had the smooth growth faces and sharp corners necessary to ensure directional tunneling. In addition, due to the different chemistry of the Tl system, we cannot anneal Au on Thallium-based crystals at the same high temperature as with YBCO, making it harder to fabricate superconducting junctions.

We have also made junctions on $Bi_{1-x}K_xBaO_3$ (BKBO) single crystals. This was done to address concerns about the effect of the corner in our corner SQUIDs and junctions, as raised by Klemm (1994) and described in Chapter 6. In an attempt to resolve the issue, we chose BKBO because it is generally believed to have a conventional *s*-wave gap and excellent quality single crystals were available from Pendgi Han and David Payne at Urbana. Junctions were prepared in a slightly different fashion than for YBCO. Based on our research group's experience in growing BKBO films and making contact to them, I ion-milled the BKBO crystal in a partial oxygen atmosphere before evaporating Ag as the barrier material. The Ag was annealed in a rapid thermal anneal furnace at 200° C or less in flowing oxygen for 30 -

90 minutes. The rest of the junction preparation was the same as for YBCO, except that liquid nitrogen was used to keep the crystal from heating during all ion-milling and evaporation steps. The completed junctions are shown in Figure 9.1, demonstrating that the technique of setting crystals in polyamide is readily transferred to crystals of different sizes. In Figure 9.2, bubbling of the Ag layer is clearly visible, and may explain our failure to produce useable junctions. The junctions occasionally had decent tunneling characteristics but never any supercurrent, so no phase-sensitive measurements were possible.

Figure 9.1. SEM photograph of Pb-Ag-BKBO tunnel junctions fabricated on the corner and edges of a BKBO single crystal set in polyamide.

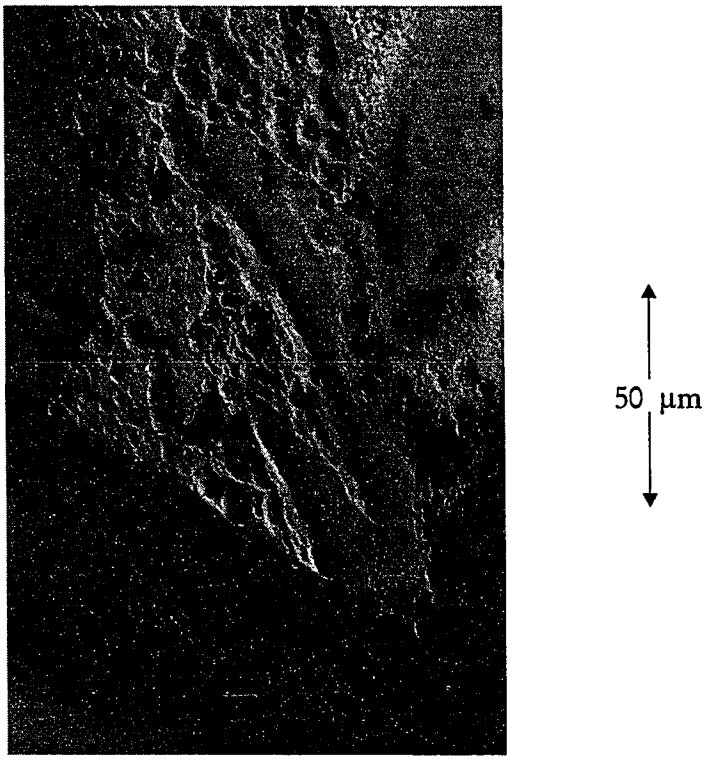

Figure 9.2. SEM close-up of a Pb-Ag-BKBO tunnel junction showing bubbling of the Ag layer. The regions of the junction with no bubbling do not have Ag underneath.

Non-orthogonal angle measurements. In addition to trying to extend our measurements to other cuprates, we also attempted to measure the relative phase of the order parameter in YBCO as a function of angle, not just between the orthogonal *a*-axis and *b*-axis directions. Our first effort was cleave YBCO crystals along the 45° direction in the *a*-*b* plane and fabricate Pb-Au-YBCO junctions on the exposed face. In this geometry, the supercurrent tunneling would be into the node direction for a $d_{x^2-y^2}$ pairing state symmetry and no supercurrent would be expected at zero field, assuming a perfectly smooth interface and no *a*-*b* anisotropy. We were excited to

discover smooth regions on the cleaved face of the crystal when it was examined using a Scanning Electron Microscope (SEM). In addition, there were jagged or serrated regions in which the surface was composed of many *a-b* corners in a row. A SEM photograph of the smooth and serrated regions is shown in Figure 9.3.

We postulated that the junctions fabricated on the two surfaces, smooth and serrated, would have very different magnetic field modulation patterns. A perfectly smooth interface in the node direction would have no supercurrent even when a sizable magnetic field was applied. On the other hand, tunneling in the serrated junction would be divided into alternating *a*-faces and *b*-faces with a characteristic length smaller than 1 μm. Assuming that the exposed *a*-faces and *b*-faces were equal in area and critical current density, the supercurrent in the many *a*-axis and *b*-axis directions would cancel each other to produce no net supercurrent at zero magnetic field, just as in the corner junction experiment described in Chapter 7. Compared to a single corner junction, however, a much larger magnetic field must be applied to the serrated junction to bring the many alternating faces into phase with each other to produce a large critical current, as shown in Figure 9.4.

The expected modulation pattern was not observed, however, as I was never able to fabricate a junction solely on a smooth region or serrated region. It was extremely difficult to cleave the YBCO crystals precisely along the 45° direction, even using twin lines as a natural guide for the razor blade. The few junctions that were made showed supercurrent with the usual Fraunhofer diffraction pattern, with no indication of unusual behavior other than a (possibly) reduced I_cR_n product. We

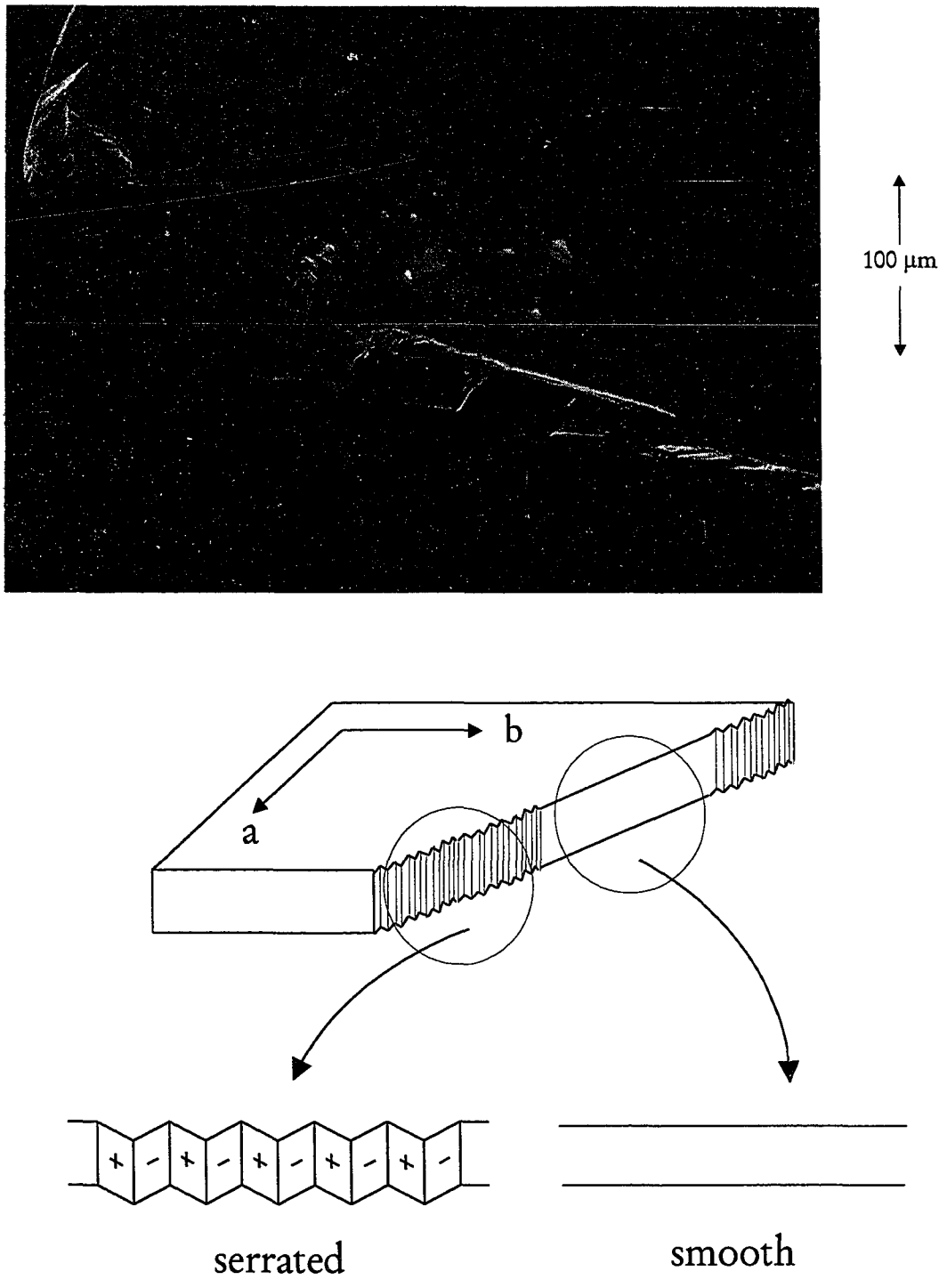

Figure 9.3. SEM photograph and drawing of serrated and smooth regions along the 45° cleaved face of a YBCO single crystal.

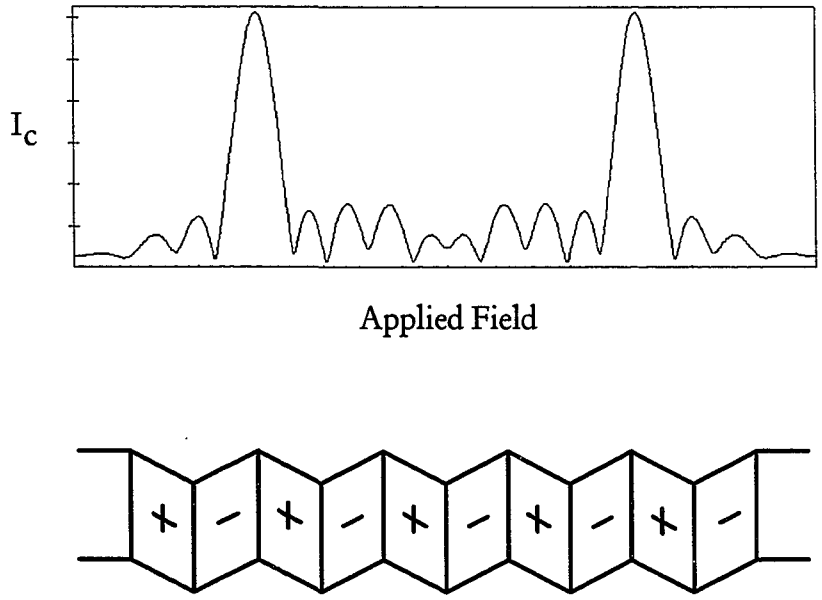

Figure 9.4 Expected diffraction pattern for a small number of serrations, with the sign of the order parameter indicated by + and − on each face.

suspect that the cleaving process always exposed substantially more *a*- or *b*-face surface area, making it impossible to see any interference effects due to the sign change of the order parameter.

c-axis tunneling. The other important experimental question that we addressed concerns the supercurrent observed in *c*-axis YBCO-Pb junctions by Sun *et al.* (1994), as discussed in Chapter 8. We wanted to understand why supercurrent was seen when a simple *d*-wave model predicted there should be no supercurrent. The following discussion is based on a paper written for the 1995 Stanford Conference on Spectroscopies in Novel Superconductors (Wollman *et al.*, to be published, 1995).

We proposed an extension of our SQUID experiments designed to understand the origin of the *c*-axis supercurrent. As shown in Figure 9.5, we wanted to construct dc SQUIDs or corner junctions by connecting Josephson junctions on the *c*-axis and the *a*- or *b*-axes of YBCO single crystals with a thin film of Pb, a conventional *s*-wave superconductor. The goal was to compare intrinsic phase shifts between the *c*-axis direction and the *a*- or *b*-axes (δ_{ac} and δ_{bc}) with the π phase shift we observed between the *a*- and *b*-axes (δ_{ab}).

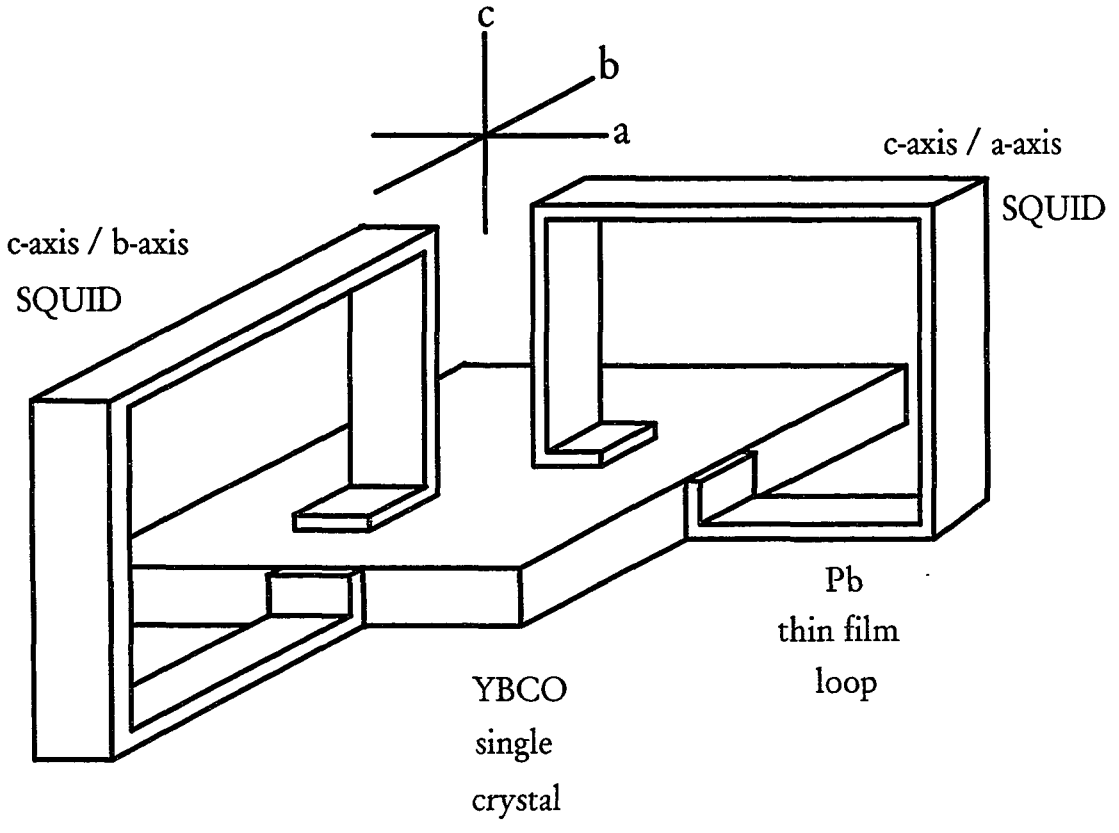

Figure 9.5. Proposed SQUID experiments designed to understand the origin of supercurrent in *c*-axis Pb-YBCO junctions.

The out-of-plane phase shifts to be measured provide crucial information about the nature of the *c*-axis supercurrent. The different scenarios that might explain the observed supercurrent can be distinguished by their very different phase shift predictions. One possibility is that the order parameter has an intrinsic *s*-wave component in addition to a pure *d*-wave symmetry. One example is a *d*-wave order parameter with an imaginary *s*-wave component. Although this is unlikely because a two component complex order parameter leads to a double transition that is not observed experimentally, I am choosing this state to illustrate possible phase shifts. Here, the angular average is non-zero due to the *s*-wave component, and the complex phase between the *s* and *d* components will be seen in the *c*-axis SQUIDs. For simplicity, we assume the positive lobes of the $d_{x^2-y^2}$ order parameter lie along the *a*-axis, and define intrinsic phase shifts with respect to the *c*-axis supercurrent. For $d+is$ order parameter with equal amounts of *d* and *s*, an *a*-axis/*c*-axis SQUID would have a phase shift of $\delta_{ac}=\frac{\pi}{4}$, compared to a phase shift of $\delta_{bc}=-\frac{\pi}{4}$ for *b*-axis/*c*-axis SQUIDs. For a non-equal mixture of *d* and *s*, such as $d+i\varepsilon\, s$, the phase shifts are $\delta_{ac}=\arctan(1/\varepsilon)$ and $\delta_{bc}=-\arctan(1/\varepsilon)$.

Another possibility is that the *c*-axis supercurrent results from the orthorhombicity of YBCO, which breaks the in-plane symmetry of the order parameter. One pair of order parameter lobes, for example the positive lobes oriented along the *a*-axis, can be larger in magnitude than the negative lobes, causing a non-zero angular average. This can occur in a $d+s$ (or $d+\varepsilon\, s$) order parameter where the

nodes are shifted away from 45°. In this scenario, as shown in Figure 9.6, an *a*-axis/*c*-axis SQUID would sample the same sign of the order parameter and would have no intrinsic phase shift. A *b*-axis/*c*-axis SQUID, on the other hand, would have an intrinsic phase shift of π. This explanation seems to us to be the most likely, as it fits certain aspects of the data in that the I_cR_n product of twinned crystals and films is substantially reduced compared to junctions on untwinned crystals (Sun *et al.*, 1994, Katz *et al.*, 1995).

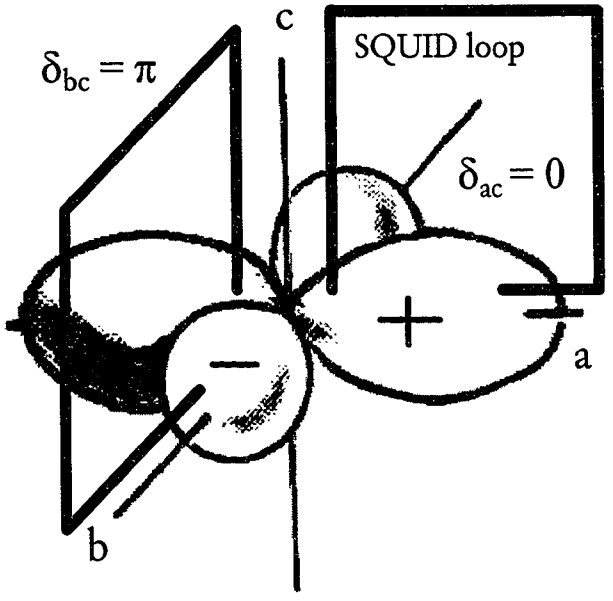

Figure 9.6. *a*-axis /*c*-axis and *b*-axis /*c*-axis SQUIDs and predicted phase shifts for orthorhombic distortion scenario.

Another possibility is that the etch needed to prepare a fresh *c*-axis surface exposes *a*- and *b*-faces which then carry supercurrent. We find that the standard 1%

(by volume) Br_2 in methanol etch is anisotropic, creating rectangular etch pits with aspect ratios of two to three in untwinned regions of YBCO single crystals. These etch pits are always elongated along the *b*-axis so that more *a*-face edges are exposed. In this scenario, the phase shifts would be identical to those described directly above. This argument is plausible but not probable, since the San Diego group obtains layer by layer etching of the *c*-axis YBCO surface as characterized with a STM, with no difference in the amount of *a*- and *b*-faces exposed (Dynes *et al.*, to be published, 1995).

Finally, it is possible to have both an intrinsic imaginary *s*-wave component of the order parameter and orthorhombic symmetry-breaking. This is equivalent to an order parameter symmetry of $d + \varepsilon e^{i\varphi} s$, where the angle φ is dependent on the relative magnitude of the orthorhombic distortion compared to the intrinsic imaginary *s* component. In this case, the phase shifts δ_{ac} and δ_{bc} would in general be different in magnitude and sign.

From an experimental standpoint, the necessary first step to making SQUIDs and measuring δ_{ac} and δ_{bc} is to obtain c-axis supercurrent. We start with excellent YBCO crystals that have been extensively characterized. A junction is prepared by etching a twinned YBCO crystal in the standard 1% Br_2 in methanol (or ethanol) solution for 5 to 15 minutes, exposing a fresh *c*-axis YBCO surface with shallow etch pits roughly 10 μm by 10 μm in lateral size. The YBCO crystal is set in polyamide and the junction areas are defined using a flexible shadow mask. A diffusion barrier (Sun *et al.*, 1994) of 10 - 20 Å of Ag is thermally evaporated, and is followed by 8000 Å of Pb. The samples are then mounted in a variable temperature cryogenic insert and

quickly cooled to 100 K. The measurements are taken in a μ-metal shielded cryostat in an rf-shielded room down to 2 K. Our junction sizes are roughly 200 μm × 200 μm, with normal state resistances ranging from 10 to 1000 Ω but generally 20 to 250 Ω.

To date, we have not been able to reproduce the *c*-axis junction supercurrent observed by the San Diego group. This failure has been my greatest disappointment during this work. Although we have tried to duplicate their procedure (A. G. Sun, private communication, 1994), we do not get as low normal state resistances as they report (0.1 Ω - 1 Ω). We speculate that we are limited by thermodynamic noise rounding, or that the I_cR_n product falls significantly with increased R_n.

On the other hand, the junctions show good quasiparticle tunneling characteristics. Tunneling is important because it should provide information about the microscopic interactions responsible for pairing in high temperature superconductivity. The conductance as a function of voltage for a typical junction is shown in Figure 9.7 for several temperatures. Following previous work (Gurvitch *et al.*, 1989), the conductance is normalized to the conductance at 100 mV, although the dynamic resistance at 100 mV for this junction only changed from 100 Ω to 95 Ω between 105 K and 8 K. The voltage polarity refers to the YBCO electrode. Below the Pb critical temperature, a Pb superconducting gap appears along with weak structure due to Pb phonons at 6 and 10 mV. The tunneling characteristics include very reproducible structure as shown in Figure 9.8 for four junctions measured at a temperature of 2 K. The normal state resistances of these junctions ranged from

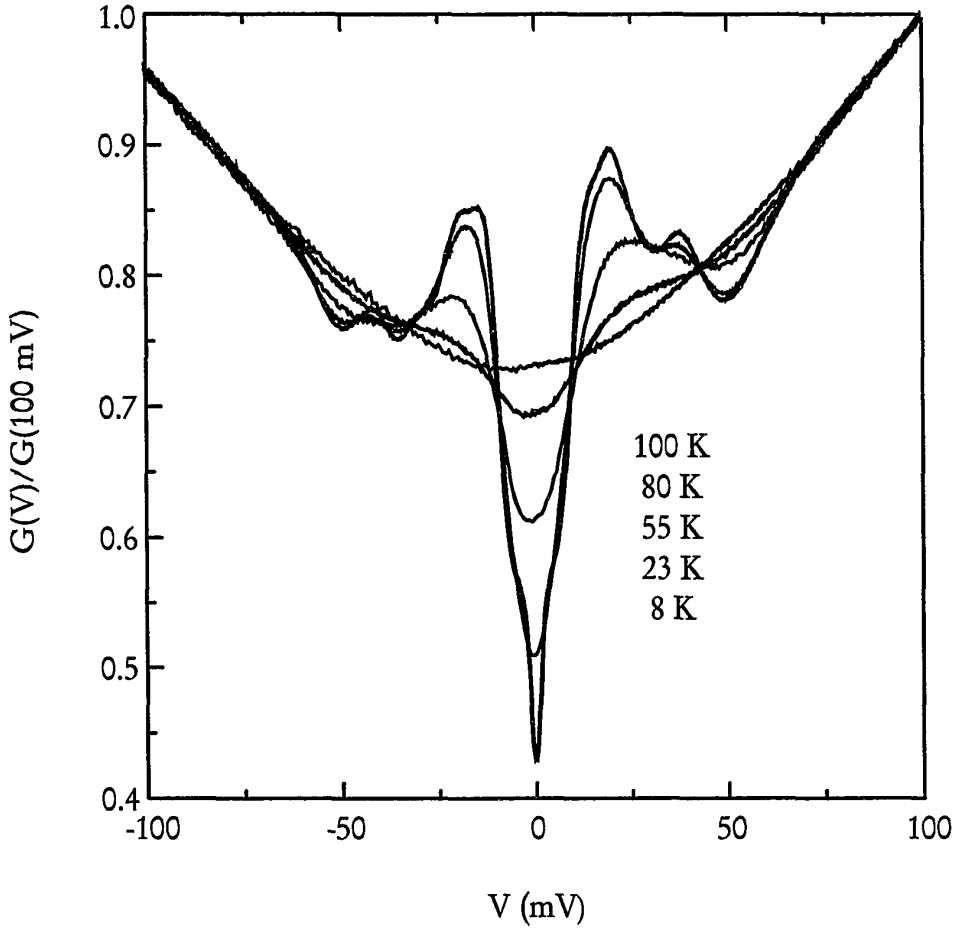

Figure 9.7. Conductance *vs.* voltage for a Pb-YBCO *c*-axis tunnel junction at the indicated temperatures.

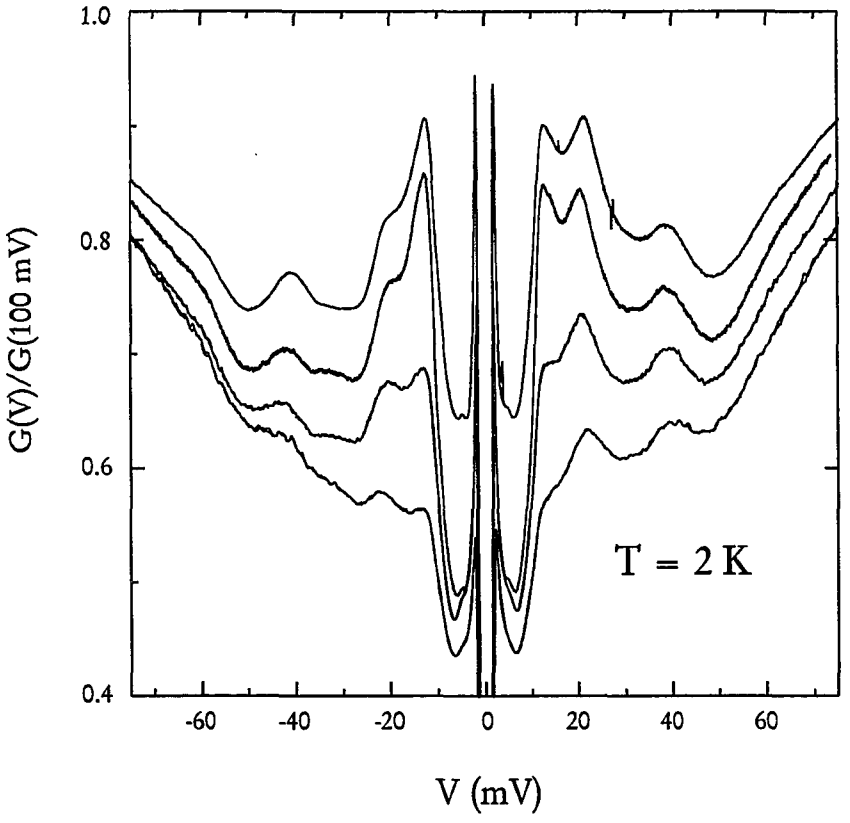

Figure 9.8. Conductance *vs.* voltage for four Pb-YBCO *c*-axis junctions at 2 K.

50 to 250 Ω. In Figure 9.9 the asymmetry of positive and negative voltages is shown for two junctions, with most features symmetric in voltage except for the peaks at roughly 38 mV and -42 mV. The junctions had leakage currents of 1% to 2% at 2 K, as seen in the current-voltage characteristic in Figure 9.10.

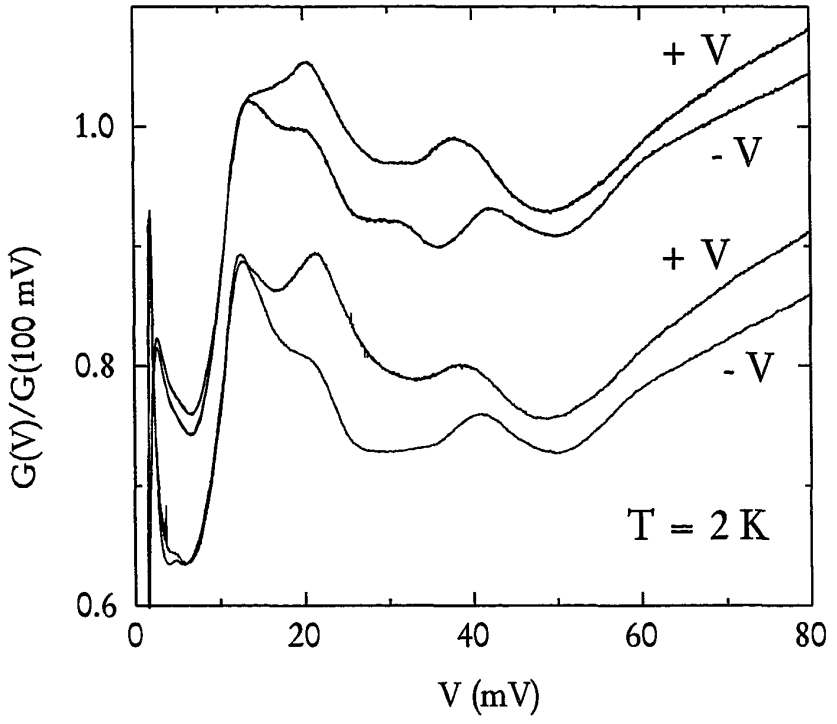

Figure 9.9. Conductance *vs.* voltage asymmetry for two Pb-YBCO *c*-axis tunnel junctions, with voltage polarity as indicated. The top set of curves has been shifted vertically by 0.15 for clarity.

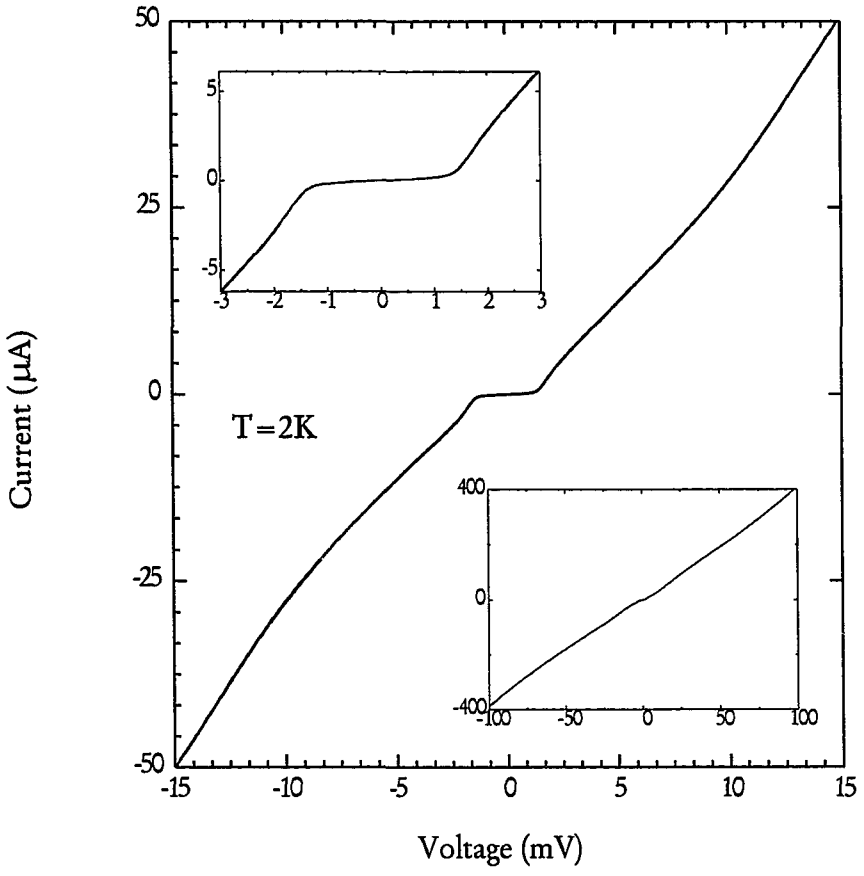

Figure 9.10. Current *vs.* voltage for a Pb-YBCO c-axis tunnel junction showing low leakage at 2 K.

Chapter 10

CONCLUSION

In this thesis, I have presented phase-sensitive measurements of bimetallic Pb-Au-YBCO dc SQUIDs and Josephson junctions designed to determine the symmetry of the superconducting order parameter in YBCO. Using the bimetallic SQUID as an superconducting phase interferometer, we find that there is an intrinsic phase shift of π in the relative phase between orthogonal directions in momentum space in YBCO, equivalent to a sign change of the gap. This sign change is consistent with a $d_{x^2-y^2}$ pairing state symmetry.

I would like to conclude with a few personal observations of life in the scientific spotlight. This has been a very visible experiment and has attracted much attention from the superconducting research community. What is particularly striking, though, is the coverage of this issue -- *s*-wave vs. *d*-wave -- by the popular science press. I am referring to several news articles and letter exchanges in the pages of *Physics Today*, *Science*, *The New Scientist*, and other publications (for example, see Levi (1993); Amato(1993); Clery (1994); Fox(1994); and Anderson (1993, 1994b, 1994c) with replies by Pines (1994b); Scalapino (1994a, 1994b)). Although part of this interest has been due to the great technological promise of the high T_c cuprate materials themselves, much of the attention has focused on the vocal and controversial opinions of many prominent theorists, particularly Philip Anderson and David Pines.

The mental image that is evoked is that of two giants, slugging it out in the middle of a pitched battle of trolls, ogres and other giants. To give you a flavor of this war of words, I have selected a few quotes from several of the exchanges. It is often difficult to determine who fired first, so I will arbitrarily start with a quote by Philip Anderson (1993) at a panel discussion on "*d*-wave Superconductivity" at the Conference on Spectroscopies in Novel Superconductors in Sante Fe, "The spin fluctuation 'theory' of high T_c superconductivity does not seem to me to have any of the characteristics in style or substance of a successful theory." Following a news article by Barbara Goss Levi in *Physics Today* (May 1993), Anderson (1994a) wrote a letter to complain that his negative comments about the spin fluctuation theory (for example, its computational complexity) had not been given enough press. Pines (1994b) felt it necessary to respond, firing back that his research "is easily subject to independent verification by a computationally literate theorist," and was followed by the additional replies of Scalapino and Shen. There were other articles and exchanges after the ones mentioned above, but I do not mean to belabor this discussion. However, I cannot resist including a quote (in Fox, 1994) from another theorist, Dick Klemm, "I think that the *d*-wave crowd is a real Mafia. They are just trying to control it [the debate] by screaming loudly." Klemm goes on to conclude that, "Sooner or later there's going to be a right and a wrong." From these exchanges, it seems to me that as much importance is placed on who is right, or more importantly, WHO IS WRONG, as is placed on the actual theories themselves.

Perhaps this vehemence is simply the result of the combative nature of theoretical physics, in which theories are proposed, attacked and defended until a victor emerges. As David Pines explained to me, theorists make a huge investment in their initial description of the problem and subsequent choice of Hamiltonian. In essence, they have placed a very large bet (their reputation, time and effort) at the outset, deciding up front what is the best approach to follow that includes all of the relevant physics. Only after carrying through their calculations do they discover if their initial intuition was accurate. After that, it becomes a poker game. The bigger the stakes, the more vigorously they will defend their theory. If they are wrong, there is often nothing else to do but fold and deal another hand (often in a different game on a new subject), as expressed in a common theorist put-down, "I hope that someday we find an experimental system for which your theory applies."

It is not my goal to malign only theorists; experimentalists are also capable of equivalent behavior, as I know from personal experience. Experimentalists typically do not have as much invested in specific experiments, however, and are able to appreciate someone else's new experiment without immediately being threatened by it. Perhaps this is because experiments only rarely compete in such a visible way as theories do, with the conflict between the photoemission results of Shen *et al.* (1993) and Ding *et al.* (1995a; 1995b) being an obvious exception. Another reason is that experiments are much more focused than theories, which must explain everything. It is also possible to devise alternative methods to measure an experimental quantity, as evidenced by the many phase-sensitive measurements (reviewed in Chapter 8) that

were inspired by our initial SQUID experiment, an experiment that thrust us into the scientific spotlight.

Of course, being in the scientific spotlight is nothing new for Urbana, which has a long tradition of excellence in superconductivity research, dating back to before Bardeen, Cooper, and Schrieffer formulated their successful theory of conventional low-temperature superconductors. Working within the interdisciplinary framework of the Materials Research Laboratory and the Science and Technology Center for Superconductivity, Urbana has fostered a climate of close collaboration between top theorists and experimentalists, making it an ideal place for this research to be successfully completed. We found that it was crucial to have access to the best possible samples of YBCO, as provided by Don Ginsberg's research group, as well as the theoretical support of Tony Leggett, who made the original suggestion for this experiment and also served as a source of right answers throughout this effort. The success of our project can be directly linked to the interdisciplinary and collaborative atmosphere at Urbana, making it ironic that our Materials Research Laboratory (designed to foster such collaborations) lost its NSF funding just after our experiments were completed.

In conclusion, being part of a very visible experiment has been a mixed blessing, as expressed in the ancient Chinese curse, "May you live in interesting times." These were definitely interesting times, making my graduate education quite exciting and eventful. On the other hand, while it is encouraging to know that your work is relevant and that others are interested in your results, being in the spotlight also forces

you to worry about the political aspects of science: how your results are being received and whether or not you are getting the credit you (think you) deserve. My graduate school experience has served to whet my appetite for all aspects of scientific research, from the actual practice of science to the politics of academic world.

REFERENCES

Alexandrov, A. S. and N. F. Mott, 1993, Supercond. Sci. Technol. **6**, 215.
Do Pairs Exist Above T_c?

Amato, I., 1993, Science **261**, 294.
Theory Meets Experiment in High T_c Superconductivity.

Anderson P. W., 1991, Phys. Rev. Lett. **67**, 3844.
"Confinement" in the One-Dimensional Hubbard Model: Irrelevance of Single-Particle Hopping.

Anderson, P. W., 1992, Science. **256**, 1526.
Experimental Constraints on the Theory of High T_c Superconductivity.

Anderson P. W., 1993, J. Phys. Chem. Solids **54**, 1457.
Remarks at the Panel Discussion on d-Wave Superconductivity.

Anderson, P. W., 1994a, Physica B **199**, 8.
Two New Developments in the Theory of High T_c Superconductivity.

Anderson, P. W., 1994b, Physics Today **47**, 11.
In Explaining High T_c, Is d-Wave a Washout?

Anderson, P. W., 1994c, Science **265**, 1789.
Superconductivity: The Real Dichotomy.

Anderson, P. W. and R. Schrieffer, 1991, Physics Today **44**, 54.
A Dialogue on the Theory of High T_c.

Anlage S. M., D. H. Wu, J. Mao, S. N. Mao, X. X. Xi, T. Venkatesan, J. L. Peng, R. L. Greene, 1994, Phys. Rev. B **50**, 523.
Electrodynamics of $Nd_{1.85}Ce_{0.15}CuO_4$ - Comparison with Nb and $YBa_2Cu_3O_{7-\delta}$.

Annett, J. F., N. Goldenfeld, and A. J. Leggett, to be published.

Annett, J. F., N. Goldenfeld, and S. R. Renn, 1990, in *Physical Properties of High Temperature Superconductors II*, edited by D. M. Ginsburg (World Scientific, New Jersey), p. 571.
The Pairing State Of $YBa_2Cu_3O_{7-\delta}$

Barone, A. and G. Paterno, 1982, *Physics and Applications of the Josephson Effect* (Wiley & Sons).

Barone A., 1994, Il Nuovo Cimento D 16, 1635.
Pairing State of High T_c Superconductors -- Comments on the Josephson Effect Experiments in the Context of the s- vs. d-Wave Debate.

Barrett, S. E., J. A. Martindale, D. J. Durand, C. H. Pennington, C. P. Slichter, T. A. Friedmann, J. P. Rice, and D. M. Ginsberg, 1991, Phys. Rev. Lett. **66**, 108.

Barzykin, V. D., Pines and D. Thelen, 1994, Phys. Rev. B **50**, 16052.
Spin Fluctuations in $La_{2-x}Sr_xCuO_4$ -- NMR Versus Inelastic Neutron Scattering.

Batlogg, B., 1991, Physics Today **44**, 44.
Physical Properties of High T_c Superconductors.

Beasley, M. R., D. Lew, and R. B. Laughlin, 1994, Phys. Rev. B **49**, 12330.
Time Reversal Symmetry Breaking in Superconductors -- A New Proposed Experimental Test.

Bednorz, J. G. and K. A. Muller, 1986, Z. Phys. **B64**, 189.
Possible High T_c Superconductivity in the Ba-La-Cu-O System.

Bickers, N. E., D. J. Scalapino, and S. R. White, 1989, Phys. Rev. Lett. **62**, 961.

Bonn, D. A., P. Dosanjh, R. Liang, and W. N. Hardy, 1992, Phys. Rev. Lett. **68**, 2390.
Evidence for Rapid Suppression of Quasiparticle Scattering Below T_c in $YBa_2Cu_3O_{7-\delta}$.

Bonn, D. A., R. Liang, T. M. Riseman, D. J. Baar, D. C. Morgan, K. Zhang, P. Dosanjh, T. L. Duty, A. MacFarlane, and G. D. Morris, 1993, Phys. Rev. **B 47**, 11314.
Microwave Determination of the Quasiparticle Scattering Time in $YBa_2Cu_3O_{6.95}$.

Brandow, B. H., 1993, J. Phys. Chem. Solids **54**, 1137.
Highly Anisotropic but Nodeless Gap from a Valence-Fluctuation Pairing Mechanism.

Braunisch, W., N. Knauf, G. Bauer, A. Kock, A. Becker, B. Freitag, A. Grutz, V. Kataev, S. Neuhausen, B. Roden, D. Khomskii, Wohlleben, D., J. Bock, and E. Preisler, 1993, Phys. Rev. B **48**, 4030.
Paramagnetic Meissner Effect in High Temperature Superconductors.

Brawner D. A. and H. R. Ott, 1994, Phys. Rev. B **50**, 6530.
Evidence for an Unconventional Superconducting Order Parameter in $YBa_2Cu_3O_{6.9}$.

Burns, G., 1992, *High Temperature Superconductivity* (Academic, New York).

Chakravarty, S., A. Sudbo, P. W. Anderson, and S. Strong, 1993, Science **261**, 337.
Interlayer Tunneling and Gap Anisotropy in High Temperature Superconductors.

Chaudhari, P. and Shawn-Yu Lin, 1994, Phys. Rev. Lett. **72**, 1084.
Symmetry of the Superconducting Order Parameter in $YBa_2Cu_3O_{7-\delta}$ Epitaxial Films.

Clarke, D. G., S. P. Strong, and P. W. Anderson, 1995, Phys. Rev. Lett. **74**, 4499.
Conductivity Between Luttinger Liquids in the Confinement Regime and c-Axis Conductivity in the Cuprate Superconductors.

Clarke, J., 1994, Scientific American **271**, 46.
SQUIDs.

Clery, D., 1994, Science **265**, 860.
New Clues to Superconductivity.

Coffey D., 1993, J. Phys. Chem. Solids **54**, 1369.
Effect of Spontaneous Decay of Superconductor Quasiparticles in the Tunneling Density of States.

Dagotto, E., 1994, Rev. Mod. Phys. **66**, 763.
Correlated Electrons in High Temperature Superconductors.

Dagotto, E., A. Nazarenko, and A. Moreo, 1995, Phys. Rev. Lett. **74**, 310.
Antiferromagnetic and Van Hove Scenarios for the Cuprates: Taking the Best of Both Worlds.

De Waele, A.Th. A. M. and R. De Bruyn Ouboter, 1969, Physica **41**, 225.
Quantum Interference Phenomena in Point Contacts Between Two Superconductors.

DeGennes, P. G., 1989, *Superconductivity In Metals And Alloys* (Addison-Wesley, New York).

Dessau, D. S., Z. X. Shen, D. M. King, D. S. Marshall, L. W. Lombardo, P. H. Dickenson, A. G. Loeser, J. DiCarlo, C. H. Park, A. Kapitulnik, and W. E. Spicer, 1993, Phys. Rev. Lett. **71**, 2781.
Key Features in the Measured Band Structure of $Bi_2Sr_2CaCu_2O_{8+\delta}$ -- Flat Bands at E_F and Fermi Surface Nesting.

Devereaux, T. P., D. Einzel, B. Stadlober, R. Hackl, D. H. Leach, and J. J. Neumeier, 1994, Phys. Rev. Lett. **72**, 396.
Electronic Raman Scattering in High T_c Superconductors -- A Probe of $d_{x^2-y^2}$ Pairing.

Ding, H., J. C. Campuzano, A. F. Bellman, T. Yokoya, M. R. Norman, M. Randeria, T. Takahashi, H. Katayama-Yoshida, T. Mochiku, K. Kadowaki, and G. Jennings, 1995a, Phys. Rev. Lett. **74**, 2784.
Momentum Dependence of the Superconducting Gap in $Bi_2Sr_2CaCu_2O_8$.

Ding, H., J. C. Campuzano, A. F. Bellman, T. Yokoya, M. R. Norman, M. Randeria, T. Takahashi, H. Katayama-Yoshida, T. Mochiku, K. Kadowaki, and G. Jennings, 1995b, Phys. Rev. Lett. **75**, 1425.
Momentum Dependence of the Superconducting Gap in $Bi_2Sr_2CaCu_2O_8$ -- Correction.

Dynes, R. C., *et al.*, 1995, to be published in J. Phys. Chem. Solids.

Fox, K. C., 1994, New Scientist 17 September, 32.
Materials Too Hot to Resist.

Geshkenbein, V. B., A. I. Larkin, and A. Barone, 1987, Phys. Rev. B **36**, 235.
Vortices with Half Magnetic Flux Quanta in "Heavy Fermion" Superconductors.

Gough, C. E., M. S. Colclough, and E. M. Forgan, 1987, Nature **326**, 855.
Flux Quantization in a High T_c Superconductor.

Greene, R. L., 1995, private communication.

Gurvitch, M., J. M. Valles, Jr., A. M. Cucolo, R. C. Dynes, J. P. Garno, L. F. Schneemeyer, and J. V. Waszczak, 1989, Phys. Rev. Lett. **63**, 1008.
Reproducible Tunneling Data on Chemically Etched Single Crystals of $YBa_2Cu_3O_7$.

Hardy, W. N., D. A. Bonn, D. C. Morgan, R. Liang, and K. Zhang, 1993, Phys. Rev. Lett. **70**, 3999.
Precision Measurements of the Temperature Dependence of λ in $YBa_2Cu_3O_{6.95}$: Strong Evidence for Nodes in the Gap Function.

Hirata, T. and Y. Asada, 1991, J. Supercond. **4**, 171.
A Review of the Size of the Energy Gap in Superconducting Oxides.

Hirschfeld, P. J. and N. Goldenfeld, 1993, Phys. Rev. B **48**, 4219.
Effect of Strong Scattering on the Low Temperature Penetration Depth of a d-Wave Superconductor.

Huang, Q., J. F. Zasadzinski, N. Tralshawala, K. E. Gray, D. G. Hinks, J. L. Peng, and R. L. Greene, 1990, Nature, **347**, 369.
Tunneling Evidence for Predominantly Electron-Phonon Coupling in Superconducting $Ba_{1-x}K_xBiO_3$ and $Nd_{2-x}Ce_xCuO_{4-y}$.

Iguchi, I. and Z. Wen, 1994, Phys. Rev. B **49**, 12388.
Experimental Evidence for a d-Wave Pairing State in $YBa_2Cu_3O_{7-\delta}$ from a Study of $YBa_2Cu_3O_{7-\delta}$ /Insulator/Pb Josephson Tunnel Junctions.

Imai, T. *et al.*, 1988, J. Phys. Soc. Jpn. **57**, 2280.

Jorgensen, J. D., 1991, Physics Today **44**, 34.
Defects and Superconductivity.

Kampf, A. P., 1994, Phys. Rep. **249**,219.
Magnetic Correlations in High Temperature Superconductivity.

Katz, A. S., A. G. Sun, R. C. Dynes, and K. Char, 1995, Appl. Phys. Lett. **66**, 105.
Fabrication of All Thin-Film $YBa_2Cu_3O_{7-\delta}$ /Pb Josephson Tunnel Junctions.

Kim, J. -T., 1995, private communication.

Kirtley, J. R., C. C. Tsuei, J. Z. Sun, C. C. Chi, L. S. Yujahnes, A. Gupta, M. Rupp, and M. B. Ketchen, 1995, Nature **373**, 225.
Symmetry of the Order Parameter in the High T_c Superconductor $YBa_2Cu_3O_{7-\delta}$.

Klemm, R.A., 1994, Phys. Rev. Lett. **73**, 1871.
Comment on "Experimental Determination Of The Superconducting Pairing State In YBCO from the Phase Coherence of YBCO-Pb dc SQUIDs."

Kotliar, G., 1988, Phys. Rev. B **37**, 3664.
Resonating Valence Bonds and d-Wave Superconductivity.

Laughlin, R., 1986, in *Quantum Hall Effect*, edited by S. M. Girvin and R. E. Prange (Springer, New York) p. 233.

Leggett, A. J., 1992, private communication.

Leggett, A. J., 1993, private communication.

Levi, B. G., 1993, Physics Today **46**, 17.
In High T_c Superconductors, Is d-Wave the New Wave?

Liu, D. Z., K. Levin, and J. Maly, 1995, Phys. Rev. B **51**, 8680.
Superconducting Order Parameter in Bilayer Cuprates -- Occurrence of π Phase Shifts in Corner Junctions.

Maki, K. and H. Won, 1994, Phys. Rev. Lett. **72**, 1758.
Spin Fluctuations of d-Wave Superconductors.

Mante, G., R. Claessen, T. Buslaps, S. Harm, R. Manzke, M. Skibowski, and J. Fink, 1990, Z. Phys. B **80**, 181.

Markiewicz, R. S., 1990, J. Phys. Condens. Matt. **2**, 6223.

Martin, S., A. T. Fiory, R. M. Fleming, L. F. Schneemeyer, and J. V. Waszczak, 1988, Phys. Rev. Lett. **60**, 2194.

Martin, S., A. T. Fiory, R. M. Fleming, L. F. Schneemeyer, and J. V. Waszczak, 1990, Phys. Rev. B **41**, 846.
Normal State Transport Properties of $Bi_{2+x}Sr_{2-y}CuO_{6\pm\delta}$ Crystals.

Mathai, A., Y. Gim, R. C. Black, A. Amar, and F. C. Wellstood, 1995, Phys. Rev. Lett. **74**, 4523.
Experimental Proof of Time-Reversal Invariant $d_{x^2-y^2}$ Symmetric Pairing in $YBa_2Cu_3O_7$.

Miller, Jr., J. H., Q. Y. Ying, Z. G. Zou, N. Q. Fan, J. H. Xu, M. F. Davis, and J. C. Wolfe, 1995, Phys. Rev. Lett. **74**, 2347.
Use of Tricrystal Junctions to Probe the Pairing State Symmetry of $YBa_2Cu_3O_{7-\delta}$.

Millis, A. J., 1994, Phys. Rev. B **49**, 15408.
Josephson Coupling Between a Disk of one Superconductor and a Surrounding Superconducting Film of Different Symmetry.

Millis, A. J., H. Monien, and D. Pines, 1990, Phys. Rev. B **42**, 167.

Moler, K. A., D. J. Baar, J. S. Urbach, R. Liang, W. N. Hardy, and A. Kapitulnik, 1994, Phys. Rev. Lett. **73**, 2744.
Magnetic Field Dependence of the Density of States of $YBa_2Cu_3O_{6.95}$ as Determined from the Specific Heat.

Monthoux, P., A. V. Balatsky and D. Pines, 1992, Phys. Rev. B **46**, 14803.
Weak-Coupling Theory of High Temperature Superconductivity in the Antiferromagnetically Correlated Copper Oxides.

Monthoux, P. and D. Pines, 1993, Phys. Rev. B **47**, 6069.
$YBa_2Cu_3O_7$ -- A Nearly Antiferromagnetic Fermi Liquid.

Monthoux, P. and D. Pines, 1994, Phys. Rev. B **49**, 4261.
Spin-Fluctuation-Induced Superconductivity and Normal State Properties of $YBa_2Cu_3O_7$.

Moriya, T., Y. Takahashi, and K. Ueda, 1990, J. Phys. Soc. Jpn. **59**, 2905.

Newns, D. M., P. C. Pattnaik, and C. C. Tsuei, 1991, Phys. Rev. B **43**, 3075.

Ogg, Jr., R. A., 1946, Phys. Rev. **69**, 243.
Bose-Einstein Condensation of Trapped Electron Pairs. Phase Separation and Superconductivity of Metal-Ammonia Solutions.

Olson, C. G., R. Liu, A. B. Yang, D. W. Lynch, A. J. Arko, R. S. List, B. W. Veal, Y. C. Chang, P. Z. Jiang, and A. P. Paulinkas, 1989, Science **245**, 731.
Superconducting Gap for Bi-Sr-Ca-Cu-O by High-Resolution Angle-Resolved Photoelectron Spectroscopy.

Ong, N. P., 1990, in *Physical Properties of High Temperature Superconductors II*, edited by D. M. Ginsberg (World Scientific, Singapore).

Ong, N. P., 1994, Physica C **235-240**, 221.
Non-Fermi Liquid Aspects of Charge Transport in the Cuprate Superconductors.

Parks, R. D., 1969, *Superconductivity, Volumes I And II* (Marcel Dekker, New York).

Pines, D., 1991, Physica C **185-189**, 120.
Spin Fluctuations and High Temperature Superconductivity in the Antiferromagnetically Correlated Oxides: $YBa_2Cu_3O_7$; $YBa_2Cu_3O_6$.

Pines, D., 1994a, Physica C **235-240**, 113.
$d_{x^2-y^2}$ Pairing and Spin Fluctuations in the Cuprate Superconductors -- Experiment Meets Theory.

Pines, D., 1994b, Physics Today **47**, 13.
Reply to "In Explaining High T_c, Is d-Wave A Washout?"

Pines, D., 1995, in *High T_c Superconductivity and the C_{60} Family*, edited by T. D. Lee and H. C. Ren (Gordon and Breach).
Spin Fluctuations and $d_{x^2-y^2}$ Pairing in the High Temperature Superconductors.

Pines, D. and Monthoux, P., 1995, to be published in J. Phys. Chem. Solids.
$d_{x^2-y^2}$ Pairing and Spin Fluctuations in the Cuprate Superconductors: A Progress Report

Quinlan, S. M. and D. J. Scalapino, 1995, Phys. Rev. B **51**, 497.
Neutron Scattering from a $d_{x^2-y^2}$-Wave Superconductor with Strong Impurity Scattering and Coulomb Correlations.

Radtke, R. J., K. Levin, H. B. Schuttler, and M. R. Norman, 1993a, Phys. Rev. B **48**, 653.
Predictions for Impurity-Induced T_c Suppression in the High Temperature Superconductors.

Radtke, R. J., K. Levin, H. B. Schuttler, and M. R. Norman, 1993b, Phys. Rev. B **48**, 15957.
Role of van Hove Singularities and Momentum-Space Structure in High Temperature Superconductivity.

Rice, J., 1992, thesis, unpublished.

Rokhsar, D. S., 1993, Phys. Rev. Lett. **70**, 493.
Pairing in Doped Spin Liquids: Anyon Versus d-Wave Superconductivity.

Rzchowski, M. S. and B. M. Hinaus, 1995, preprint.
Extrapolation Procedures in High T_c Gap-Function Experiments.

Scalapino, D. J., 1994a, Science **266**, 1626.
Letter -- Significance of $d_{x^2-y^2}$ Pairing in the Cuprates.

Scalapino, D. J., 1994b, Physics Today **47**, 120.
Reply to "In Explaining High T_c, Is d-Wave A Washout?"

Scalapino, D. J., 1995, Phys. Rep. **250**, 330.
The Case for $d_{x^2-y^2}$ Pairing in the Cuprate Superconductors.

Schafroth, M. R., 1955, Phys. Rev. **100**, 463.
Superconductivity of a Charged Ideal Bose Gas.

Schrieffer, J. R., 1992. Physica Scripta **T42**, 5.
Critical Issues in the Theory of High Temperature Superconductivity.

Shen, Z. X., D. S. Dessau, B. O. Wells, D. M. King, W. E. Spicer, A. J. Arko, D. Marshall, L. W. Lombardo, A. Kapitulnik, P. Dickinson, S. Doniach, J. DiCarlo, A. G. Loeser, and C. H. Park, 1993, Phys. Rev. Lett. **70**, 1553.
Anomalously Large Gap Anisotropy in the a-b Plane of $Bi_2Sr_2CaCu_2O_{8+\delta}$.

Sigrist, M. and T. M. Rice, 1992, J. Phys. Soc. Jpn. **61**, 4283.
Paramagnetic Effect in High T_c Superconductors -- A Hint for d-Wave Superconductivity.

Sigrist, M. and T. M. Rice, 1994, J. Low Temp. Phys. **95**, 389.
On the Phenomenology of Superconductivity in Cuprate Materials.

Sigrist, M. and T. M. Rice, 1995, Rev. Mod. Phys. **67**, 503.
Unusual Paramagnetic Phenomena in Granular High Temperature Superconductors -- A Consequence of d-Wave Pairing?

Sire, C., C. M. Varma, A. E. Ruckenstein, and T. Giamarchi, 1994, Phys. Rev. Lett. **72**, 2478.
Theory of the Marginal-Fermi Liquid Spectrum and Pairing in a Local Copper Oxide Model.

Slichter, C. P., 1994, in *Strongly Correlated Electronic Materials*, edited by K. S. Bedell *et al.* (Addison-Wesley, New York) p. 427.
Experimental Evidence for Spin Fluctuations in High Temperature Superconductors.

Solymar, L., 1972, *Superconductive Tunnelling and Applications* (Wiley-Interscience, New York).

Sun, A. G., 1994, private communication.

Sun, A. G., D. A. Gajewski, M. B. Maple, and R. C. Dynes, 1994, Phys. Rev. Lett. **72**, 2267.
Observation of Josephson Pair Tunneling Between a High T_c Cuprate ($YBa_2Cu_3O_{7-\delta}$) and a Conventional Superconductor (Pb).

Tesche, C. D. and J. Clarke, 1977, J. Low Temp. Phys. **29**, 301.
dc SQUID: Noise and Optimization.

Thompson, D. J., M. S. M. Minhaj, L. E. Wenger, and J. T. Chen, 1995, Phys. Rev. Lett. **75**, 529.
Observation of Paramagnetic Meissner Effect in Niobium Disks.

Tinkham, M., 1975, *Introduction to Superconductivity* (McGraw-Hill, New York).

Tsuei, C. C. *et al.*, 1990, Phys. Rev. Lett. **65**, 2724.

Tsuei, C. C., J. R. Kirtley, C. C. Chi, L. S. Yujahnes, A. Gupta, T. Shaw, J. Z. Sun, M. B. Ketchen, 1994, Phys. Rev. Lett. **73**, 593.
Pairing Symmetry and Flux Quantization in a Tricrystal Superconducting Ring of $YBa_2Cu_3O_{7-\delta}$.

Ueda, K., T. Moriya, and Y. Takahashi, 1992, J. Phys. Chem. Solids **53**, 1515.
Antiferromagnetic Spin Fluctuations and High T_c Superconductivity.

Van Duzer, T. and C. W. Turner, 1981, *Principles of Superconductive Devices and Circuits* (Elselvier-North Holland, New York).

Van Harlingen, D. J., 1993, private communication.

Van Harlingen, D. J., 1995, Rev. Mod. Phys. **67**, 515.
Phase-Sensitive Tests of the Symmetry of the Pairing State in the High Temperature Superconductors -- Evidence for $d_{x^2-y^2}$ Symmetry.

Van Harlingen, D. J. and D. A. Wollman, 1994a, *Proceedings of the Seventh International Symposium On Superconductivity* -- Kitakyushu, Japan, July 5-9, 1994.
Determining the Symmetry of the Superconducting Pairing State from Phase Coherence in Josephson Junctions and dc SQUIDs.

Van Harlingen, D. J., D. A. Wollman, D. M. Ginsberg, and A. J. Leggett, 1994b, Physica C **235-240**, 122.
Phase-Sensitive Tests of the Symmetry of the Pairing State in the High Temperature Superconductors -- Evidence for $d_{x^2-y^2}$ Symmetry in YBCO.

Varma, C. M., 1995a, Phys. Rev. Lett. **75**, 898.
Theory of Copper-oxide Metals.

Varma, C. M., 1995b, preprint.
Symmetry of the Superconducting State in Copper-oxides.

Varma, C. M., P. B. Littlewood, S. Schmitt-Rink, E. Abrahams, and A. E. Ruckenstein, 1989, Phys. Rev. Lett. **63**, 1996.
Phenomenology of the Normal State of Cu-O High Temperature Superconductors.

Vijayaraghavan, R. and L. C. Gupta, 1995, Int. J. Mod. Phys. B **9**, 633.
Magnetic and Superconducting Properties of High T_c Superconductors.

Volovik, G. E., 1993, JETP Lett. **58**, 469.
Superconductivity with Lines of Gap Nodes: Density of States in the Vortex.

Wakai, R., 1987, thesis, unpublished.

Wollman, D. A., D. J. Van Harlingen, J. Giapintzakis, and D. M. Ginsberg, 1995, Phys. Rev. Lett. **74**, 797.
Evidence for $d_{x^2-y^2}$ Pairing from the Magnetic Field Modulation of $YBa_2Cu_3O_7$ - Pb Josephson Junctions.

Wollman, D. A., D. J. Van Harlingen, J. Giapintzakis, and D. M. Ginsberg, to be published in J. Phys. Chem. Solids.
Tunneling in Pb-YBCO Junctions: Determining the Symmetry of the Pairing State.

Wollman, D. A., D. J. Van Harlingen, W. C. Lee, D. M. Ginsberg, and A. J. Leggett, 1993, Phys. Rev. Lett. **71**, 2134.
Experimental Determination of the Superconducting Pairing State in YBCO from the Phase Coherence of YBCO-Pb dc SQUIDs.

Wollman, D. A., D. J. Van Harlingen, W. C. Lee, D. M. Ginsberg, and A. J. Leggett, 1994a, Physica B **194**, 1669.
Phase Coherence in YBCO-Pb SQUIDs -- Direct Experimental Determination of the Symmetry of the Pairing State in High Temperature Superconductors.

Wollman, D.A., D. J. Van Harlingen, and A. J. Leggett, 1994b, Phys. Rev. Lett. **73**, 1872.
Reply to Comment on "Experimental Determination of the Superconducting Pairing State in YBCO from the Phase Coherence of YBCO-Pb dc SQUIDs."

Yagil, Y., N. Hass, G. Desgardin, and I. Monot, 1995, Physica C **250**, 59.
Experimental Evidence for Strong Electron-Phonon Coupling to Selected Phonon Modes in Point-Contact Spectroscopy of $YBa_2Cu_3O_{7-\delta}$.

Yu, F., M. B. Salamon, A. J. Leggett, W. C. Lee, and D. M. Ginsberg, 1995, Phys. Rev. Lett. **74**, 5136.
Tensor Magnetothermal Resistance in $YBa_2Cu_3O_{7-x}$ *via Andreev Scattering of Quasiparticles.*

Yu, R. C., M. B. Salamon, and W. C. Lee, 1992, Phys. Rev. Lett. **69**, 1431.

VITA

David Anders Wollman was born on January 31, 1968, in Galesberg, Illinois. At the age of three his family relocated to the more geologically interesting area of western Pennsylvania. After growing up as an "academic brat" (his parents taught history and humanities at Geneva College), he left to study physics on a four-year academic scholarship (Freshman Distinguished Alumni Scholarship) at the beautiful campus of Michigan State University in East Lansing, Michigan in 1986. There he met his future wife, Susan, and found purpose, direction, and responsibility. He was an undergraduate professorial assistant to Dr. Michael Dubson, and decided to go into experimental condensed matter physics after realizing that he really enjoyed working in the machine shop. In 1990, he graduated Summa Cum Laude with a Bachelor of Science degree in Physics, and was invited to join several honorary societies (Phi Beta Kappa, Phi Kappa Phi, Sigma Pi Sigma, Pi Mu Epsilon).

Dave returned to the flatlands of Illinois with a National Science Foundation Graduate Fellowship that allowed him to pursue his graduate education at the University of Illinois at Urbana-Champaign. He joined the research group of Dr. Dale Van Harlingen in 1990 to investigate properties of mesoscopic systems, but was caught up in the excitement of the cuprate superconductors. He has published several papers and has given an invited talk on the symmetry of the superconducting state in YBCO.

In 1995 Dave was named a National Research Council Post-doctoral Fellow at NIST in Boulder, Colorado. He will work with John Martinis to develop a new x-ray detector for microanalysis while enjoying the scenic views of the Rocky Mountains.